



Universität Hamburg

Erg K⁺ channels in mouse
(*Mus musculus* (Linnaeus, 1758)) gonadotropes

Dissertation

zur Erlangung des Doktorgrades
-Dr. rer. nat.-
am Department Biologie der Universität Hamburg

vorgelegt von

Crenguța Elena Dinu

Râmnicu Sărat, Rumänien

Hamburg
July, 2010

Genehmigt vom Fachbereich Biologie
der Fakultät für Mathematik, Informatik und Naturwissenschaften
an der Universität Hamburg
auf Antrag von Professor Dr. J. SCHWARZ
Weitere Gutachterin der Dissertation:
Priv.-Doz. Dr. S. LÜTHJE
Tag der Disputation: 03. September 2010

Hamburg, den 17. August 2010



A. Temming
Professor Dr. Axel Temming
Leiter des Fachbereichs Biologie

Discover Clinical Research LLC

6610 Crestwood Court
San Antonio Texas 78249

Telephone: 210 877-2226
Fax 210 694-6083
Cell 210 367-8227
www.discoverclinicalresearch.com

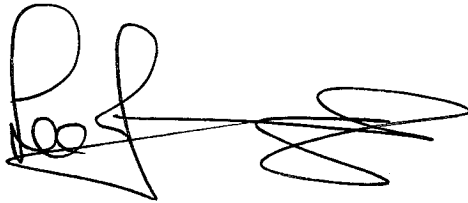
July 21, 2010

Re: Doctoral Thesis for Crenguta Elena Dinu, University of Hamburg

To Whom It May Concern.

I, Lee Jennings, the undersigned, certify that I am a native English speaker. I have read Crenguta Elena Dinu's draft doctoral thesis and have provided the relevant advice in relation to English composition and grammar that I believe should be incorporated into the final thesis. I affirm the thesis' general language, grammar and spelling are correct and should be readily understood by any native English speaker.

Sincerely,

A handwritten signature in black ink, appearing to read 'Lee Jennings', with a stylized flourish extending to the right.

Lee Jennings Ph.D.
President
Discover Clinical Research LLC.

List of contents

I.	Abstract/Zusammenfassung	1
II.	Introduction	3
II.1.	Classification of K⁺ channels α-subunits	3
II.2.	EAG K⁺ channels family	4
II.3.	EAG K⁺ channel structure	5
II.4.	Erg K⁺ channels	6
II.4.1.	Influence of ions and temperature on erg K ⁺ currents	7
II.4.2.	Erg K ⁺ channel kinetics	8
II.4.3.	Erg K ⁺ channel modulation	9
II.5.	Physiology of erg K⁺ currents	10
II.5.1.	Role of erg K ⁺ channels in the pituitary gland	11
II.6.	Aim of the study	16
III.	Materials and methods	17
III.1.	Mice	17
III.2.	Gonadotrope cells	18
III.2.1.	Primary cell culture	18
III.2.2.	Acute pituitary slice	19
III.3.	Calcium imaging	20
III.3.1.	Principle of the method	20
III.3.2.	Measurement of fura-2 fluorescence/experimental procedure	21
III.3.3.	Data analysis	22
III.4.	Electrophysiology	22
III.4.1.	Electrophysiological parameters	22
III.4.2.	Voltage clamp and patch clamp	23

III.4.3.	Patch clamp recording configurations	25
III.4.4.	Equipment and experimental setup	26
III.4.5.	Electrodes	27
III.4.6.	Solutions	28
III.4.7.	Experimental procedure	30
III.4.8.	Data analysis	30
III.5.	ELISA	32
III.5.1.	Technique principle	32
III.5.2.	Media and cell culture preparation	33
III.5.3.	Stimulation protocol	33
III.5.4.	ELISA procedure	34
III.5.5.	Data analysis	34
IV.	Results	35
IV.1.	Physiological characterization of genetically labeled mouse gonadotropes	35
IV.1.1.	Fluorescence and immunofluorescence	35
IV.1.2.	The membrane potential was changed by GnRH	36
IV.1.3.	GnRH increased $[Ca^{2+}]_i$	40
IV.1.4.	Membrane depolarization increased $[Ca^{2+}]_i$ and decreased outward current	40
IV.1.5.	Na^+ currents	41
IV.2.	Erg K^+ currents in mouse gonadotropes	43
IV.2.1.	Blockage of erg K^+ channels increased $[Ca^{2+}]_i$ in acute pituitary slices	43
IV.2.2.	Availability and activation of erg K^+ currents in cultured gonadotropes	44
IV.2.3.	Erg conductance changed by external K^+ concentration	46
IV.2.4.	Temperature dependence of erg K^+ currents	47
IV.2.5.	Blockage of erg K^+ channels depolarized gonadotropes	51

IV.2.6.	Blockage of erg K ⁺ channels increased [Ca ²⁺] _i in cultured gonadotropes	52
IV.2.7.	E-4031 and GnRH increased the [Ca ²⁺] _i	53
IV.2.8.	E-4031 and GnRH reduced net outward currents	54
IV.2.9.	Modulation of erg K ⁺ current by GnRH	55
IV.3.	LH secretion in mouse gonadotropes	59
V.	Discussion	61
V.1.	Heterogeneity of mouse gonadotropes	61
V.2.	Biophysical properties of erg K⁺ currents in gonadotropes	62
V.3.	Inhibition of erg K⁺ currents by GnRH	65
V.4.	The GnRH-activated signaling cascade involves influx of Ca²⁺	66
VI.	References	69
VII.	Appendix	81
VII.1.	Contributions	81
VII.2.	List of tables	81
VII.3.	List of figures	81
VII.4.	Abbreviations	83
VIII.	Acknowledgements	88

I. Abstract/Zusammenfassung

Ether-á-go-go-related gene (erg) K⁺ channels are prominently expressed in the pituitary gland. Their presence and function has previously been described in lactotropes where erg K⁺ channel modulation by thyrotropin-releasing hormone is important in inducing the 2nd phase of prolactin secretion (reviewed by (Bauer and Schwarz 2001)). This thesis now describes an erg K⁺ current in primary mouse gonadotropes and its function in the control of Ca²⁺ influx and discusses its possible role in the control of luteinizing hormone (LH) secretion initiated by gonadotropin-releasing hormone (GnRH). GnRH induces an increase in the intracellular Ca²⁺ concentration ([Ca²⁺]_i) by Ca²⁺ release from intracellular stores and Ca²⁺ influx through voltage-dependent Ca²⁺ channels.

Erg K⁺ currents were recorded in 80–90% of fluorescently-labeled gonadotropes of a knock-in mouse strain in which Cre recombinase is coexpressed with the GnRH receptor. Specifically blocking erg K⁺ currents with E-4031 depolarized the resting membrane potential by 5–8 mV and led to an increase in [Ca²⁺]_i, which was abolished by the L-type Ca²⁺ channel blocker nifedipine. GnRH inhibited erg currents by reducing the maximal current and in half of the cells additionally by shifting the activation curve to more positive potentials. In conclusion, the erg current contributes to the maintenance of the resting potential in gonadotropes, thereby securing a low [Ca²⁺]_i by restricting Ca²⁺ influx. In addition, erg K⁺ channels are blocked by GnRH by an as-yet unknown signal cascade

In der Hypophyse sind Ether-á-go-go-related-gene (erg)-K⁺-Kanäle weit verbreitet. Zuvor wurde bereits ihre Funktion in laktotropen Zellen beschrieben, in denen Modulation der erg-K⁺-Kanäle durch das Thyreotropin-Releasing-Hormon (TRH) für die zweite Phase der Prolaktinausschüttung wichtig ist (Review von (Bauer and Schwarz 2001)). Diese Doktorarbeit beschreibt einen Erg-K⁺-Strom in gonadotropen Zellen aus der Maus, seine Funktion bei der Kontrolle des Kalziumeinstroms und diskutiert seine mögliche Rolle bei der Kontrolle der Ausschüttung des Luteinisierenden Hormons (LH), welche durch das Gonadotropin-Releasing-Hormon (GnRH) verursacht wird. GnRH führt zu einem Anstieg in der intrazellulären Ca²⁺-Konzentration ([Ca²⁺]_i) durch Ca²⁺-Ausschüttung aus intrazellulären Speichern und Ca²⁺-Einstrom durch spannungsabhängige Ca²⁺-Kanäle.

Erg-K⁺-Ströme traten in 80–90% fluoreszenzierender gonadotroper Zellen einer Knock-In-Mauslinie auf, in der Cre-Rekombinase mit dem GnRH-Rezeptor koexprimiert wird. Spezifische Blockade der Erg-K⁺-Ströme durch E-4031 führte zu einer Depolarisation des Ruhemembranpotentials in Höhe von 5–8 mV und zu einem [Ca²⁺]_i-Anstieg, der durch den L-Typ-Ca²⁺-Kanalblocker Nifedipine verhindert wurde. GnRH inhibierte den Erg-Strom durch eine Reduktion des maximalen Stromes und in der Hälfte der Zellen zusätzlich durch eine Verschiebung der Spannungsabhängigkeit der Aktivierung zu positiveren Potentialen. Zusammenfassend gesagt, trägt der Erg-Strom in gonadotropen Zellen zur Beibehaltung des Ruhemembranpotentials und einer niedrigen niedrigen intrazellulären Ca²⁺-Konzentration durch Einschränkung des Ca²⁺-Einstroms bei. Des Weiteren werden Erg-K⁺-Kanäle durch GnRH durch eine bis jetzt unbekanntes Signalkaskade inhibiert.

II. Introduction

The first description of a K^+ ion current was presented as a part of action potential mechanism in squid giant axons by Hodgkin and Huxley in 1952 (Hodgkin and Huxley 1952; Hodgkin and Huxley 1952). The K^+ current was responsible for the repolarization of the action potential. K^+ currents have been found in all excitable cells which display action potentials mediated by Na^+ or Ca^{2+} , but also in non-excitable cells, with K^+ channels being the most ubiquitous of all and present in all eukaryotic cells. K^+ channels form a diverse and large group of ion channel families involved in a broad range of physiological functions (Pongs 1992; Chandy and Gutman 1995). They vary in their kinetics, voltage-dependence, pharmacology, single-channel behavior and other properties. Their diversity is not dependent on the cell type as different K^+ channels can be found in the same cell and also in different cell types the same K^+ channel can be found. The diversity is due to the large number of genes coding for principal subunits (α -subunit) of K^+ channel, alternative splicing generating multiple mRNA transcripts from a single gene, heteromeric assembly of different principal subunits, as well as possible RNA editing and posttranslational modifications (Coetzee, Amarillo et al. 1999).

II.1. Classification of K^+ channels α -subunits

There are several types of K^+ channels, classified accordingly to their principal α -subunit structural properties. The first group contains proteins with six transmembrane domains (TMD) (S1-S6) and a conserved P (pore or H5) domain. The voltage-gated K^+ (K_v) family (with eight subfamilies: K_v1 – K_v6 and K_v8 – K_v9 ; (Gutman, Chandy et al. 2005)) belongs to this group, as well EAG-like family, and many others (Fig. II.1). The second group consists of proteins with two TMDs and contains inward rectifier K^+ (K_{ir}) channels with seven subfamilies ($K_{ir}1$ – $K_{ir}7$: (Kubo, Adelman et al. 2005)). The third group, known as two-pore subunits, contains four putative TMDs (M1–M4) and two P domains (P1 and P2) assembled as dimers contrary to the 6TMD and 4 TMD which are most likely forming tetrameric proteins (Lesage, Guillemare et al. 1996). Functionally, α -subunits of this group express K^+ selective channels that respond to changes in extracellular K^+ concentration in a manner

described by the Goldman-Hodgkin-Katz equation, and are referred to as “leak” K^+ channels (Goldstein, Wang et al. 1998).

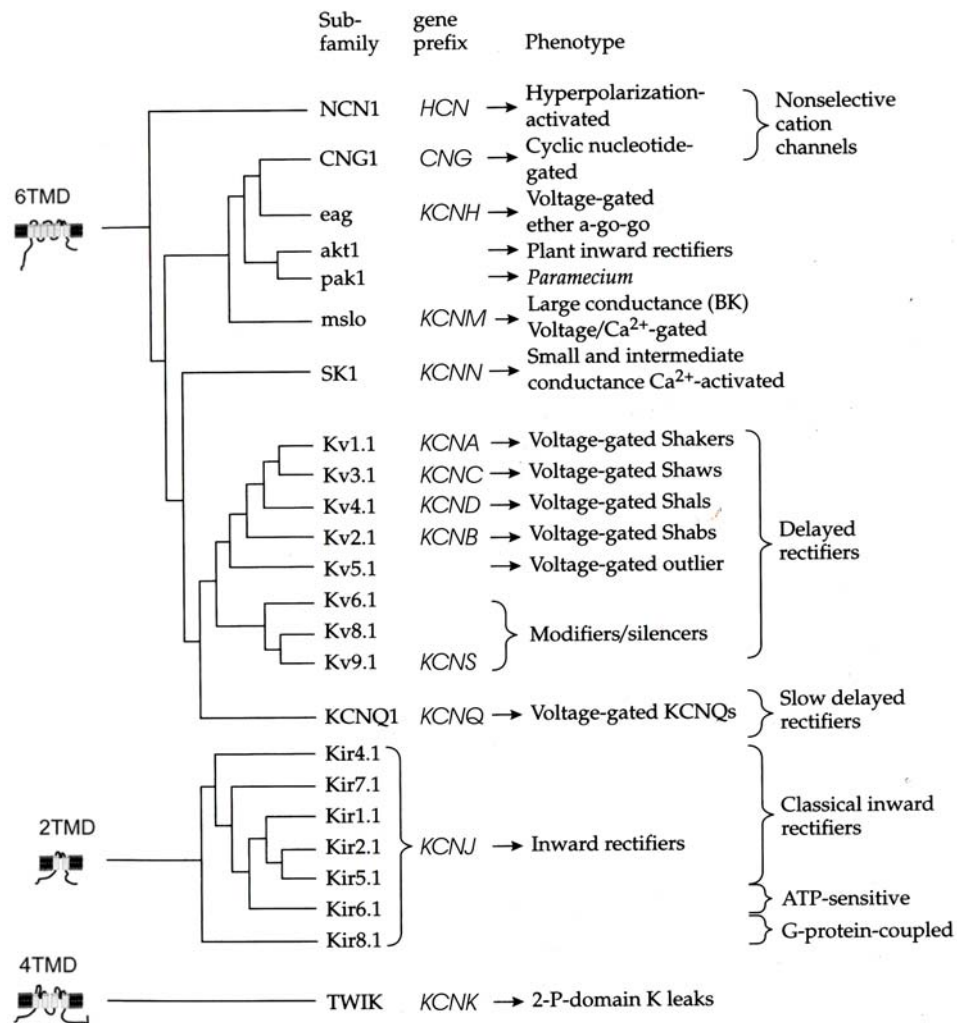


Fig. II.1: Schematic representation of principal K^+ subunits families and subfamilies. They are classified into three groups according to the membrane topology of the subunit – with six, two and four transmembrane domains (6TMD, 2TMD, 4TMD). Each group of principal subunits is divided into discrete subfamilies on the basis of sequence similarity and each family can be further subdivided into several subfamilies which often contain closely related members (adapted from (Hille 2001)).

II.2. EAG K^+ channels family

This work was concentrated on characterization of the voltage-dependent erg K^+ channels (erg1, erg2 and erg3, corresponding to $K_v11.1$, $K_v11.2$ and $K_v11.3$ or K_{cnh2} , 6 and 7 based on the IUPHAR nomenclature: (Gutman, Chandy et al. 2005)). Erg K^+ channels belong to the family of EAG (**ether-a-go-go**) K^+ channels. They were first cloned from a *Drosophila melanogaster* mutant, which under ether anesthesia exhibited leg-shaking behavior

reminiscent of the famous “go-go” dance, hence the peculiar name (Warmke, Drysdale et al. 1991). They have 6 TMDs (Fig. II.1) and a special inward rectification function (Warmke and Ganetzky 1994; Trudeau, Warmke et al. 1995) not corresponding to the inward rectification of the classical K_{ir} channels which have only 2TMDs.

The EAG family is divided into three different subfamilies: *eag*, *eag*-related gene (*erg*), and *eag*-like K^+ channel (*elk*) (Warmke and Ganetzky 1994; Ganetzky, Robertson et al. 1999) (Fig. II.2). Each subfamily of EAG K^+ channels has more than one member (Fig. II.2): 2 *eag* channels (*eag1*: (Ludwig, Terlau et al. 1994; Saganich, Vega-Saenz de Miera et al. 1999)), three *erg* channels (*erg1*: (Shi, Wymore et al. 1997; Bauer, Engeland et al. 1998)) and three *elk* channels (Engeland, Neu et al. 1998; Shi, Wang et al. 1998).

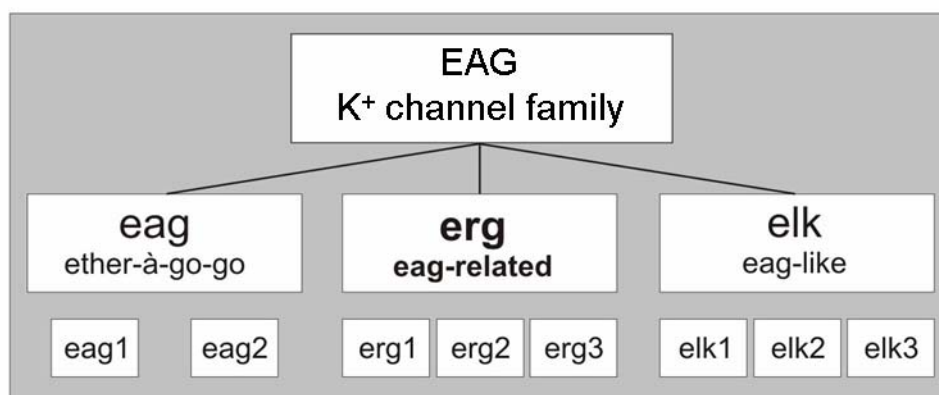


Fig. II.2: The ether-à-go-go gene K^+ channel family (EAG). The EAG family consists of three subfamilies: *eag* (ether-à-go-go gene) with 2 members, *elk* (eag-like gene) with 3 members and *erg* (eag-related gene) with 3 members (adapted from (Bauer and Schwarz 2001)).

II.3. EAG K^+ channel structure

Functional *erg* channels consist of four subunits with six transmembrane domains (S1-S6) which assemble into homo- or heterotetramers of different composition (Fig. II.3, C). The fourth transmembrane segment (S4) functions as a voltage sensor (Bauer and Schwarz 2001). The inner wall of the channel is constructed by S5 and S6 segments together with the pore region which is involved in forming the K^+ selectivity filter (Schwarz and Bauer 1999). The N-terminal part of the *erg* channels contains an EAG domain which is responsible for the slow deactivation of the human *erg* channels (HERG) by binding to the S4-S5 linker (Schonherr and Heinemann 1996; Morais Cabral, Lee et al. 1998; Wang, Trudeau et al. 1998; Chen, Zou et al. 1999; Vilorio, Barros et al. 2000; Wang, Myers et al. 2000). This domain is

not present in any other K^+ channel family. The function of the C-terminus has a cyclic nucleotide binding domain (cNBD) (Fig. II.3) is still controversial. While direct binding of cyclic nucleotides to erg1 channels was ruled out (Robertson, Warmke et al. 1996; Brelidze, Carlson et al. 2009), modulation of erg currents containing erg1b subunits by cGMP was reported (Mewe, Mauerhofer et al. 2010). One explanation for these differences is that the experiments were done in different cell types, with different eag subunits and with different techniques.

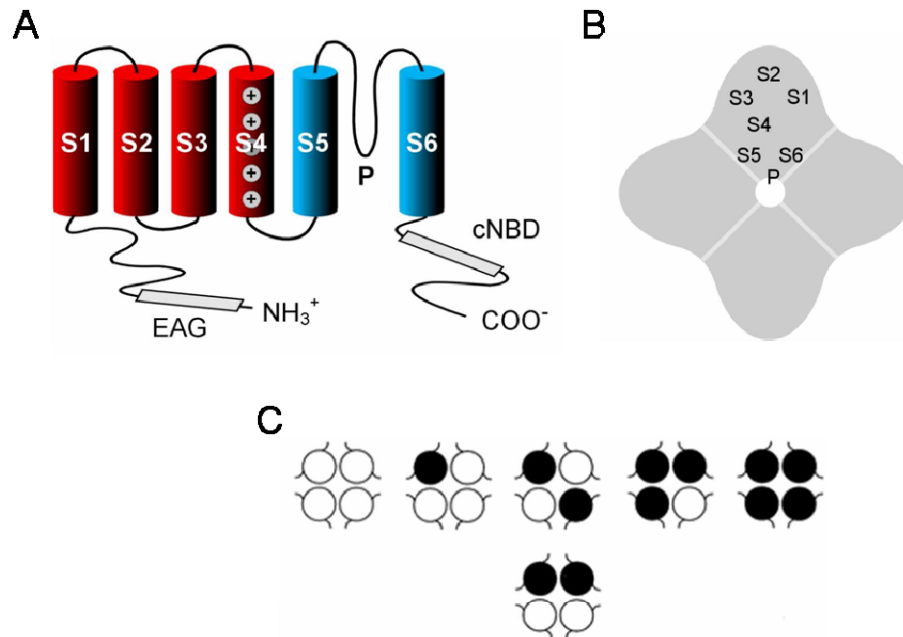


Fig. II.3: Structure of EAG K^+ channels. A, the α -subunit of EAG K^+ channels consists of six TMDs (S1-S6), an EAG domain at the N-terminus and a cNBD at the C-terminus. B, Proposed tetrameric structure of an EAG channel with the pore region P and S6 forming the inner core of the channel and S1-S5 forming the outer parts and with S4 as the voltage sensor (adapted from (Bauer and Schwarz 2001)). C, Schematic representation of possible heteromultimeric channel composition (adapted from (Wimmers, Bauer et al. 2002)).

II.4. Erg K^+ channels

The first cloned erg channel was the human erg1 (HERG1 or KCNH2: based on the IUPHAR nomenclature: (Gutman, Chandy et al. 2005)) in 1994 (Warmke and Ganetzky 1994). Later, rat and mouse homologues of all eag subfamilies members have been cloned. Three splice variants and alternative transcripts of mouse erg1 (Merg1; Kcnh2) were cloned: Merg1a' lacks the first 59 amino acids of the N-terminus of Merg1a (London, Trudeau et al. 1997). Merg1b and its human homologue has a short alternative 36 amino acids N-terminus (Lees-

Miller, Kondo et al. 1997; London, Trudeau et al. 1997). In human heart another splice variant, HERG_{USO}, has been identified which lacks part of the cNBD domain together with the C-terminal domain and ends with an alternative sequence instead (Kupersmidt, Snyders et al. 1998). There are also β -subunits coexpressed with *erg1*: MinK and MiRP1 were found to coimmunoprecipitate with HERG1 in heterologous system and they affect the amplitude, shift the activation curve and influence the modulation of the HERG channel (Yang, Kupersmidt et al. 1995; McDonald, Yu et al. 1997; Bianchi, Wible et al. 1998; Abbott, Sesti et al. 1999; Cui, Melman et al. 2000). Another β -subunit, MiRP2 (KCNE) was found to completely suppress HERG currents when coexpressed in *Xenopus* oocytes (Schroeder, Waldegger et al. 2000). They are no β -subunits or proteins known to interact with *erg2* and *erg3*.

II.4.1. Influence of ions and temperature on *erg* K⁺ currents

The study of *erg* channels isolated from other channels was made possible by the discovery of specific *erg* channel blockers. Most of them belong to the class III antiarrhythmic drugs, like the: methanesulfonanilides E-4031, WAY-123,389 and dofetilide (Sanguinetti, Jiang et al. 1995; Spector, Curran et al. 1996; Weinsberg, Bauer et al. 1997). Also toxins purified from the Mexican scorpions *Centruroides elegans elegans* (CeErg4 or KTx1.7 and CeErg5 or KTx1.8: (Restano-Cassulini, Olamendi-Portugal et al. 2008)) and *Centruroides noxius Hoffmann* (*erg*toxin: (Gurrola, Rosati et al. 1999)) specifically block different *erg* channels in a dose-dependent manner and depending on the cell type. The advantage of these venom toxins is that they are reversible. By specifically blocking all *erg* channels, E-4031 (used in the present work) and WAY-123,389 are appropriate tools for *erg* currents identification.

The properties of *erg* channels are influenced by the extracellular ion concentration, especially K⁺ (Shibasaki 1987; Sanguinetti, Jiang et al. 1995; Sturm, Wimmers et al. 2005) and Ca²⁺ (Ho, Earm et al. 1996; Johnson, Mullins et al. 1999). Elevated external K⁺ concentration ($[K^+]_e$) slows deactivation, inactivation and recovery from inactivation kinetics and shifts activation to more negative potentials. External Ca²⁺ concentration ($[Ca^{2+}]_e$) accelerates the deactivation kinetics and shifts the activation to more positive potentials. An increase in the $[K^+]_e$ also reduces the steady-state inactivation and increases the conductance of *erg* channels, which leads to larger currents. Therefore, to facilitate evaluation of the biophysical properties of the relatively small native *erg* current in gonadotropes, in this study $[K^+]_e$ was increased and $[Ca^{2+}]_e$ buffered to nanomolar concentrations.

Electrophysiological experiments are often carried out at room temperature. This leads to deviations in kinetics, voltage dependence and amplitude in comparison to the conditions at human body temperature and thus might also influence the study of modulation of the erg current. (Zhou, Gong et al. 1998) (1998) studied for the first time the properties of erg channels at physiological temperature. They transfected human embryonic kidney (HEK) 293 cells with HERG channel cDNA and they noticed that the current density was increased and the activation, inactivation, recovery from inactivation and deactivation kinetics were more rapid at 35° C. (Vandenberg, Varghese et al. 2006) (2006) investigated the temperature dependence of HERG channels in Chinese hamster ovary (CHO) cells. They found different temperature coefficients (Q_{10}) for the various biophysical parameters of the HERG current between the measurements at room temperature and the ones near physiological body temperature (35° C). The Q_{10} represents the rate of change of a biological or chemical parameter for a 10-degree rise in the temperature:

$$Q_{10} = \frac{\alpha_1}{\alpha_2}^{10/(T_2-T_1)}$$

where α_1 and α_2 represent the parameters and T_1 and T_2 represent the temperature in degree Celsius (α_1 at T_1 and α_2 at T_2). In biological systems the Q_{10} is usually between 1 and 3 indicating no to positive thermal dependence.

II.4.2. Erg K^+ channel kinetics

The erg channels expressed in heterologous systems mediates membrane currents with characteristic kinetic properties. Upon depolarization from -60 mV to positive potentials the erg current activates slowly reaching a steady-state after several seconds (Snyders and Chaudhary 1996; Wang, Liu et al. 1997). This corresponds to the successive opening of the channels which involves the movement of the voltage sensor (S4) to the external side in a screw-like manner inducing structural changes (Jiang, Lee et al. 2003). The reverse process is called deactivation. After opening the channels close due to collapse of the outer pore region, a mechanism known as C-type inactivation (Schonherr and Heinemann 1996; Smith, Baukrowitz et al. 1996; Herzberg, Trudeau et al. 1998; Fan, Jiang et al. 1999). Contrary to classical voltage-dependent K^+ channels, erg channels show a kinetic based on the “inverse gating” with faster inactivation than activation and much faster recovery from inactivation than deactivation (Trudeau, Warmke et al. 1995; Smith, Baukrowitz et al. 1996; Spector, Curran et al. 1996; Wang, Liu et al. 1997). The small steady-state outward current is due to a

large steady-state inactivation. Due to a slower deactivation compared to the recovery from inactivation, there is a huge flow of current during repolarization (Fig. II.4).

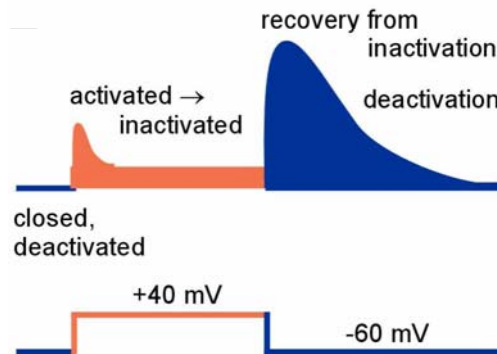


Fig. II.4: Schematic representation of the erg-mediated current. At negative holding potentials erg K^+ channels are closed (deactivated). After depolarization, a small steady-state outward current is elicited. Upon repolarization a large transient current occurs because of very fast recovery from inactivation and slow deactivation (Adapted from (Bauer and Schwarz 2001)).

There are significant differences in the kinetic properties between erg channels composed of different erg subunits. The voltage-dependence of activation is different for each subunit with erg3 currents being activated at the most negative potentials, erg2 currents at the most positive potentials and erg1a and erg1b in the middle (London, Trudeau et al. 1997; Shi, Wymore et al. 1997). The time courses of activation are influenced in the same way: erg2 having the slowest activation time constant and erg3 the fastest one. When comparing the deactivation in different tissues the order of voltage-dependence is the same even with different external K^+ concentrations (Schledermann, Wulfsen et al. 2001; Wimmers, Bauer et al. 2002; Hirdes, Schweizer et al. 2005). In vivo, the erg channels are not homomeric, i.e. the erg1a and erg1b are often expressed together and the properties of heteromeric channels are very different from the properties of homomeric channels (Lees-Miller, Kondo et al. 1997; London, Trudeau et al. 1997; Jones, Roti Roti et al. 2004).

II.4.3. Erg K^+ channel modulation

Little is known about erg channel modulation by neurotransmitters and/or hormone receptors. Erg current are often modulated by G-protein-coupled receptors (GPCRs) and their downstream secondary messenger molecules. The most investigated pathway in respect to erg channels was the pathway activated by the thyrotropin-releasing hormone (TRH) receptor. Studies done in *Xenopus* oocytes show that the structural integrity of HERG channels is required for TRH modulation (Alonso-Ron, Barros et al. 2009) and secondly that TRH may inhibit HERG currents via PKC (Barros, Gomez-Varela et al. 1998). Studies done also on a

pituitary tumor cell line (GH₃/B₆) show that TRH inhibits *erg1a*, *erg2* and *erg3* by reduction of maximal current and shift of activation (Schledermann, Wulfsen et al. 2001) and also reduces *erg1b* (Kirchberger, Wulfsen et al. 2006). The β ₁-adrenergic receptor is G_s-protein coupled. β ₁-adrenergic stimulation exerts a complex regulation of Kv11.1 (*erg1*) channels by acting at different levels, including direct binding of cAMP (Cui, Melman et al. 2000; Cui, Kagan et al. 2001) and PKA phosphorylation (Karle, Zitron et al. 2002; Thomas, Kiehn et al. 2004). PKA-dependent phosphorylation of the β ₁-adrenergic receptor promotes its association with 14-3-3 ϵ proteins disrupting the interaction between Kv11.1 and 14-3-3 ϵ (Tutor, Delpon et al. 2006). Stimulation of G_q-protein coupled receptors cause HERG current reduction (for the α _{1A}-adrenergic receptor: (Thomas, Kiehn et al. 2004; Zankov, Yoshida et al. 2009); for M1 and M3-muscarinic receptors: (Hirdes, Horowitz et al. 2004; Cockerill, Tobin et al. 2007)). The α _{1A}-adrenergic receptor induced shift in the activation curve of HERG and accelerated the deactivation kinetics which could be prevented by inhibition of both PKC and PKA (Thomas, Kiehn et al. 2004). The *erg* current modulation may be caused by PIP₂ consumption since PIP₂ loading leads to augmentation of HERG/I_{Kr} current (Zankov, Yoshida et al. 2009) and attenuation of α _{1A}-adrenergic modulation (Bian, Cui et al. 2001), but in other studies no effect of PIP₂ on *erg* currents was seen (Schledermann, Wulfsen et al. 2001; Hirdes, Horowitz et al. 2004).

II.5. Physiology of *erg* K⁺ currents

Erg channels are present widely in the body (brain, muscle, endocrine glands, testes, smooth muscle, esophagus, stomach, bladder, jejunum and colon) and mediate a variety of physiological functions. The physiological role of HERG in the heart is the best studied among all the *erg* channel functions. In the sinoatrial node (SA) *erg1* currents contribute to the mechanism underlying pacemaking (Verheijck, van Ginneken et al. 1995; Zaza, Micheletti et al. 1997) and in atrial and ventricular myocytes, I_{Kr} is important in the plateau formation and repolarization of the cardiac action potential (Spinelli, Moubarak et al. 1993): during the plateau phase of the ventricular action potential, I_{Kr} only has a small amplitude which supports the formation of the plateau potential and at repolarization the transient *erg* outward current increases and repolarizes the action potential together with classical inward rectifier K⁺ channels (Fig. II.5) (Hancox, Witchel et al. 1998; Zhou, Gong et al. 1998). Thus,

a blockage or loss-of-function mutation of erg K^+ channels prolongs the cardiac action potential leading to a prolongation of the QT interval in the ECG (long QT-syndrome: LQT-2) which can induce early after-depolarizations causing heart arrhythmia and “torsade de pointes” leading to ventricular fibrillation and sudden death (Curran, Splawski et al. 1995).

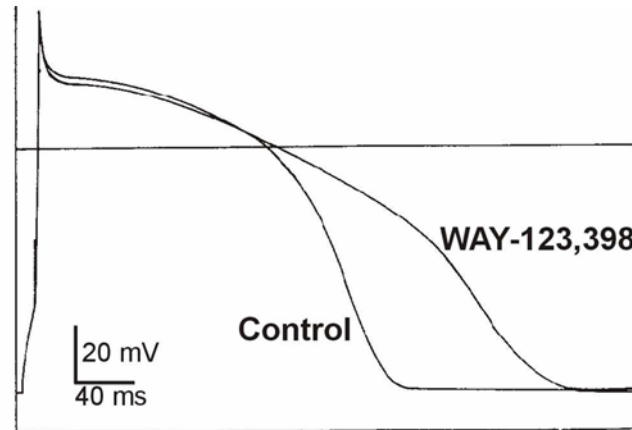


Fig. II.5: Physiological function of erg currents in cardiac myocytes. Recording of an action potential from a cat ventricular myocyte. Blocking of the erg currents by WAY-123.389 prolonged the action potential (Adapted from (Spinelli, Moubarak et al. 1993)).

II.5.1. Role of erg K^+ channels in the pituitary gland

Another system where erg channels were very intensively studied is the pituitary gland. The pituitary gland is a small endocrine gland part of the hypothalamic-pituitary-gonadal (HPG) axis and controls the hormonal regulation of many body functions. In mammals, the pituitary gland is composed of three lobes: anterior (adenohypophysis), intermediate and posterior (neurohypophysis) (Kelberman, Rizzoti et al. 2009). The activity of the anterior pituitary is controlled by releasing hormones from the hypothalamus and controls downstream organ by production of hormones (Hiller-Sturmhofel and Bartke 1998). The anterior pituitary contains five major hormone secreting cell types: somatotropes secrete growth hormone (GH), lactotropes secrete prolactin (PRL), corticotropes secrete adrenocorticotrophic hormone (ACTH), thyrotropes secrete thyroid stimulating hormone (TSH), and gonadotropes secrete follicle-stimulating hormone (LH) and/or luteinizing hormone (FSH) (Daughaday, Kapadia et al. 1985). According to their targets (ovary and testes, liver, bone, adrenal, thyroid and mammary gland) these hormones play important roles in the regulation of very important physiological processes such as stress, growth and reproduction. The posterior pituitary releases vasopressin (ADH) and oxytocin (OT) (Zhu, Gleiberman et al. 2007). Both are synthesized by peptidergic neurons in the supraoptic (SON) and paraventricular nuclei (PVN) of the hypothalamus (Hadley and Levine 2007). Vasopressin is involved in the water reabsorption in the kidneys, glycogenolysis in the liver, and vasoconstriction (Ball 2007).

Oxytocin stimulates smooth muscle contraction and is involved in parturition and milk ejection during nursing (Gainer and Wray 1994). The pituitary gland intermediate lobe contains melanotropes which produce melanocyte-stimulating hormone (MSH) (Evans, Manning et al. 1994) which stimulates the production and release of melanin in skin and hair (Slominski, Tobin et al. 2004).

Hormone secretion by lactotropes is regulated by changes in excitability of the membrane (reviewed by (Corrette, Bauer et al. 1995)). In these cells as well as in other pituitary tumor cell lines (GH₃/B₆: (Bauer, Meyerhof et al. 1990); GH₃: (Barros, Mieskes et al. 1993)) erg channels contribute to the maintenance of the resting membrane potential (Corrette, Bauer et al. 1995) and are inhibited by TRH. TRH induces a biphasic increase in the intracellular [Ca²⁺] ([Ca²⁺]_i) (Malgaroli, Vallar et al. 1987; Reid, Bauer et al. 1996): the first phase of the TRH response is characterized by release of Ca²⁺ from intracellular stores and the second phase has two components: the capacitive Ca²⁺ entry triggered by Ca²⁺ depletion of the intracellular stores and the influx of Ca²⁺ via the voltage-dependent Ca²⁺ channels. Depolarization of the membrane potential due to reduction of the erg current by the TRH-induced signal cascade contributes to the second phase. The physiological role of the erg channels in pituitary lactotropes is schematically shown in Fig. II.6.

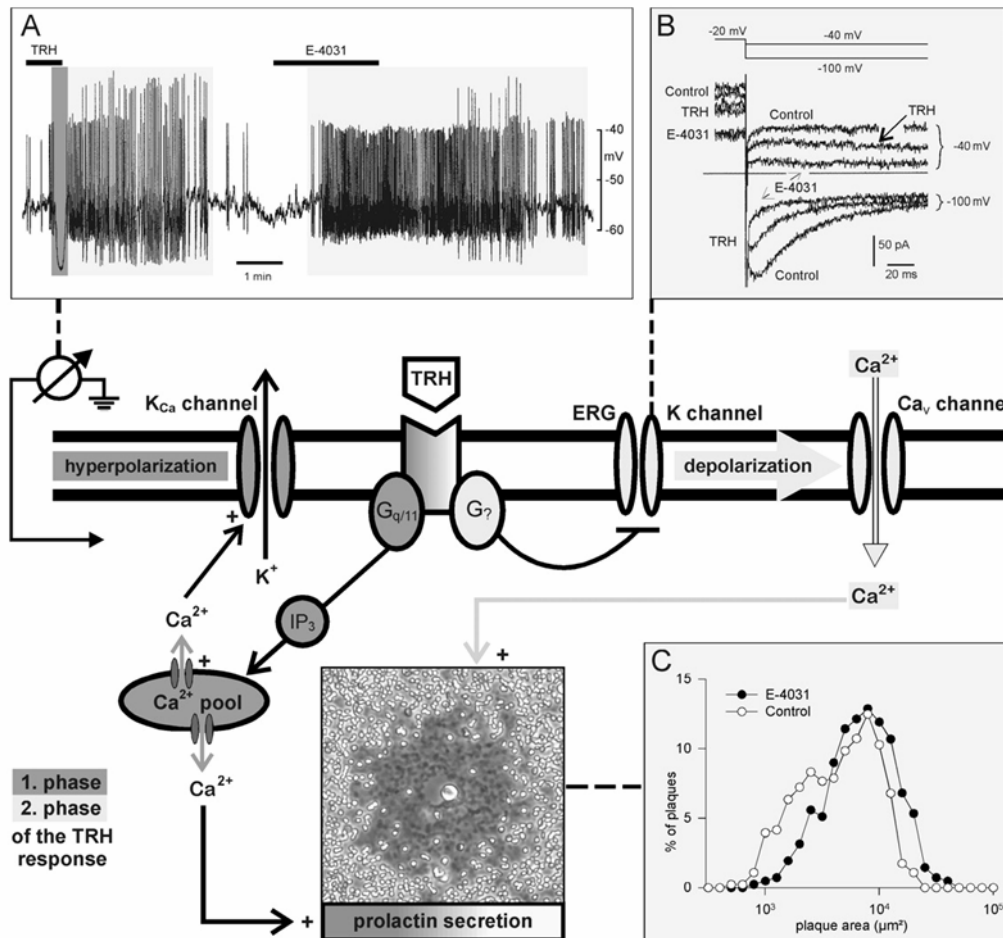


Fig. II.6: Diagram illustrating the effects of reduction of the erg current in prolactin secretion. A, Recording of the membrane potential of a GH₃/B₆ cell. Application of 500 nM TRH induced a biphasic electrical response consisting of a transient hyperpolarization and a subsequent increase in the frequency of action potentials. Application of 1 μM E-4031 induced an increase in the frequency of the action potentials imitating the second phase of the TRH response. B, erg current recorded in a GH₃/B₆ cell. TRH induced a reduction of the erg-mediated outward and inward currents, which are both completely blocked by 10 μM E-4031. C, Measurement of prolactin secretion from single lactotrophs with the reverse hemolytic plaque assay. Incubation with E-4031 induced a shift in the frequency distribution to larger plaque areas. IP₃, inositol 1,4,5-triphosphate; Ca_v, voltage-dependent Ca²⁺ channels (Adapted from (Schwarz and Bauer 1999)).

Unlike the other pituitary cells, gonadotropes secrete two hormones (LH and FSH) which are secreted from monohormonal (18% LH and 22% FSH) containing cells, as well as from multihormonal gonadotropes containing both LH and FSH (about 60% of the cells) (Childs 2006). LH and FSH have specific functions in males and female, for example LH stimulates ovaries to produce steroids in females and stimulates Leydig cells to produce testosterone in males; FSH stimulates ovaries to produce estradiol and progesterone in females and stimulates Sertoli cells to produce androgen-binding protein for spermatogenesis in males. Gonadotropin-releasing hormone (GnRH) binds to the GnRH receptor (GnRHR) expressed by gonadotropes and regulates the synthesis and secretion of LH and FSH (Clayton and Catt 1981). The GnRHR has 328 amino acids and is a member of the seven-transmembrane

G-protein coupled receptor family (Stojilkovic, Reinhart et al. 1994) and was first cloned from mouse (Reinhart, Mertz et al. 1992). It has a short N-terminal extracellular domain and no C-terminal intracellular tail, which is involved in rapid receptor desensitization and internalization (Sealfon, Weinstein et al. 1997). The mouse GnRHR is 97% homologous to the rat GnRHR, 89% to the human GnRHR, and 87% to the ovine GnRHR (Jeong and Kaiser 2006).

GnRH has multiple actions on gonadotropes and, as acute/short time exposure GnRH elicits secretion and induces changes in the membrane potential (Kukuljan, Stojilkovic et al. 1992; Stojilkovic, Kukuljan et al. 1992). The classical picture shows that GnRH stimulates membrane oscillations of a plateau-bursting type (Fig. II.7, A). Application of GnRH induces major changes in the electrical activity of gonadotropes which include an increase in the firing of action potentials followed by membrane potential oscillations with different frequencies depending on GnRH concentration. Each cycle of oscillations is initiated by a rapid hyperpolarization with slow depolarization which leads to firing of action potentials (Fig. II.7, B and C). In some cells action potentials trigger the release of Ca^{2+} from ryanodine-sensitive intracellular stores but not in the case of gonadotropes (Fig. II.7, D) where the influx of Ca^{2+} comes exclusively through voltage-dependent Ca^{2+} channels (VDCC) and they generate global Ca^{2+} oscillations in gonadotropes (Iida, Stojilkovic et al. 1991; Van Goor, Zivadinovic et al. 2001) (Fig. II.7, E and F).

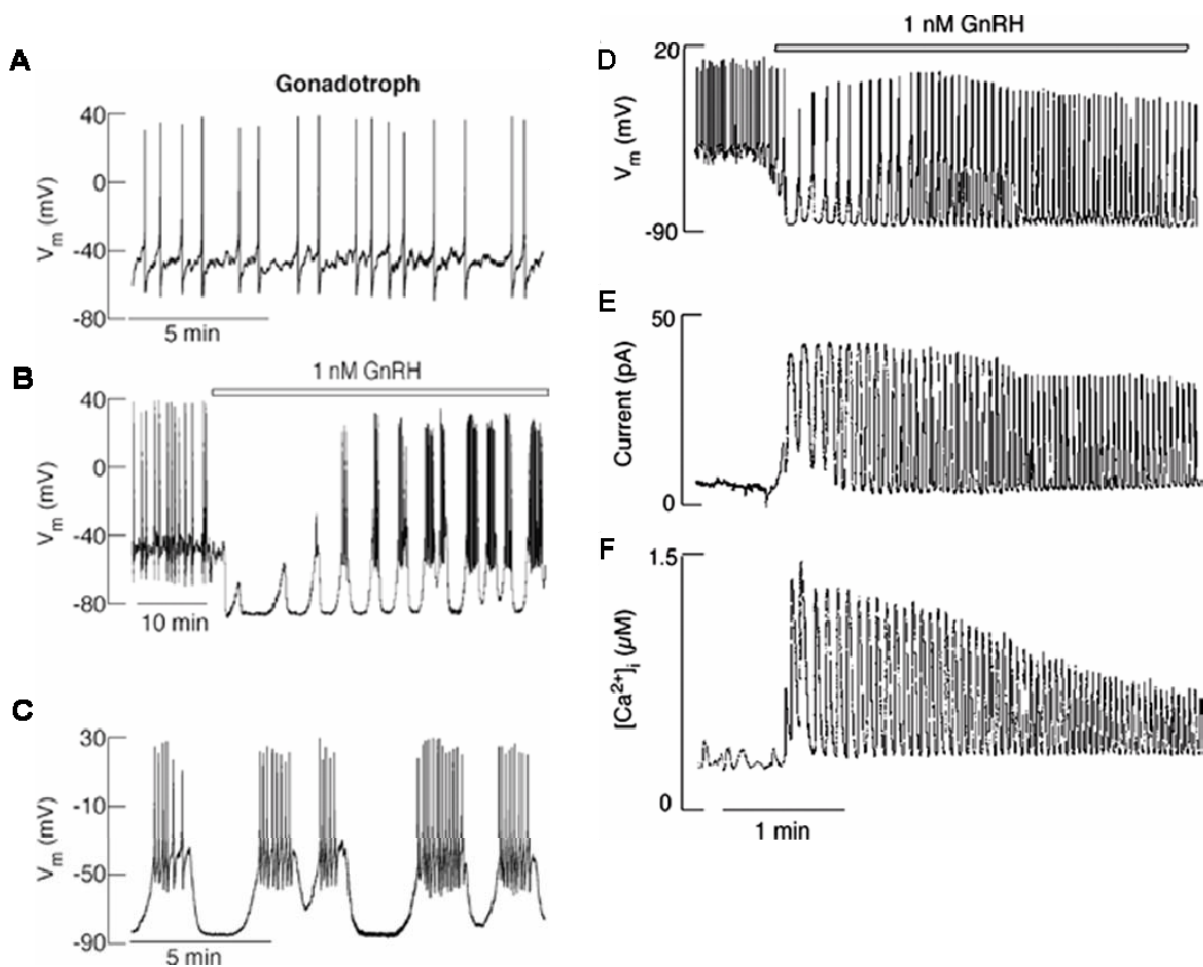


Fig. II.7: Gonadotropes membrane potential at rest, GnRH-induces electrical activity and Ca^{2+} signaling. A, Pattern of spontaneous action potentials in a gonadotrope cell. B, Pattern of membrane potential changes under GnRH stimulation. C, Same cell as in B at an enlarged time scale. Activation of gonadotropes by GnRH induces changes in the membrane potential (D) caused by changes in the membrane currents (E) which are associated with changes in the global $[Ca^{2+}]_i$ (Adapted from (Stojilkovic 2006)).

Differences in the expression level of different channels in the membrane could explain the different patterns of action potentials, the influx of Ca^{2+} through VDCC and hormone secretion. In order to know the mechanism that connects all these events culminating in LH and FSH secretion in the gonadotropes, it is very important to look for the ionic currents present in these cells and what role they play. Gonadotrope cells express a large number of plasma membrane channels including tetrodotoxin (TTX)-sensitive Na^+ channels, VDCC, transient and delayed rectifying K^+ channels and Ca^{2+} -sensitive K^+ channels (reviewed in (Stojilkovic 2005)).

II.6. Aim of the study

A new mouse model has been created (Wen, Schwarz et al. 2008) which allows the study of all gonadotropes from the whole population of pituitary cells by direct visualization among other pituitary cells. This mouse allows the specific characterization of mouse gonadotropes and the study of possible mechanisms underlying hormone secretion. Among other ion channels which have been reported also in gonadotropes of other species (ovine: (Heyward, Chen et al. 1995); rat: (Tse and Hille 1993)), additionally an erg channel has been found. The aim of this thesis was to study the electrophysiological properties of gonadotropes with special attention to erg K^+ currents. To study the role of this channel in the basic physiological mechanism underlying secretion in gonadotropes it is very important to investigate the biophysical characteristics of this channel, i.e. voltage-dependence, kinetics, influence of external K^+ concentration and temperature and modulation by GnRH.

III. Materials and methods

Experiments were performed on mouse gonadotropes from two transgenic mouse lines and wild-type C57BL/6J mice. Patch-clamp technique, Ca^{2+} imaging and ELISA technique were the three major techniques used for characterization and functional analysis of gonadotropes.

III.1. Mice

Animal care and experimental procedures were performed in accordance with the guidelines established by the animal welfare committee of the University of Hamburg. Mice were kept under standard light-dark cycle with food and water *ad libitum*.

One transgenic mouse line used in this study was GRIC/R26-YFP. Mice were generated by Ulrich Boehm and co-workers (Wen, Schwarz et al. 2008). They generated mice in which Cre recombinase was coexpressed with the *GnRHR* gene. Using gene targeting in embryonic stem cells the *GnRHR* gene was modified by inserting an internal ribosome entry site (IRES) sequence just after the coding sequence of the gene, followed by a Cre recombinase complementary DNA. Transcription of the mutant GnRHR allele yielded a bicistronic messenger RNA, from which the GnRHR and Cre recombinase were independently translated (Eggan, Baldwin et al. 2004). The altered stem cells were then used to generate GnRHR-IRES-Cre “knock-in” (GRIC^{neo+}) mice. To remove the neomycin resistance cassette, GRIC^{neo+} animals were bred to Flp recombinase deleter mice (Rodriguez, Buchholz et al. 2000) resulting in GRIC^{neo-} (GRIC) mice. To monitor Cre recombinase activity, GRIC mice were bred to ROSA26-YFP (R26-YFP) mice. This reporter strain carries a targeted insertion of *YFP* gene (yellow-fluorescent protein gene) in the ubiquitously expressed ROSA26 locus (Srinivas, Watanabe et al. 2001). Due to *loxP* flanked (floxed) strong transcriptional termination sequence the *R26-YFP* allele terminates transcription prematurely. The mice were crossed with Cre-expressing mice and Cre-mediated excision of the floxed termination sequence lead to constitutive YFP expression (Fig. III.1). In the double heterozygous GRIC/R26-YFP mice, the GnRHR cells express YFP from the recombined *R26-YFP* allele and can be identified by their fluorescence signal. All GRIC/R26-YFP mice used in this study were 11 to 31 weeks old males.

The other mouse line used in this study, GRIC/eR26- τ GFP was generated by Oliver Mai from Ulrich Boehm’s laboratory (Wen et al., submitted) because of too low YFP-expression in

GnRHR neurons in GRIC/R26-YFP mice. In the GRIC/eR26- τ GFP mouse line, the τ GFP-positive neurons could be easily detected in live brain sections without antibody labeling. Gonadotropes of these mice could also be easily detected. They used the same technique of gene targeting in embryonic stem cells to generate another Cre reporter mouse strain. This strain expresses a fusion of the microtubule-associated protein tau with GFP (green fluorescent protein) (Rodriguez, Feinstein et al. 1999) under control of β -actin promoter/CMV (cytomegalovirus) enhancer (CAGS) (Lobe, Koop et al. 1999) in the *ROSA26* locus after Cre-mediated excision of a stop sequence. The recombinant stem cells were then used to generate ROSA26-CAGS- τ GFP (eROSA26- τ GFP) mice. eROSA26- τ GFP mice were then bred to GRIC mice to specifically express τ GFP under control of the enhanced ROSA26 promoter in GnRHR neurons (Fig. III.1).

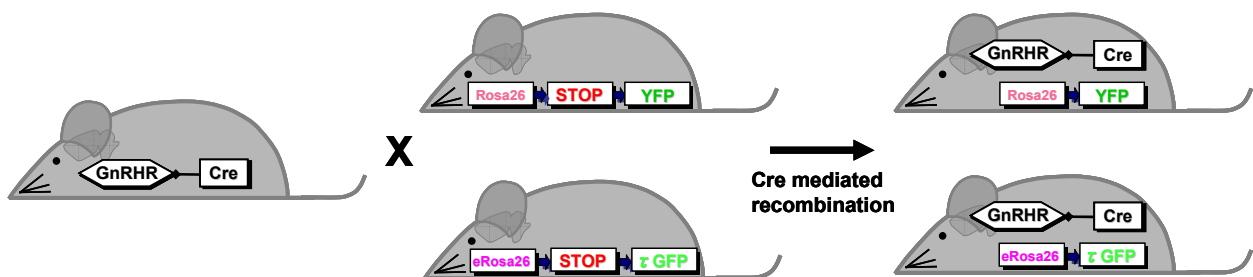


Fig. III.1: Cre recombinase mediated YFP and GFP expression in gonadotropes. Breeding strategy to activate YFP and GFP expression in GnRHR-expressing cells. Coexpression of Cre recombinase with GnRHR leads to excision of the floxed stop cassette which in turn activates ROSA26 driven transcription of YFP in GRIC/R26-YFP double knock-in mice and transcription of τ GFP under the enhanced ROSA26 promoter in eROSA26- τ GFP double knock-in mice (adapted from (Wen, Schwarz et al. 2008); Wen et al., submitted).

III.2. Gonadotrope cells

III.2.1. Primary cell culture

Mice were anesthetized with isoflurane (Abbot GmbH&Co. KG, Wiesbaden, Germany) and decapitated. Pituitaries were collected in cold (4°C) Earle's balanced salt solution (EBSS) (Invitrogen Corp., Paisley, UK), cut in 3 pieces and kept for digestion in papain solution (20 U/ml; Worthington Biochemical Corp., Lakewood, NJ; USA) for 30-45 min at 37°C in a humidified incubator with 5% CO₂. Dispersion was facilitated by aspiration and expulsion of the tissue pieces (trituration) every 15 min with a fire-polished glass Pasteur pipette. The cells were collected by centrifugation for 10 min at 1000 x g at room temperature (RT). The pellet

was washed three times with plating medium containing minimal essential medium (MEM, Invitrogen) + 0.6% glucose + 10% horse serum (Invitrogen). The pellet was then resuspended in 600 μ l plating medium using three different Pasteur pipettes with decreasing openings. The cell suspension was then plated on six coated 11 mm glass coverslips per pituitary (0.01% poly-L-lysine and 1 mg/l laminin in 0.1 M borate buffer) placed in 35 mm cell culture dishes (Nunc GmbH & Co. KG, Langselbold, Germany). For cells maintained for 24 h in culture, after plating they were fed with the same medium (plating medium). If the cells were kept in culture for more than one day, they were fed after plating with culture medium containing Neurobasal A medium (Invitrogen) + 1% Glutamax (100x, Invitrogen) + 0.1% sodium pyruvate (stock of 25 mg/ml in distilled water, Sigma) + 2% B27 (Invitrogen) freshly added in the day of culture. This dissociation method will be called “papain method” The cells were kept at 37° C in a humidified incubator with 5% CO₂ for 1-15 days.

In some electrophysiological and calcium imaging experiments, a modified protocol for preparing the cell culture was used: Pituitaries were transferred into Hank’s F10 dispersion medium (Sigma) supplemented with 10 mM D-glucose, 10 mM HEPES and 0.5 mg/ml BSA (pH adjusted to 7.3 with NaOH). Pituitary pieces were digested with collagenase type CLS II (Biochrom KG, Berlin, Germany; 678 U/ml in dispersion medium) for 30 min at 37°C. The tissue was gently triturated with a glass pipette, centrifuged for 15 min at 4°C, and resuspended in growth medium containing low-glucose DMEM (Life Technologies, Inc., Gaithersburg, MD) enriched with 10% fetal bovine serum (Biochrom KG; containing 11.39 pg/ml estradiol, 0.03 ng/ml progesterone and 0.02 ng/ml testosterone as reported by the supplier), 1.78 mM L-glutamine (Life Technologies), penicillin (100 U/ml), and streptomycin (1 mg/ml). Then the cells were plated on poly-L-lysine coated 11-mm glass coverslips placed in 35 mm cell culture dishes (Nunc GmbH & Co. KG) and fed with growth medium. This method will be called “collagenase method”.

There were no difference between these two protocols in the appearance of pituitary cells and percentage of successful experiments.

III.2.2. Acute pituitary slice

Pituitary slices were used for Ca²⁺-imaging experiments. GRIC/R26-YFP mice were anaesthetized with isoflurane and decapitated. The skull and the brain were rapidly removed and the pituitary was carefully dissected out and placed in ice-cold carbogenated artificial cerebrospinal fluid (ACSF) containing 124 mM NaCl, 25 mM NaHCO₃, 8 mM KCl, 1.25

mM NaH₂PO₄, 5 mM glucose, 0.8 mM MgCl₂. The whole gland was then embedded in 2% low-melting point (37°C) agarose in ACSF. The hardened agarose block was glued with cyanoacrylate (Ultra Gel, Henkel AG&Co., Wien, Austria) on the sample plate of the vibratome (Leica VT1200 S, Wetzlar, Germany) and covered with ice-cold ACSF. Pituitary gland was sectioned in 200 µm thick slices at 4°C. The freshly cut slices were transferred into an incubation beaker containing carbogenated ACSF with 1 mM CaCl₂ at 37°C for 30 min and used within six hours at RT.

III.3. Calcium imaging

III.3.1. Principle of the method

In this study the dual-wavelength ratiometric dye fura-2 (Fig. III.2, (Grynkiewicz, Poenie et al. 1985)) was used to monitor and measure global changes in the intracellular Ca²⁺ concentration ([Ca²⁺]_i). The polycarboxylate anion fura-2 cannot cross the lipid bilayer membrane. To load the cells with the dye, the acetoxymethyl (AM) ester form (fura-2AM) of the indicator was used to mask the negatively charged carboxyl groups. After entering the cell, AM esters of the indicator are cleaved by cytoplasmatic esterases trapping fura-2 inside the cell and the carboxyl groups are now able to bind Ca²⁺ and to trap the fluorescent indicator inside the cell (Kao 1994).

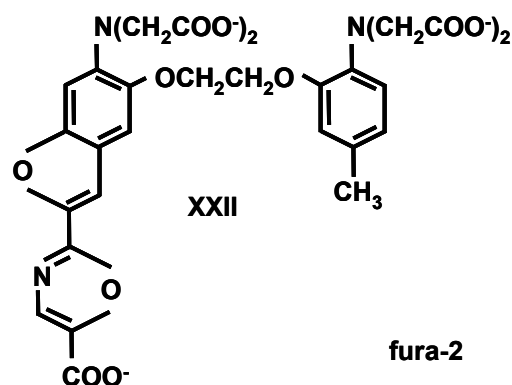


Fig. III.2: Chemical structure of fura-2 (Adapted from (Grynkiewicz, Poenie et al. 1985))

The Ca²⁺-free and Ca²⁺-bound forms of this dye have emission peaks at two different spectral excitation wavelengths. A Ca²⁺ increase causes an increase of emission intensity at 340 nm

but a decrease of the emission intensity at 380 nm excitation (Fig. III.3). Calculating the ratio between the emission intensities at these two excitation wavelengths minimizes artifacts unrelated to changes in $[Ca^{2+}]_i$ like bleaching.

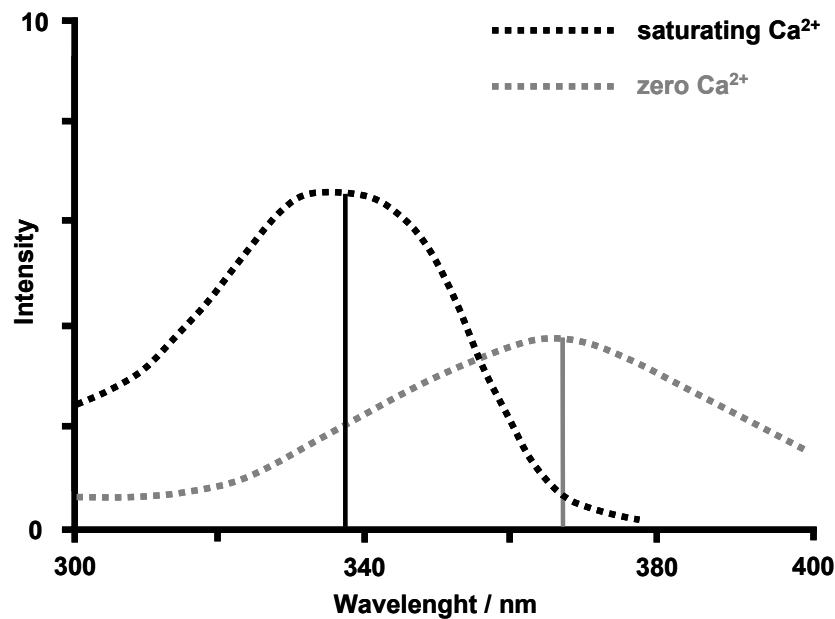


Fig. III.3: Excitation spectra of 1 μ M fura-2 (Adapted from (Grynkiewicz, Poenie et al. 1985)). Ordinate: emission intensity at 510 nm (arbitrary unit). X-axis: excitation wavelength.

III.3.2. Measurement of fura-2 fluorescence/experimental procedure

For Ca^{2+} -imaging experiments an area which had at least two YFP-positive cells was selected. Cultured cells were loaded with fura-2AM (Merck chemicals, Darmstadt, Germany) in the dark for 30-45 min at 37°C. Fura-2AM was dissolved in DMSO (stock 1 mM) with 5 μ M final concentration in 5 K^+ CC Ringer solution (see table III.1 for composition). Pituitary slices were loaded for 45 min at RT with 5 μ M fura-2AM in carbogenated ACSF. In order to elicit and monitor the fura-2 fluorescence, a polychromator V (TILL Photonics, Gräfelfing, Germany) and a Sensicam camera (PCO Imaging, Kelkheim, Germany) were used. Images were acquired every 260 or 500 ms with 10 ms exposure time using TILLVision software (TILL Photonics). Emission at 510 nm was measured with alternating excitations at 340/380 nm. The experiments were carried out at RT under a water-immersed objective of an Axioskop2 FS plus microscope (Carl Zeiss SMT, Göttingen, Germany). The solutions were bath perfused at 3 ml/min in approximately 1 ml volume. GnRH (Sigma L8008 LHRH; Sigma Aldrich, St. Louis, MO, USA) with 0.2% BSA, nifedipine (Sigma), or E-4031 (Eisai, Tokyo, Japan) were added to the Ringer solutions (see table III.1 composition of Ringer solutions).

III.3.3. Data analysis

Ratio images (340/380 nm) of matching frames of the two movies were calculated after background subtraction of the fluorescence in an area with no cells and no fura-2 loaded formations. The ratio fluorescence intensity is called F. The changes in F averaged from the cytoplasmic area of individual cells, were analyzed in Igor (WaveMetrics, Lake Oswego, OR). The plots were normalized by dividing F to the minimal fluorescence during the 10 s before application (F_0). To calculate changes in $[Ca^{2+}]_i$, the F/F_0 was divided by the average F/F_0 during 1 min before drug application. Significance was tested with paired or unpaired Student's *t* tests for single comparisons or one-way ANOVA for multiple comparisons.

III.4. Electrophysiology

III.4.1. Electrophysiological parameters

In electrophysiological measurements, currents can flow through capacitors, resistors, ion channels, amplifiers and other entities and always in a complete circuit. The most direct way of investigating ion channel function is to record the charge movement across the membrane. The movement of charge (*q*) in time (*t*) is defined as current (*I* measured in amperes (A))

$$I = \frac{q}{t}$$

The driving force needed to move the charge is voltage (*V*, measured in volts (V)). The ion channel represents the path for the current flow and the ease with which charge moves through the channel is resistance (*R*, measured in ohms (Ω)). The relationship between *V*, *I* and *R* is defined by Ohm's law:

$$V = IR \quad I = \frac{V}{R}$$

The resistance of a single channel or an ensemble of channels is represented by the reciprocal conductance (*G*, measured in siemens (S) = A/V). This parameter is a basic biophysical property of an ion channel, given that in most cases the opening of an ion channel is an "all-or-nothing" phenomenon. The conductance of an ion channel can be described as:

$$G = \frac{1}{R} \quad G = \frac{I}{V}$$

Ion channel current can be represented as a function of membrane voltage (I/V curve). The slope of this curve represents the ion channel conductance, and if the I/V curve is not linear, this result suggests that channel conductance changes with changes in membrane potential (i.e., it is voltage-dependent).

Capacitance (C, measured in farads (F)) is a measure of the charge separated by the cell membrane.

$$C = \frac{q}{V}$$

The capacitive charge is uniformly distributed over the membrane so that it can be used as a reliable index of cell size. Current is typically calculated as current density (normalized to cell capacitance) to control for differences in cell size and is given as pA/pF.

These parameters define and characterize each excitable cell. A simple schematic view of how these parameters contribute to maintenance of the membrane potential is presented in Fig. III.4.

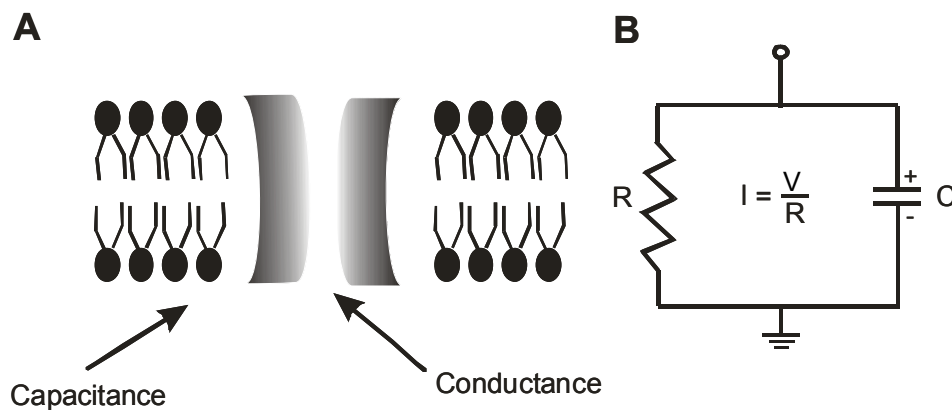


Fig. III.4: Membrane behavior compared with an electrical circuit. A, The lipid bilayer of biological membranes contains many conducting channels and separates internal and external solutions by a thin insulating layer where the membrane is a capacitor and the channel is a conductor. B, In the electrical circuit, the membrane is represented as a resistor of value R in parallel with capacitance C of the membrane conductor. The voltage across the capacitor is measured from the two terminals (Adapted from (Hille 2001))

III.4.2. Voltage clamp and patch clamp

The voltage clamp allows the membrane voltage to be manipulated independently of the ion currents and this enables the study of membrane channels. Kenneth Cole and George Marmont introduced the concept of voltage clamp in squid axon (Marmont 1949; Cole and

Moore 1960). They discovered that the cell's membrane potential could be maintained at a certain value by impaling the cell with two electrodes, the voltage-recording electrode and the current-delivering electrode, and connecting a feedback circuit in which a membrane potential amplifier measures the membrane voltage and sends output to an feedback amplifier. The feedback amplifier, which is an operational amplifier, subtracts the membrane voltage from the command voltage (e.g. desired potential given by the pulse protocol), received from the signal generator, and amplifies the signal and sends it to the axon via the current-delivering electrode (Fig. III.5). This current is equal and opposite to the spontaneous membrane ion currents at any given voltage.

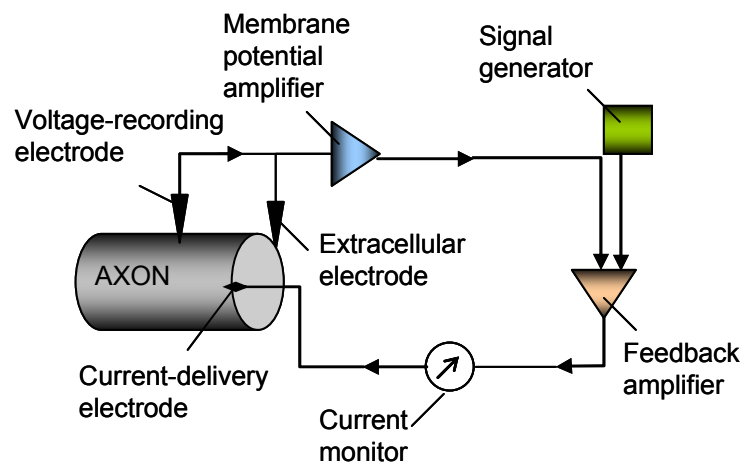


Fig. III.5: Voltage clamp negative feedback circuit. The transmembrane voltage is recorded through a voltage-recording electrode, relative to the ground, and a current-delivering electrode passes current into the cell. The electrodes are connected to an amplifier which measures the membrane potential and feeds the signal into a feedback amplifier. The feedback amplifier gets the input from the signal generator that determines the command potential, and it subtracts the membrane potential from the command potential. This amplifier magnifies any difference and sends an output to the current-delivering electrode. The clamp circuit produces a current equal and opposite to the membrane ion current

With this method it is possible to investigate the voltage dependence of particular ion channels. Contrary to voltage clamp, in the current-clamp mode the membrane potential is free to vary and the amplifier records the voltage generated by the cell membrane. This mode is useful when investigating the behavior of the cell membrane in response to substances that inhibit or stimulate ion channels from the membrane.

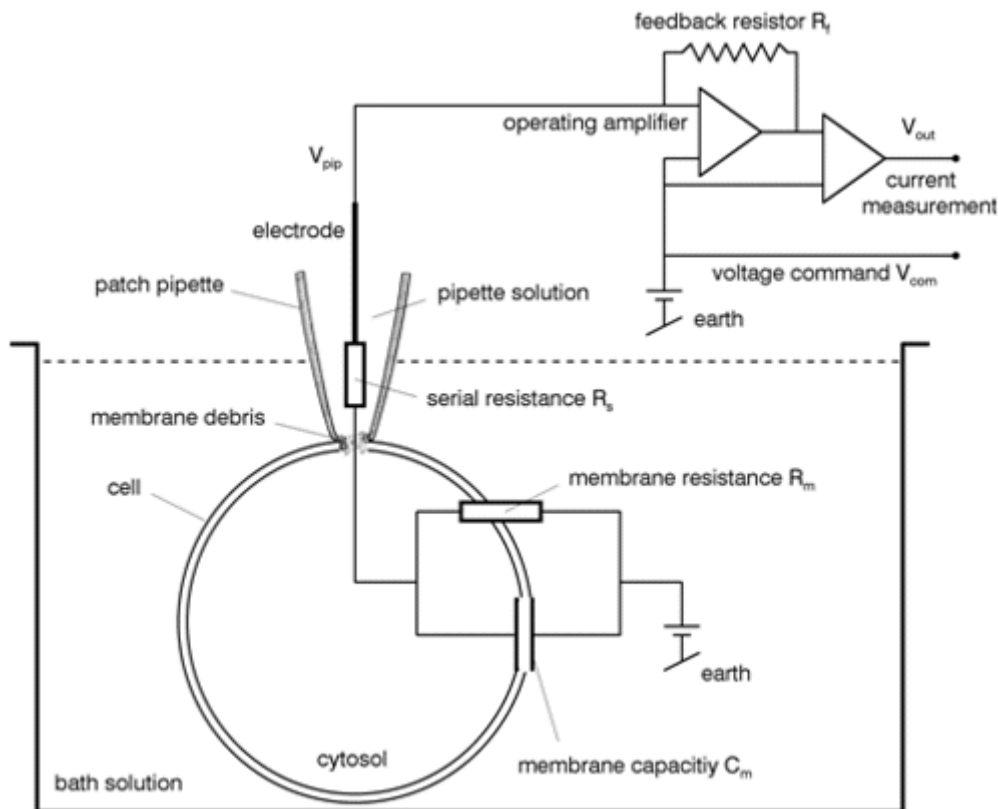


Fig. III.6: Simplified diagram of the patch-clamp amplifier and substitute circuit of the whole-cell configuration. R_f represents the feed-back resistance, V_{com} is the command voltage, V_{pip} is the pipette potential, V_{out} is the output voltage proportional to the current.

III.4.3. Patch-clamp recording configurations

The patch-clamp technique, first described by Neher and Sakmann in 1980's (Hamill, Marty et al. 1981; Neher and Sakmann 1992), represents a particular voltage-clamp procedure. Depending on which configuration is used, the electrical activity of a single ion channel, or the ensemble activity of a large number of channels within a small patch of membrane, or the activity of all channels within a cell can be measured. All these different configurations involve the initial formation of a high resistance seal between the tip of the recording pipette and the cell membrane. The **cell-attached configuration** is obtained by lowering the tip of the pipette onto the cell followed by the application of negative pressure to the recording pipette to create the gigaseal (in the order of $10^9\Omega$, gigaohms). This configuration allows measurement of single ion channels located within the patch of membrane in the pipette tip. By quickly withdrawing the pipette from the cell after attaining the cell-attached configuration while maintaining the gigaseal between the patch of membrane and the pipette, one can obtain the **inside-out configuration**. In this configuration, the internal side of the membrane is in contact with the bath solution. The inside-out patch is useful when studying the effects of manipulating the internal environment on single ion channel function. The

whole-cell configuration was obtained by applying negative pressure and/or high voltage pulse to the recording pipette after attaining the cell-attached configuration. The whole-cell configuration allows the study of the ensemble response of all ion channels within the cell's membrane. One disadvantage of this configuration is that intracellular components can diffuse out of the cell into the patch pipette, with significant effects on ion channel function (Strauss, Herbrink et al. 2001). Especially when studying signaling pathways leading to ion channel modulation a variation of the whole-cell patch-clamp configuration, the **perforated-patch configuration**, is preferred. This configuration is achieved by using a patch pipette that contain e.g. nystatin, a pore forming compound (ionophore) that allows the passage of monovalent cations while essentially blocking the diffusional transport of polyvalent ions, second-messenger substances, and other regulatory cytoplasmic substances (Lippiat 2008). After attaining the whole-cell configuration one can slowly withdraw the recording pipette and obtain a bleb of membrane separated from the cell which can form a patch on the tip of the pipette. This represents the **outside-out patch configuration** in which the extracellular membrane is in contact with the bath solution. This configuration is useful for studying the effects of different compounds applied to the external membrane on single ion channel function. Of the various configurations, the whole-cell and perforated patch-clamp configuration were used in this study (Fig. III.7).

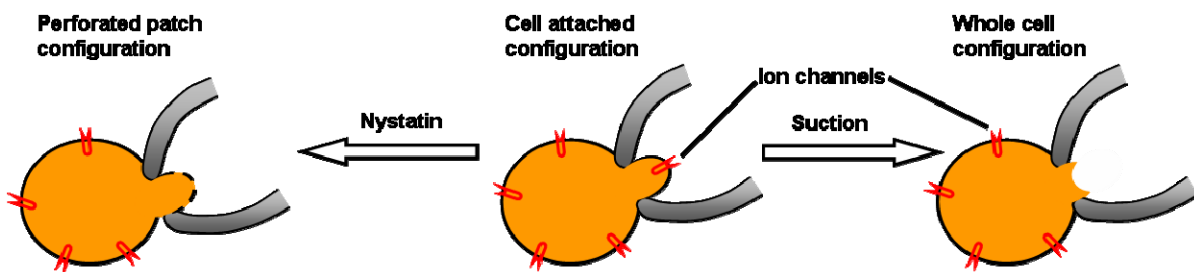


Fig. III.7: Schematic diagram of various patch-clamp recording configurations. Initially, a high resistance gigaseal is formed by gentle suction between the tip of the recording pipette and the cell membrane, called cell-attached configuration. Then, the whole-cell configuration is created by either rupturing the cell membrane patch with suction or the perforated-patch whole-cell configuration is formed by the addition of nystatin in the pipette solution

III.4.4. Equipment and experimental setup

The electrophysiological experiments were done by using a conventional patch-clamp setup. The glass coverslip coated with cells was placed in a home-made recording-bath chamber with a small volume of Ringer solution, under an inverted light microscope (Axiovert 405M, Carl Zeiss MicroImaging GmbH, Hamburg, Germany). The YFP- and GFP-positive cells were visualized with a lamp exciting fluorescence (FluoArc, Zeiss). The patch pipette with the

internal recording electrode and the reference electrode were connected to the headstage, which was mounted on a micromanipulator (Patchman, Eppendorf AG, Hamburg, Germany) used to navigate the recording electrode. The headstage's role was to record the input from the recording electrode and reference electrode (placed in the external bath) and to interface with the amplifier for data acquisition. The bath chamber was continuously washed with Ringer solution using a perfusion system composed of three parts: one peristaltic pump (Minipuls 3, Gilson Inc., Middleton, WI, USA), an electromechanical-valve controller (ValveBank8.2, AutoMate Scientific Inc., Berkeley, CA, USA) and a home-made 8-channel manifold with the tip of the perfusion in close vicinity of the cell. The recording-bath chamber together with the microscope, micromanipulator, and headstage were placed on an air table (TMC, Technical Manufacturing Corporation, Peabody, MA, USA) with pressurized cylinders to isolate these components from vibrations, and placed within a Faraday cage. The cage was electrically grounded to shield the setup from ambient electrical noise. The acquired signal from the headstage was passed to a patch-clamp amplifier (EPC-9, HEKA Elektronik, Dr Schulze GmbH, Lambrecht/Pfalz, Germany), which controlled the membrane voltage (voltage clamp) or current (current clamp), filtered the input signal, compensated the capacitance, and generated square waves for the stimulation protocols. The amplifier interfaced with a computer for data acquisition and analysis. To control the temperature of the external solution in some experiments a temperature controller system was used consisting of a WK 14 water bath (Colora, Lörrach, Germany) connected to a home-made recording-chamber holder with tubes isolated against temperature equalization. The tempered water from the water bath was continuously circulating and ensuring a constant temperature around the cells. To achieve "cold" (20°C) temperature around the cells, the water bath temperature was maintained at 11°C and the perfusion solutions were kept on ice. For "hot" (30°C) experiments the water bath was kept at 46°C with the perfusion solutions maintained at RT. The actual temperature around the cells was continuously measured with a thermocouple element.

III.4.5. Electrodes

Recording patch pipettes were capillaries made of borosilicate glass (GC150F-10, Harvard Apparatus Ltd., UK) which were pulled and polished with an electrode puller (Model P-97, Sutter Instrument, Novato, CA, USA, or with a DMZ-Universal Puller, Zeitz-Instruments Vertriebs GmbH, Martinsried, Germany). The pipette resistance was between 2 – 4 MΩ when filled with intracellular solution. Before each experiment, the pipettes coated with a special

silicone solution in heptane that readily forms a covalent, microscopically thin water-repellant film on glass (Sigmacote, Sigma) in order to increase the contact surface between pipette and cell membrane. Because voltage drops proportionally to the series resistances in an electrical circuit, the pipette resistance should ideally be at least two orders of magnitude the cell membrane's resistance after achieving the whole-cell condition. Therefore, the pipette series resistance after achieving the whole-cell condition should ideally be below 10 M Ω . Part of the pipette series resistance can be automatically compensated for by the patch-clamp amplifier by increasing the command voltage. The reference electrode consisted of a silver wire with an AgCl pellet which insures a low resistance.

III.4.6. Solutions

To optimize conditions for identification and characterization of different ion currents, customized extracellular and intracellular solutions have been used. The solutions are listed in tables III.1 (erg currents) and III.2 (sodium currents).

GnRH and nystatin stock solutions (6 mg/100 ml) were dissolved in DMSO and kept at -20°C. All the other chemicals were dissolved in water. Except were indicated, all chemicals were purchased from Sigma-Aldrich. The solutions were bath perfused at 3 ml/min in approximately 1 ml volume.

III. Materials and methods

Table III.1: Ionic composition of different extracellular (Ringer) solutions and intracellular solution used for recording of the erg currents

Solution name	Substance concentration in mM						
	CaCl ₂	MgCl ₂	NaCl	KCl	EGTA	HEPES	glucose
3 K ⁺ CC Ringer	1	0.8	145	3	-	10	5
5 K ⁺ CC Ringer	1	0.8	143	5	-	10	5
8 K ⁺ CC Ringer	1	0.8	140	8	-	10	5
5 K ⁺ VC Ringer	-	-	135	5	2.5	10	5
40 K ⁺ VC Ringer	1	4	100	40	2.5	10	5
140 K ⁺ VC Ringer	1	4	0	140	2.5	10	5
Intracellular	1	2	-	140	2.5	10	-

The pH was adjusted to 7.3 with 1 N NaOH for the Ringer solutions and with 1 M KOH for intracellular solution; CC = current-clamp, VC = voltage-clamp.

Table III.2: Ionic composition of extra- and intracellular solutions used for recording sodium currents.

Solution name	Substance concentration in mM										
	NaCl	KCl	MgCl ₂	CaCl ₂	CsCl	TEA-Cl	4-AP	EGTA	MgATP	HEPES	Glucose
Extracellular solution	135	5	4	1	-	10	5	-	-	10	5
Intracellular solution	5	-	2	-	130	-	-	1	2	10	-

The pH was adjusted to 7.3 with 1 M NaOH for the extracellular solution and with 1 M CsOH for intracellular solution.

III.4.7. Experimental procedure

Pituitary cells grown on glass coverslips were taken out from the incubator; the coverslip was broken into 5-6 smaller pieces, washed once with 5 K⁺ VC Ringer and placed in the bath chamber. Gonadotropes were identified by their bright fluorescence using a 500- to 520-nm excitation filter set (Filter set 46, Zeiss). After selection of a particular cell under the YFP filter, the experiment was continued in the bright-field mode of the microscope. For electrophysiological experiments only single cells were chosen. After cell-attached configuration was obtained, fast current transients due to the capacitance between the pipette and the bath solution were compensated using the fast compensation adjustment of the amplifier. After whole-cell configuration was obtained, slow current transients due to the cell membrane capacitance were compensated using the slow capacitance adjustment at the amplifier and subsequently the series resistance (R_s) of the small pipette tip was compensated by 70%-80%. The holding potential was adjusted to the voltage protocol that was applied. Before switching to current-clamp mode, the holding potential was adjusted so that the net current flow was close to zero.

For stimulation and data acquisition Pulse 8.65 software (HEKA Elektronik, Dr Schulze GmbH, Lambrecht/Pfalz, Germany) in combination with an EPC-9 patch-clamp amplifier (HEKA) were used. Data were low-pass filtered at 3 kHz. The sampling rate varied depending on the current that was recorded and recording mode (voltage or current clamp) from 10 kHz for Na⁺ currents to 1 kHz for current-clamp data.

III.4.8. Data analysis

Data were analyzed with PulseFit (HEKA), Igor (WaveMetrics) and Excel (Microsoft Corp., Redmond, WA) and presented as mean \pm SEM. The data shown have not been corrected for the liquid junction potential (< 4 mV). The current-clamp experiments were performed in perforated-patch configuration and a Donnan potential was present. The Gibbs-Donnan effect arises when charged molecules do not distribute evenly by diffusion on both sides of the membrane, creating an electric field that influences the movement of charged molecules. The exact value of the Donnan potential is uncertain and could amount to about 10 mV. Because liquid junction potential and Donnan potential are additive, in the current clamp experiments, the membrane potential could be 14 mV more negative than the pipette potential. In addition, in the perforated-patch configuration, the hypertonicity of the cells should induce a cell swelling. However, during the course of the experiments, which could last up to 30 min, cell

swelling of gonadotropes was not observed, similar to the observations in lacrimal gland cells (Horn and Marty 1988).

Sodium currents

To measure sodium currents, gonadotropes were whole-cell patch-clamped with the solutions given in table III.2. Voltage activation and inactivation protocols described in Fig. IV.5 and Fig. IV.6, were applied. For analysis of Na⁺ current activation, the leakage current defined as the current measured at membrane potentials between -120 and -70 mV was extrapolated linearly and subtracted from the total current.

The conductance of the sodium current was calculated with the equation:

$$G_{Na} = \frac{I_{Na}}{E_m - E_{Na}} \quad (1)$$

With G_{Na} = Na⁺ conductance, I_{Na} = peak Na⁺ current, E_m = membrane potential, E_{Na} = Na⁺ current reversal potential calculated from the Nernst equation for equilibrium potentials.

The current-voltage curve of inactivation was normalized to the maximum current and then fitted with a Boltzmann equation:

$$\frac{I}{I_{max}} = \frac{1}{1 + e^{(V_{1/2} - V_m)^k}} \quad (2)$$

With I = current measured at variable membrane potentials, I_{max} = maximum current, $V_{1/2}$ = membrane potential at which I is 50% of the I_{max} , k = slope factor of the sigmoid fit.

Potassium erg currents

The erg currents were elicited by different voltage protocols in a high extracellular potassium ($[K^+]_e = 40$ mM) and isolated from other currents as difference between currents before and after selective pharmacological block by 1 μ M E-4031. At negative holding potentials erg currents are fully deactivated. The maximal tail current amplitudes recorded at -100 mV were plotted against variable pre-pulse potentials and fitted by a Boltzmann equation (2). In the case of the erg currents, I = tail current recorded at -100 mV after pre-pulse at variable membrane potentials, I_{max} = maximum current generated by Igor best sigmoid fit to the data, $V_{1/2}$ = voltage at which 50 % of the channels are activated, k = slope factor showing the inflection potential of activation. To determine the time constants of erg current activation, the envelope of tail pulse protocol was recorded.

To analyze the voltage dependence and time constants of deactivation and recovery from inactivation, erg currents were elicited with an “availability” protocol (Fig. IV.9).. Time constants of recovery from inactivation (τ_{rec}) and slow and fast deactivation (τ_{slow} , τ_{fast}) were determined by fitting the E-4031-sensitive currents elicited by the test potentials from -120 mV to -70 mV (Schledermann, Wulfsen et al. 2001) with the sum of three exponential functions. At 34°C the time course of current recovery from inactivation was too fast at potentials negative of -90 mV to be distinguished from capacitative and instantaneous currents, so only the decaying phase of tail current was fitted with a single exponential function (Vandenberg, Varghese et al. 2006).

The spontaneous resting membrane potential in different K⁺ CC solutions (table III.1) and in response to E-4031 and GnRH in the current-clamp configuration was measured during one minute before treatment and during one minute to three minutes after treatment. When the cells were clamped at voltages close to their normal resting potential, the net changes of the holding current in time in response to E-4031 and GnRH were recorded.

III.5. ELISA

III.5.1. Technique principle

Enzyme-linked immunosorbent assay (ELISA) also known as enzyme immunoassay (EIA) is a biochemical technique used to detect and quantify specific antigen-eliciting molecules involved in biological processes (Leng, McElhaney et al. 2008). This technique can be used on most of the biological samples, such as plasma, serum, urine and cell extracts (Rauer and Conrad 2001). The principle of the technique uses a polyclonal antibody attached to solid phase (microtiter wells) immobilization and an antibody in the antibody-enzyme conjugate solution (Fig. III.8). The sample was added to the plate and was allowed to react simultaneously with two antibodies resulting in antigen molecules being sandwiched between the solid phase and enzyme-linked antibodies. After some time, the wells were washed to remove the unbound labelled antibodies and 3,3',5,5'-tetramethylbenzidine (TMB) solution was added resulting in the development of a blue colour. The reaction was stopped by addition of HCl resulting in yellow colour compound. The absorbance was measured spectrophotometrically at 450 nm. The colour intensity was proportional to the amount of bound enzyme and was directly related to the amount of unlabeled product in the sample.

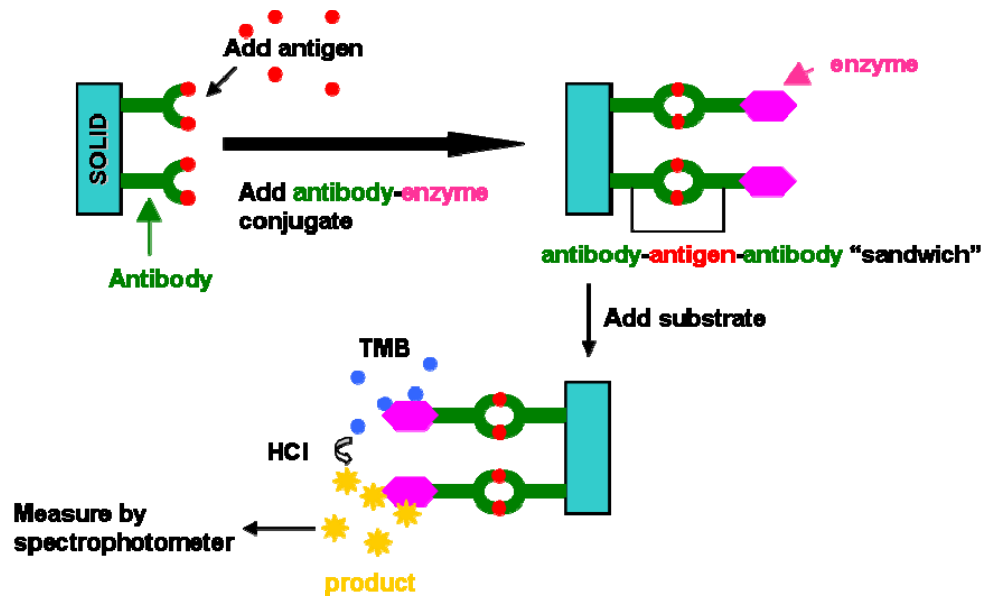


Fig. III.8: Sandwich ELISA technique steps. The well plate was prepared with a known quantity of capture antibody and the nonspecific binding sites were blocked. The antigen-containing sample was added to the plate together with the enzyme linked antibodies. The sample was incubated with the antibodies for a while to allow a specific binding. Unbound antibody-enzyme conjugates were washed away. A specific chemical (3,3',5,5'-tetramethylbenzidine, TMB) which was converted to a coloured solution was added. The colour reaction was stopped by HCl. The absorbency of the plate wells was measured to determine the presence and quantity of antigen.

III.5.2. Media and cell culture preparation

Pituitary cells pooled from two to four pituitary glands were prepared using the papain dissociation method and media of cell culturing (III.2, first paragraph). 280 μl to 350 μl of plating medium per pituitary were used for resuspension of the pellet. 70 μl of cell suspension was plated into each coated well of 96-well plates with round bottom instead of glass coverslips (0.01% poly-L-lysine and 1mg/l laminin in 0.1 M borate buffer). After 1.5 h of plating, 100 μl of plating medium was added to each well. Cells from one pituitary gland were distributed to 5 wells. The *control medium* contained: MEM (Invitrogen) and 1 mg/ml BSA. The compounds added to the control medium were: \blacklozenge E-4031: 1 μM ; \blacklozenge GnRH: 0.01 nM, 0.1 nM, 1 nM or 10 nM; \blacklozenge E-4031 1 μM + GnRH 0.1 nM.

III.5.3. Stimulation protocol

Experiments were performed after 24 h in culture. Very carefully the medium was removed and the cells were washed twice with 100 μl control medium. Starting at time zero, the cells were incubated in 100 μl control medium. Every 30 min, an amount of 90 μl of the medium were carefully collected, stored at -80°C , and replaced by fresh medium. This procedure was repeated four times (for 120 min) in order for the gonadotrope cells to reach a low constant

basal secretion level (Turgeon and Waring 1990). At time point 120 min, four different treatments were applied: control, E-4031, GnRH, E-4031+GnRH. After 30 min, 90 μ l of the medium was collected and, in the wells treated with E-4031, a subsequent addition of E-4031+GnRH followed. For the dose-response curve, the same stimulation protocol was performed, only the treatments were changed. At time point 120 min, 0.01 nM, 0.1 nM, 1 nM and 10 nM GnRH were applied to four different wells. Like for the different treatments protocol, all concentrations were tested on pituitary cells coming from the same mouse.

III.5.4. ELISA procedure

Luteinizing hormone (LH) concentration was determined using a rodent LH test kit (Endocrine Technologies Inc., Newark, CA). The test kit was used following manufacturer's instructions with some modifications:

- The standard calibration curve was determined for each ELISA measurement using dilutions from 0 – 5 ng/ml of provided 50 ng/ml standard solution with dilution solution.
- The incubation time with the enzyme was increased by 30 min and the incubation was performed on an orbital shaker (IKA Labor Technik, IKA Werke GmbH&Co. KG, Staufen, Germany) at 400 motions/min at 37°C.
- The five washing steps were performed on the shaker at 250 motions/min.
- TMB solution (3,3',5,5' – tetramethylbenzidine (TMB) plus hydrogen peroxide) incubation was done in the dark for 20 min at RT while shaking (250 motions/min).

Within half an hour after developing of the yellow color, due to the reaction with HCl, the microtiter wells were read at the spectrophotometer (μ Quant, Bio-Tek Instruments Inc., Winooski, VT) and exported as Excel file.

III.5.5. Data analysis

Data were analyzed with Excel and presented as mean \pm SEM. For each well the LH concentration was measured before and during treatment. Because of high variability in basal LH concentration due to variations in the number of gonadotropes and their secretion status in each well, the LH concentration during treatment was divided by the control value of each individual well. Differences between multiple groups were determined by a multivariate analysis of variance (MANOVA) and Bonferroni *post hoc* test.

IV. Results

The goal of this thesis was to characterize the biophysical properties and assess the physiological role of erg currents in gonadotropes. Living gonadotropes could be easily identified in transgenic GRIC/R26-YFP and GRIC/eR26- τ GFP mice, which were generated by the lab of Ulrich Boehm and first described in collaboration with our lab in Wen et al., 2008. The first description of erg currents by our lab was recently published in Hirdes et al., 2010.

IV.1. Physiological characterization of genetically labeled mouse gonadotropes

In order to confirm that the genetically altered gonadotropes are not different to native cells, several physiological parameters were measured and are described in the following section.

IV.1.1. Fluorescence and immunofluorescence

Pituitary slices prepared from GRIC/R26-YFP mice contained brightly fluorescent cells in the anterior pituitary, but no fluorescent signal was observed in the posterior part (data not shown), consistent with the distribution of gonadotropes cells in mouse pituitary (Baker and Gross 1978). Fluorescent cells were found with a frequency of 15.4%. Analysis of fixed pituitary sections from GRIC/R26-YFP mice using antibodies against LH and FSH (Fig. IV.1) proved that 99.9% of gonadotropin-containing cells were co-labeled by YFP fluorescence (4535 cells out of 4540 cells analyzed on 10 pituitary sections derived from three mice), demonstrating a faithful activation of the *ROSA26-YFP* reporter gene in gonadotropes (Wen, Schwarz et al. 2008). YFP-fluorescence without immunofluorescent LH/FSH signal was observed in 1.8% of cells (83 of 4623 cells analyzed in 10 pituitary sections derived from three mice: (Wen, Schwarz et al. 2008)).

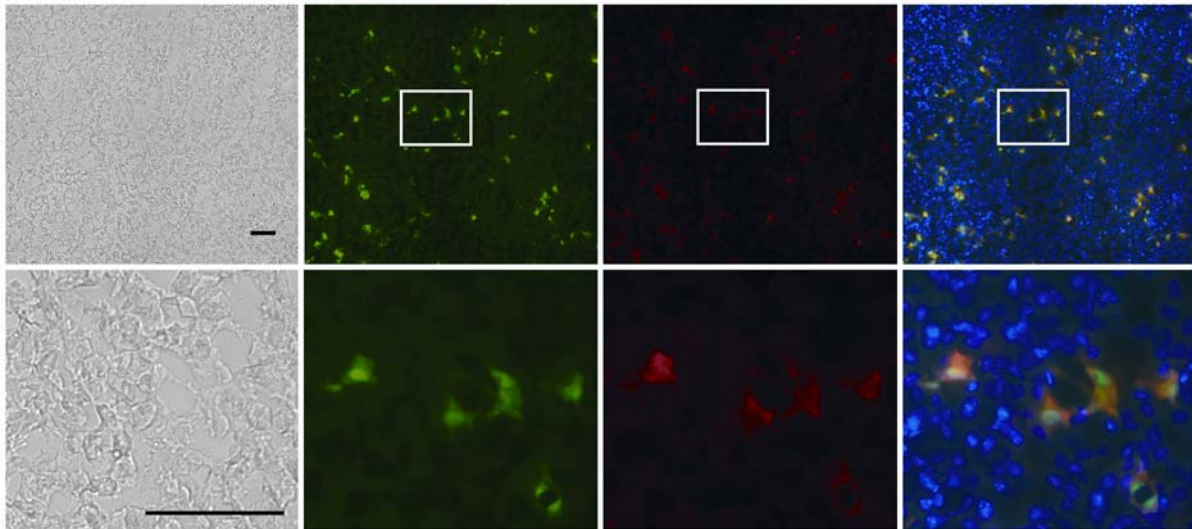


Fig. IV.1: YFP expression in gonadotropes. Immunofluorescence images of pituitary sections from GR1C/R26-YFP mice using antibodies against LH and FSH. All gonadotropin-containing cells (red) display YFP fluorescence (green). Corresponding bright-field images are shown on the left. The merged images (right) show nuclei counterstained with 4',6 - diamidino - 2 - phenylindole (blue). Scale bars, 50 μm (adapted from (Wen, Schwarz et al. 2008)).

IV.1.2. The membrane potential was changed by GnRH

The resting membrane potential of gonadotropes was recorded in current-clamp mode of perforated-patch clamp configuration with the 5K^+ CC Ringer solution and intracellular solution described in Table III.1. The resting membrane potential varied between -13 and -75 mV with a mean of -52 ± 3 mV ($n = 28$). Due to the Donnan potential and the liquid junction potential, the exact value of the resting membrane potential is more negative (see Materials and Methods). The spontaneous electrophysiological behavior of gonadotropes varied. There were spontaneously active cells ($n = 6$, Fig. IV.2, A) exhibiting action potentials with frequencies ranging from 0.3 to 1.2 Hz with a mean of 0.7 ± 0.1 Hz. The amplitudes of action potentials varied from 53 and 93 mV with a mean of 72 ± 7 mV. The action potential overshoot was between 3 and 16 mV with a mean of 12 ± 2 mV. The action potential width at -20 mV was 5.4 ± 0.9 ms. The majority of gonadotropes were silent at rest ($n = 22$).

The resting potential of gonadotropes was measured in different $[\text{K}^+]_e$. Despite the concomitant change of the reversal potential for K^+ , the resting potential remained at about -50 mV in all different $[\text{K}^+]_e$ solutions: in 3K^+ CC Ringer it was -49 ± 2 mV ($n = 11$), in 5K^+ CC Ringer it was -48 ± 3 mV ($n = 11$) and in 8K^+ CC Ringer it was -53 ± 2 mV ($n = 17$) (Fig. IV.2, B).

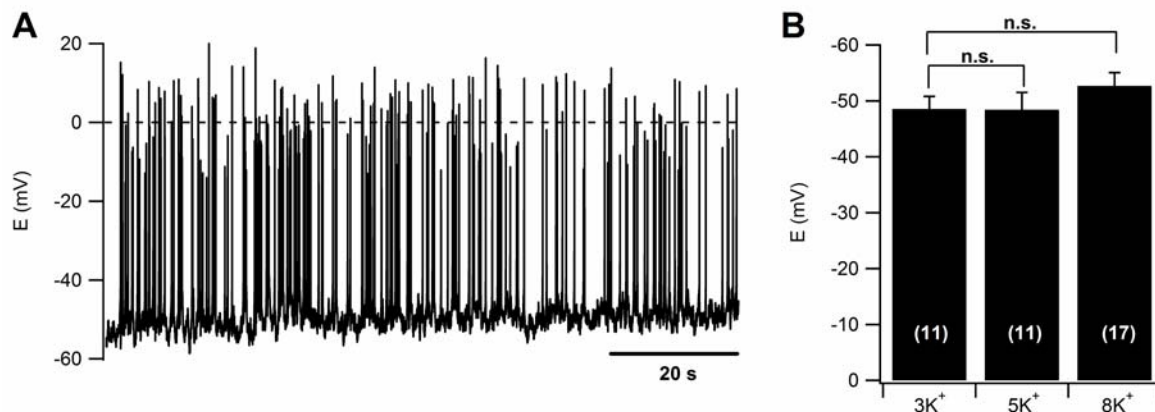


Fig. IV.2: Recording of resting membrane potential of gonadotropes. A, Example of spontaneously active gonadotrope cell recorded in 5 K⁺ CC Ringer. The resting membrane potential was -50 mV with action potentials having a frequency of 1.23 Hz, mean amplitude of 65 mV and an overshoot of about 16 mV. The action potential width at -20 mV was 4 ms. B, Resting membrane potential of gonadotropes in different K⁺ CC Ringer solutions. Number of analyzed gonadotropes for each condition is given in parentheses. Significance was tested with an unpaired two-tailed Student's t test, n.s., not significant.

Application of 1 and 10 nM GnRH induced different changes in the membrane potential of gonadotropes. 80% of gonadotropes (36 out of 45, examples in Fig. IV.3, A-D) responded to GnRH application while 20% (9 of 45) remained in the previous state (example in Fig. IV.3, E). The resting membrane potential varied and also the response to GnRH. The following classification of cells according to the membrane potential was made:

- Group of cells with membrane potentials between -13 and -40 mV (n = 8). 3 cells from this group responded to GnRH with a large sustained hyperpolarization to potentials between -60 and -75 mV (Fig. IV.3, B). The other 5 cells responded to GnRH with production of slow oscillations of the membrane potential with frequencies of about 0.2 Hz (Fig. IV.3, C)
- Group of cells with membrane potentials between -45 and -75 mV (n = 28). Some cells responded to GnRH with transient hyperpolarizations, which then led to ongoing firing of action potentials (Fig. IV.3, A). Application of GnRH initiated periodic hyperpolarizations of the membrane potential for few seconds (Fig. IV.3, D). There were also cells which depolarized as response to GnRH. The depolarization induced by GnRH was in average 6 ± 1 mV but varied also up to 10 or 48 mV (n = 6).

Application of apamin (0.1 or 1 μ M), a selective blocker of small conductance Ca²⁺-dependent potassium channels (SK) (Stocker 2004), stopped the oscillations induced by GnRH (n = 7) demonstrating that the hyperpolarizing oscillations were generated by periodic opening of SK channels. The apamin and GnRH effects were reversible upon washout. The initial response could be repeated with a second GnRH application after an interval of about 5

min (n = 2, data not shown). It was tested, whether the amount of membrane hyperpolarization was dependent on the GnRH concentration. Concentrations of 1, 10, 50 and 100 nM GnRH were tested and the amount of depolarization increased with the increase in the GnRH concentration (data not shown).

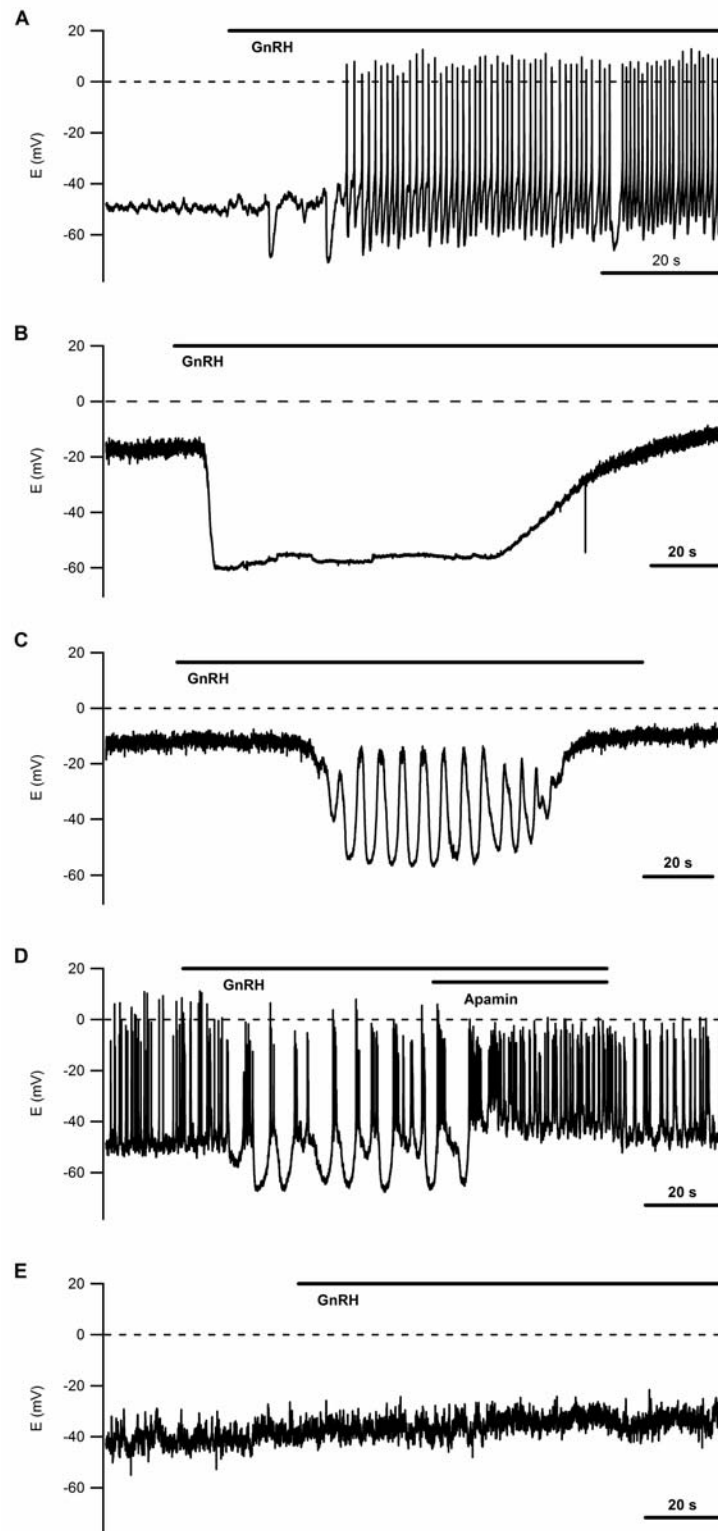


Fig. IV.3: GnRH induced different types of membrane potential responses. A, GnRH (1 nM) induced brief hyperpolarizations of the membrane potential (E (mV)) followed by action potential firing. B, GnRH (1 nM) induced a long lasting hyperpolarization of 40 mV. C, GnRH (10 nM) induced hyperpolarized slow oscillations of the membrane potential with a frequency of 0.2 Hz. D, GnRH (10 nM) induced hyperpolarized oscillations with action potentials on top. Subsequent application of apamin (1 μ M) blocked the oscillations. Washout of both GnRH and apamin restored the normal resting membrane potential. E, GnRH (1 nM) induced a depolarization of the membrane potential of about 6 mV.

IV.1.3. GnRH increased the $[Ca^{2+}]_i$

To investigate the changes in the intracellular Ca^{2+} concentration ($[Ca^{2+}]_i$) induced by GnRH, calcium imaging experiments were performed on cultured gonadotropes. Fura-2 fluorescence was measured as an indicator for changes in $[Ca^{2+}]_i$.

GnRH was added to the $5 K^+$ VC Ringer together with BSA 0.1 – 0.2% to avoid the adhesion of GnRH to the application system tubing. Application of GnRH on mouse gonadotropes generated a broad range of $[Ca^{2+}]_i$ response patterns with the majority having a significant increase in $[Ca^{2+}]_i$. Application of 10 nM GnRH caused oscillations in $[Ca^{2+}]_i$ with frequencies between 0.08 and 0.25 Hz and a mean of 0.17 ± 0.02 Hz ($n = 15$) (Fig. IV.4, B) and some cells responded with a plateau-like increase (Fig. IV.4, A) GnRH never induced an increase in $[Ca^{2+}]_i$ in non-fluorescent cells.

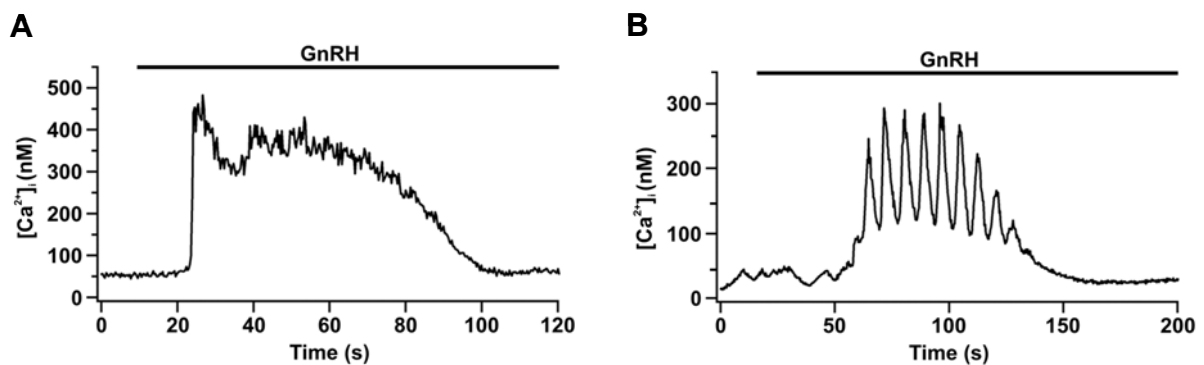


Fig. IV.4: Calcium imaging revealed heterogeneity of GnRH responses. Examples of $[Ca^{2+}]_i$ responses after application of 10 nM GnRH. A, Plateau-like response with an initial transient increase. B, Slow oscillating cell with a frequency of 0.12 Hz.

IV.1.4. Membrane depolarization increased the $[Ca^{2+}]_i$ and decreased outward current

Voltage-dependent Ca^{2+} current activates near -50 mV (Wen, Schwarz et al. 2008). To confirm these data a new set of combined voltage-clamp and calcium-imaging experiments were performed. Experiments were done on gonadotropes in the perforated-patch configuration to prevent fura-2 and $[Ca^{2+}]_i$ washout. After the seal was obtained, the cells were immediately voltage clamped at -70 mV at which presumably all voltage-dependent calcium channels are closed (Scherubl and Hescheler 1991) until the series resistance was low enough to start the recording. After the whole-cell configuration was obtained, the cells were depolarized to -50 mV. Upon this change in the membrane potential F/F_0 increased by $35 \pm 8\%$ ($n = 4$, Fig. IV.5, A) and there was also a reduction in the outward current 15 ± 4 pA ($n = 4$, Fig. IV.5, B).

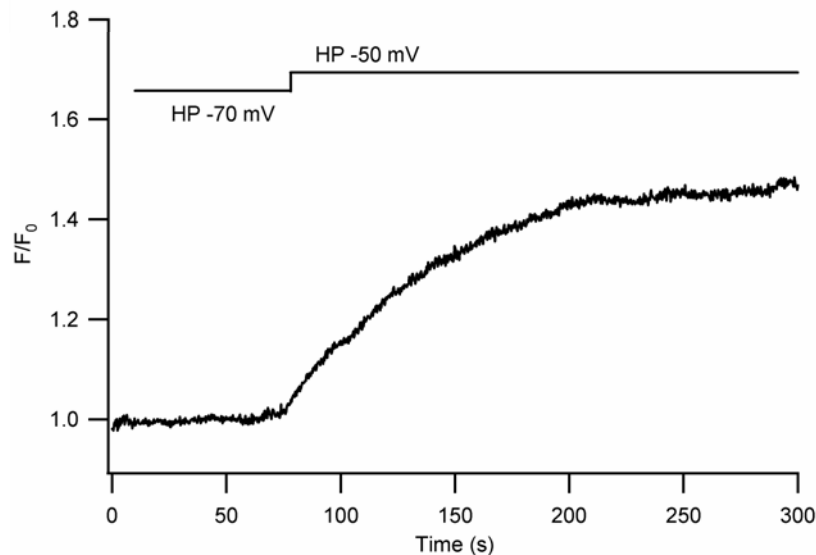


Fig. IV.5: Effects of depolarizing the membrane potential of mouse gonadotropes. Calcium-imaging experiment in which the $[Ca^{2+}]_i$ increased by 45% upon a depolarization from -70 to -50 mV.

IV.1.5. Na^+ currents

Voltage-clamp experiments with the conventional whole-cell configuration on cultured gonadotropes from GRIC/R26-YFP mice were performed to measure Na^+ currents, which have previously been described for rat (Tse and Hille 1993) and for female mouse gonadotropes (Waring and Turgeon 2006)

Na^+ currents could be isolated using an intracellular solution with Cs^+ replacing K^+ and an extracellular solution with TEA and 4-AP to block K^+ currents (see Table III.2). The pulse protocol for recording Na^+ current activation started from a holding potential of -70 mV. Characteristic for Na^+ currents is that they are transient currents, i.e. current that change its direction from inward to outward currents at the reversal potential close to the Nernst equilibrium potential for Na^+ ions. Na^+ currents have also outward rectification, in this case the depolarizing steps induce increase in the inactivation state of the current (Hille 2001). For these reasons it was necessary to apply a hyperpolarizing prepulse to -120 mV for 50 ms to remove steady-state Na^+ channel inactivation. Afterwards the Na^+ currents were activated using a series of 10 ms depolarizing steps from -120 to +70 mV in 10 mV increments (Fig. IV.6, A inset). The Na^+ current started to activate near -40 mV and exhibited a maximum inward current near -10 mV. Peak inward current amplitudes varied considerably between different cells from 0.14 to 2.4 nA. The current densities were calculated by dividing by the corresponding cell capacitance and varied between 19 and 365 pA/pF with a mean of 120 ± 30 pA/pF ($n = 10$, three mice, Fig. IV.4, A). Na^+ conductance was half maximal at $V_{1/2} = -23.7 \pm 1.4$ mV with a slope factor of $k = 6.00 \pm 0.45$ mV (Fig. IV.6, B).

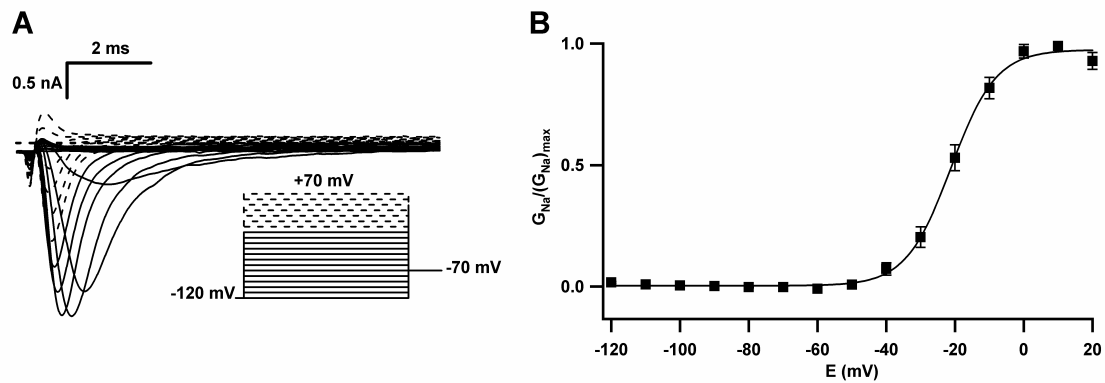


Fig. IV.6: Na⁺ currents activation. A, Family of superimposed traces of Na⁺ currents. Continuous and interrupted current traces were elicited by the corresponding voltages in the pulse protocol (inset). B, Na⁺ conductance was calculated from equation (1) (see Materials and Methods). Mean \pm SEM of the normalized conductance values ($n = 10$) were plotted against membrane potential and fitted with a Boltzmann function ($V_{1/2} = -21.2$ mV, $k = 6.5$ mV).

Steady-state inactivation of Na⁺ currents was determined by a two step protocol, whereby a 100 ms conditioning pulse at potentials from -120 mV to 0 mV from a holding potential of -70 mV, was followed by a 5 ms test pulse at 10 mV (Fig. IV.7, A inset). The voltage-dependence of Na⁺ steady-state inactivation was calculated by plotting the normalized currents evoked by the test potentials against the pre-pulse potentials, The curve was fitted with a Boltzmann function and yielded the midpoint of inactivation at $V_{1/2} = -71.2 \pm 1.7$ mV and a slope factor of $k = 11.1 \pm 0.6$ mV ($n = 12$, Fig. IV.7, B).

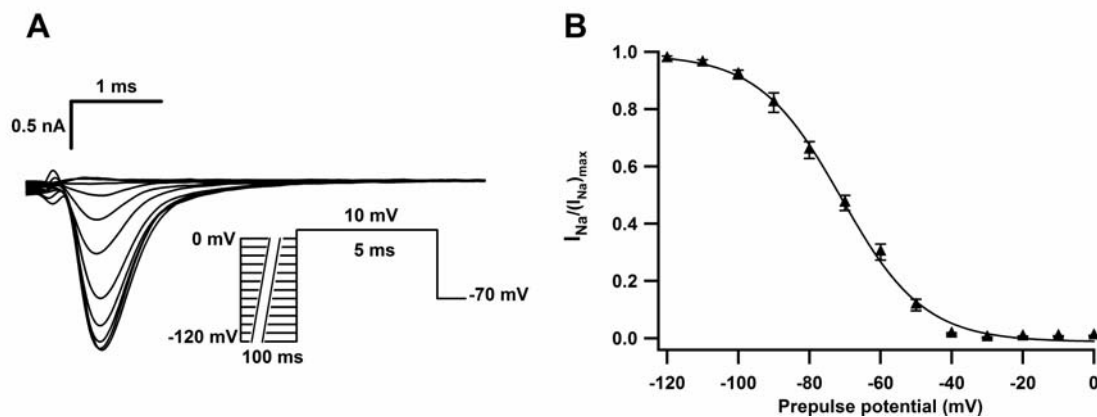


Fig. IV.7: Voltage dependence of steady-state inactivation of Na⁺ currents. A, Family of superimposed traces of Na⁺ currents. Continuous current traces were elicited at the test pulse to 10 mV after the corresponding pre-pulse voltages in the pulse protocol (inset). B, The normalized mean peak Na⁺ currents were fitted with a Boltzmann function with $V_{1/2} = -71$ mV and $k = 11.6$ mV ($n = 12$).

IV.2. Erg K⁺ currents in mouse gonadotropes

For erg K⁺ currents characterization and search for their role in mouse gonadotropes, several physiological parameters were measured and are described in the following section. Patch-clamp experiments were performed for biophysical characterization (i.e. activation and inactivation voltage-dependence and kinetics, K⁺ and temperature dependence) of the erg K⁺ currents and their modulation by GnRH. Calcium-imaging experiments show the physiological effects of erg K⁺ currents on the increase of [Ca²⁺]_i. Acute LH secretion measurements were performed in order to elucidate the physiological significance of the erg K⁺ currents in mouse gonadotropes.

IV.2.1. Blockage of erg K⁺ channels increased [Ca²⁺]_i in acute pituitary slices

To show that erg K⁺ channels have impact on the physiology of gonadotropes in intact tissue, some Ca²⁺-imaging experiments were performed on pituitary slices. Pituitary slices were prepared from GRIC/R26-YFP mice and fluorescent gonadotropes were found as isolated cells or as small agglomerated cell groups, which were often located at the slice periphery.

To test whether blockage of erg K⁺ channels would increase [Ca²⁺]_i, a specific blocker of erg K⁺ channels (E-4031), was applied on acutely sliced pituitaries. Under the YFP filter, the pituitary slices contained brightly fluorescent cells located at the surface of the slice, but also cells less bright indicating that they might be located more deep in the pituitary slice (Fig. IV.8, A). Under the fura-2 fluorescence was possible to make a clear difference between the cells located at the surface or deep in the pituitary slice (Fig. IV.8, B and C). Erg K⁺ current is highly dependent on the external concentration having a higher conductance in a high [K⁺]_e but normal ACSF had only 2.5 mM K⁺; Experiments were performed in 8K⁺ ACSF, concentration close to the physiological [K⁺]_e and large enough for erg K⁺ currents. In Fig. IV.8, B and C, it is shown that application of E-4031 increased fura-2 fluorescence in two cells out of three, indicating that not all gonadotropes express erg K⁺ channels. There were also non-fluorescent cells which responded to 1 μM E-4031. These cells were most likely lactotropes which also expressed erg K⁺ currents (Bauer, Schafer et al. 1999; Schafer, Wulfesen et al. 1999). The time course of F/F₀ increase was slow, reaching a plateau within about 1 min (Fig. IV.8, D). The mean F/F₀ increase was 10.2 ± 1.6% (n = 21) (Fig. IV.8, E).

The evaluation was restricted to gonadotropes in the periphery of the slice, where there was less overlap with other fura-2 fluorescent cells.

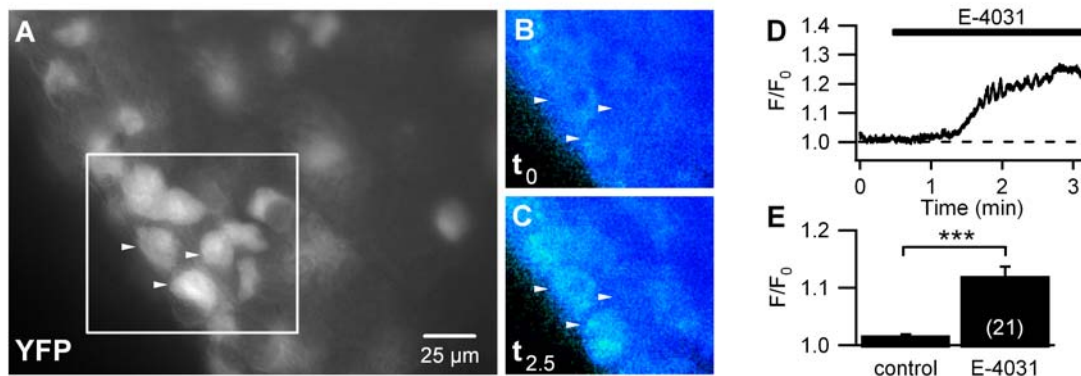


Fig. IV.8: Blockage of erg channels increases $[Ca^{2+}]_i$ in gonadotropes in acute pituitary slices. A, Section of a pituitary slice with fluorescent gonadotropes. Boxed area is shown in B and C. White arrowheads point to the same gonadotropes in A, B and C. Images of fura-2 fluorescence before (t_0 , B) and during ($t_{2.5 \text{ min}}$, C) application of E-4031 ($1 \mu\text{M}$). An increase in the fluorescence was observed in two of the arrowed three gonadotropes. D, time course of E-4031-induced increase in F/F_0 in a gonadotrope. E, mean \pm SEM of F/F_0 of all analyzed gonadotropes before (control) and 60 to 180 s after onset of E-4031 application ($n = 21$), level of significance, $P < 0.001$.

IV.2.2. Availability and activation of erg K^+ currents in cultured gonadotropes

Electrophysiological experiments were performed in perforated-patch and classical whole-cell configuration. For detection and isolation of the erg K^+ currents extracellular and intracellular solutions with specific composition were used (see Materials and Methods). The availability protocol is especially suited to detect erg K^+ currents and to analyze their voltage-dependent gating kinetics. In order to isolate specifically the erg currents, a high extracellular potassium ($[K^+]_e = 40 \text{ mM}$) was used to increase the inward tail current and the specific blocker E-4031 ($1 \mu\text{M}$) was applied to block all the erg K^+ currents (Fig. IV.9, A-C). To fully activate the erg channels and partially inactivate A-type K^+ channels, a prepulse to 20 mV was applied from a holding potential of -20 mV. Subsequently, 1-s test pulses ranged from 10 mV to -120 mV and were followed by a -100 mV potential step (Fig. IV.8, A inset). At test potentials more negative than -50 mV the erg currents characteristically exhibited a “hook-like” shape (Fig. IV.9, A-C boxed area) because of fast recovery from inactivation and slow deactivation. The currents remaining after deactivation or “available” inward tail currents at -100 mV were plotted against test potentials and fitted with a Boltzmann equation (2). The measurements were performed in the perforated-patch configuration. The availability curve showed that 50% of the erg current was “available” at -67 mV: $V_{1/2} = -67.1 \pm 1.9 \text{ mV}$, slope factor

$k = 10.5 \pm 1.3$ mV, $n = 13$ (example in Fig. IV.9, D). Erg current density, as determined from the maximal tail current amplitude and the cell capacitance (8 ± 1 pF) was 14 ± 2 pA/pF.

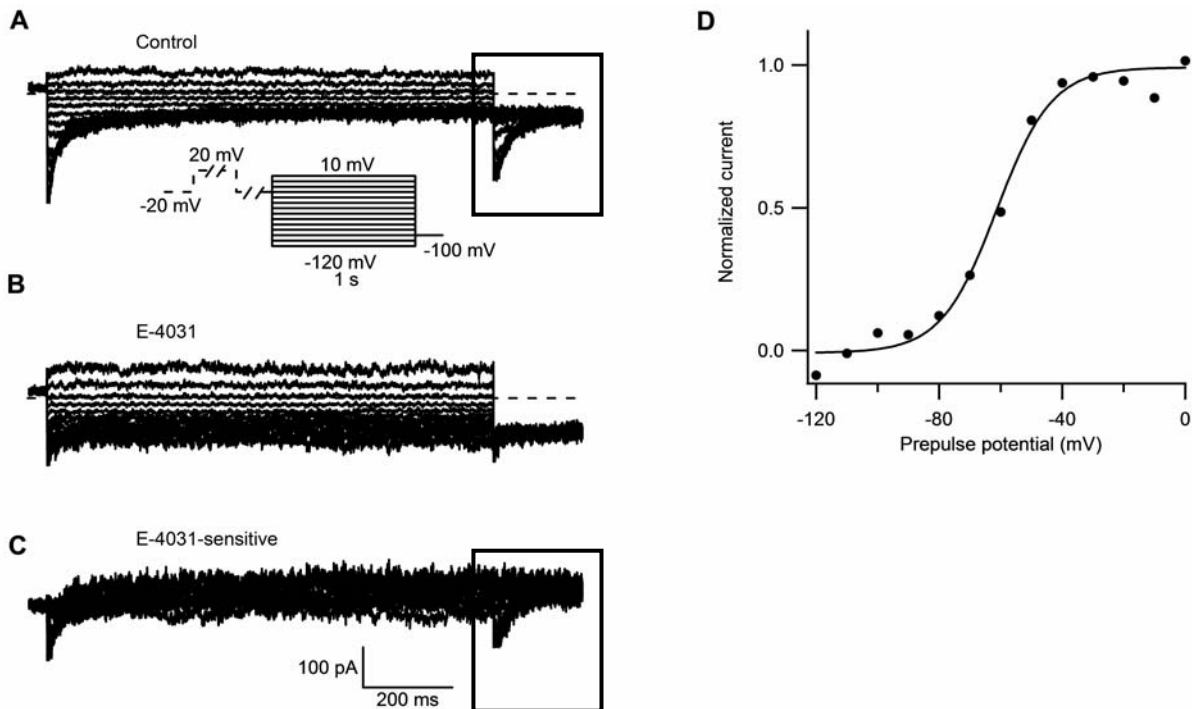


Fig. IV.9: Availability of erg currents in cultured gonadotropes. A, Membrane currents measured with the availability protocol as shown in the inset. B, Membrane currents measured with the same protocol as in A, but in the presence of E-4031 ($1 \mu\text{M}$). C, E-4031-sensitive currents, obtained by subtraction of currents shown in B from those in A. D, Peak amplitude of the tail current measured in C was normalized and plotted against preceding test-pulse potentials and fitted with a Boltzmann function yielding $V_{1/2} = -61$ mV and $k = 9$ mV.

The voltage dependence of steady-state activation was also measured in a solution with high extracellular potassium ($[\text{K}^+]_e = 40$ mM) and the specific blocker E-4031 ($1 \mu\text{M}$) was applied in order to isolate the specific erg K^+ currents after subtraction. For the steady-state activation the test pulses were prolonged to 4 s, because erg currents activate very slowly (Schönherr, Rosati et al. 1999). From a holding potential of -80 mV test pulses between -80 and $+10$ mV in steps of 10 mV were applied, followed by a step to -100 mV (Fig. IV.10, A inset) which elicited the erg-activated K^+ currents with the specific “hook-like” shape (Fig. IV, A boxed area). Plotting the normalized tail-current amplitudes versus test-pulse potentials yielded the activation curve (Fig. IV.10, B). Erg current started to activate at potentials positive of -60 mV and 50% was activated at $V_{1/2} = -41.7 \pm 1.9$ mV ($k = 7.5 \pm 0.9$ mV; $n = 3$), close to the observed resting membrane potentials in gonadotropes (see Fig. IV.2).

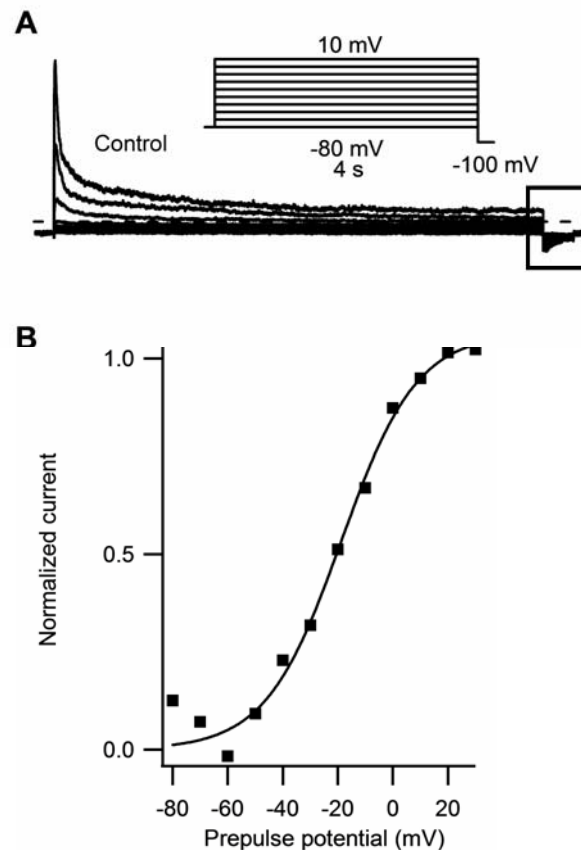


Fig. IV.10: Activation of erg currents in cultured gonadotropes. A, Membrane currents measured with the activation protocol as shown in the inset. B, Peak amplitude of the tail current shown in A (boxed area) were plotted against the preceding test-pulse potentials and fitted with a Boltzmann function yielding $V_{1/2} = -19$ mV and a slope $k = 14$ mV.

IV.2.3. Erg conductance changed by external K^+ concentration

Native and heterologously expressed *erg1* K^+ channels (Shibasaki 1987; Kiehn, Lacerda et al. 1996) are characterized by increased single-channel conductance with increase in the external K^+ concentration $[K^+]_e$. Heterologously expressed *rat erg2* and *erg3* K^+ currents (Sturm, Wimmers et al. 2005) have also been shown to have a strong dependence of the whole-cell conductance to the external K^+ . In gonadotropes, the dependence of native *erg* K^+ currents to $[K^+]_e$ was measured in 40 mM and 150 mM $[K^+]_e$. Currents were elicited with the availability protocol using the perforated-patch configuration. Elevating the $[K^+]_e$ on the one hand side shifted the reversal potential for K^+ towards more depolarized potentials, thereby increasing the driving force for the *erg* currents evoked by the pulse to -100 mV (Fig. IV.11). On the other hand the expected current increase was amplified by another factor due to the increase in *erg* K^+ channel conductance (Shibasaki 1987). First, the maximal current amplitudes were divided by the two different driving forces at -100 mV based on the experimentally observed reversal potentials averaging at $E_{rev} = -17$ mV for 40 mM and $E_{rev} = 2$ mV for 150 mM $[K^+]_e$.

Then the conductance in 150 mM was divided by the conductance in 40 mM $[K^+]_e$ giving a factor of 1.6.

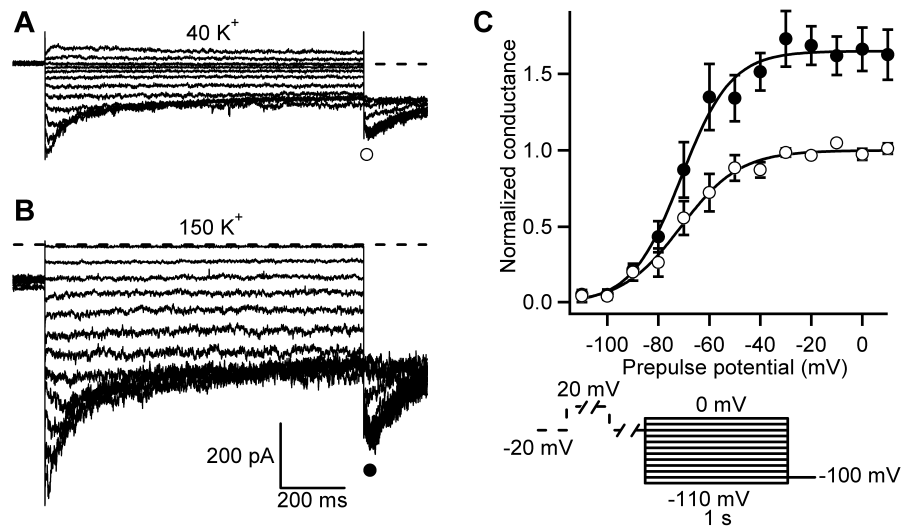


Fig. IV.11: Increase in $[K^+]_e$ elevates erg channel conductance. Membrane currents recorded with the availability pulse protocol (see panel C) in $[K^+]_e = 40$ mM (A) and 150 mM (B). C, The mean conductance in 40 mM $[K^+]_e$ was normalized to 1, the mean conductance in 150 mM $[K^+]_e$ accordingly, and both plotted against the test-pulse potential. Means were fitted with Boltzmann functions (40 mM K^+ , open circles: $E_{0.5} = -71$ mV, $k = 12$ mV; 150 mM K^+ , filled circles: $E_{0.5} = -71$ mV, $k = 10$ mV; $n = 8$).

IV.2.4. Temperature dependence of erg K^+ currents

Temperature is another important biophysical property of erg K^+ currents and it was also important to observe the behavior of erg K^+ channels at temperatures more close to the physiological ones. It has been shown in a heterologous expression system that temperature is influencing the voltage dependence of steady-state activation and inactivation of HERG K^+ channels and that the rates of inactivation and recovery from inactivation are more sensitive to changes in temperature than the rates of activation and deactivation (Vandenberg, Varghese et al. 2006). The amplitude of erg K^+ currents was increased by at least 2.2 up to 4.7 fold by at least 10°C degrees increase in the temperature (Zhou, Gong et al. 1998; Vandenberg, Varghese et al. 2006). Because the experimental setup did not allow for fast temperature changes, the experiments were done on separate groups of cells. Gonadotropes from GRIC/eR26- τ GFP mice were patch-clamped in the conventional whole-cell configuration in 40 K^+ VC Ringer (for solution composition see Materials and Methods).

The availability of erg K^+ currents was significantly shifted by 10 mV towards more positive potentials and the slope factor was significantly increased by an increase in temperature. At 30°C the maximal tail current amplitude was 166% compared to the value at 20°C (Fig. IV.12).

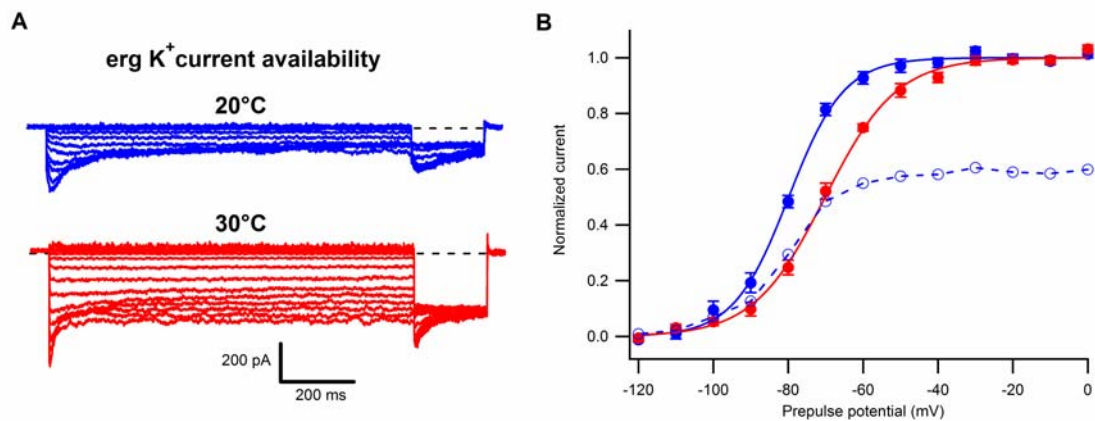


Fig. IV.12. Temperature dependence of erg K^+ currents availability. A, Erg current availability elicited by the pulse protocol shown in Fig. IV.9 was shifted from $V_{1/2} = -80$ mV at 20°C ($k = 8$ mV, $n = 10$) to $V_{1/2} = -69$ mV at 30°C , ($k = 11$ mV, $n = 13$) and the maximally available current was increased by about 60%. Continuous lines represented Boltzmann fits and the dashed lines represented the curves at 20°C normalized to the curves at 30°C . B, Membrane currents recorded with the availability pulse protocol on gonadotrope cells from GRIC/eR26- τ GFP mice using the conventional whole-cell configuration recorded at 20°C (blue symbols) and at 30°C (red symbols) in $[\text{K}^+]_e = 40$ mM.

The activation parameters were not significantly changed by an increase in the temperature with the exception of slope factor which decreased (Fig. IV.13). In table IV.1 are summarized the parameters for the Boltzmann fits of both activation and inactivation.

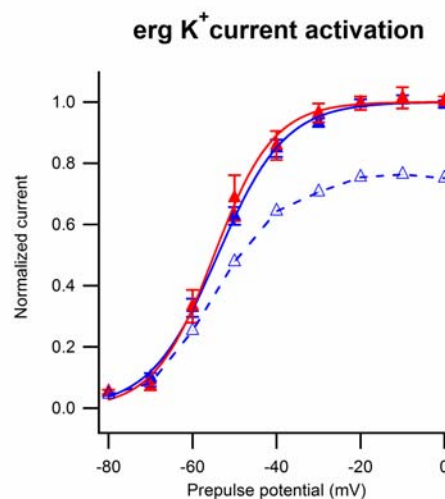


Fig. IV.13. Temperature dependence of erg K^+ current activation. Erg current activation elicited by the pulse protocol shown in Fig. IV.10 was not shifted by temperature increase (20°C : $V_{1/2} = -54$ mV, $k = 8$ mV, $n = 12$; 30°C : $V_{1/2} = -55$ mV, $k = 8$ mV, $n = 10$), but the maximal current was increased by about 30%.

Table IV.1: Temperature dependence of erg current activation, availability and current density in gonadotropes

Parameter	20°C	30°C	P value
Availability $V_{1/2}$ [mV]	-81 ± 1 (n = 10)	-70 ± 1 (n = 13)	1.9E-07 ***
Availability k [mV]	8 ± 1 (n = 10)	11 ± 1 (n = 13)	0.04 *
I_{\max} availability [pA]	-92 ± 9 (n = 10)	-153 ± 15 (n = 13)	0.003 **
Current density availability [pA/pF]	24 ± 3 (n = 10)	39 ± 4 (n = 13)	0.008 **
Activation $V_{1/2}$ [mV]	-54 ± 1 (n = 12)	-54 ± 2 (n = 10)	0.943 n.s.
Activation k [mV]	8 ± 1 (n = 12)	6 ± 1 (n = 10)	0.012 *
I_{\max} activation [pA]	-108 ± 8 (n = 12)	-139 ± 20 (n = 10)	0.13 n.s.
Current density activation [pA/pF]	27 ± 3 (n = 12)	33 ± 4 (n = 10)	0.214 n.s.

Fig. IV.14 shows typical examples of tail currents recorded at -100 mV from cells at 20°C and 30°C (blue and red color, respectively). There was an initial increase in the inward current with the time constant of 2 ms at 30°C which reflects the recovery from inactivation, followed by a decrease in the current with a slower time constant (110 ms) reflecting the deactivation. These two components of the current were individually fitted using a single exponential function. The result was that the processes of recovery from inactivation and deactivation had different temperature sensitivities. The Q_{10} factor was calculated as the change in rate or conductance (α) for each 10°C change in the temperature (T, (Hille 2001)).

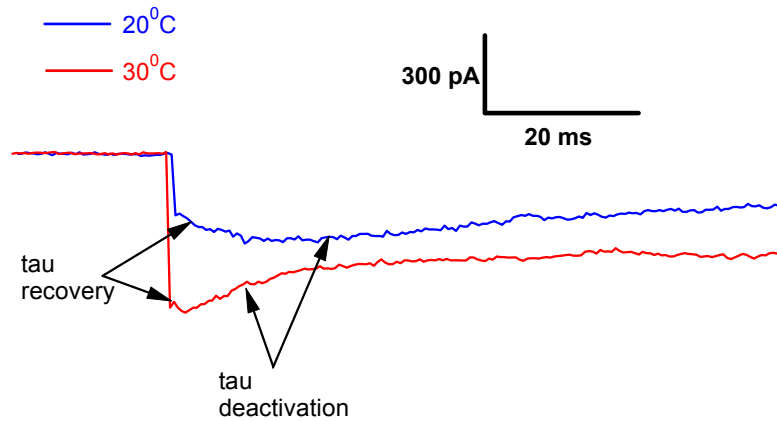


Fig. IV.14: Effects of temperature on the erg current rates of recovery from inactivation and deactivation. Example of current traces recorded at -100 mV at 20°C and 30°C from two different gonadotrope cells during an availability protocol shown in Fig. IV.8, A. The blue and red traces show recordings at 20 and 30°C , respectively, and the arrows point to the current trace region fitted with a single exponential function for each voltage step.

Table IV.2 summarizes the rates of recovery from inactivation and deactivation at different potentials and the corresponding calculated Q_{10} values. The rates of recovery from inactivation were very fast at potentials more negative than -100 mV and the time resolution of the recordings did not permit a reliable calculation. The rates for deactivation were too slow at potentials more positive than -90 mV and for this reason were omitted from final evaluation.

Table IV.2: Temperature dependence of time courses of recovery from inactivation and deactivation with the corresponding Q_{10} values

Voltage [mV]	Deactivation			Recovery from inactivation		
	$\tau_{20^{\circ}\text{C}}$ [ms]	$\tau_{30^{\circ}\text{C}}$ [ms]	$Q_{10\text{deact}}$	$\tau_{20^{\circ}\text{C}}$ [ms]	$\tau_{30^{\circ}\text{C}}$ [ms]	$Q_{10\text{rec}}$
-120	56.9 ± 2.5	20.8 ± 1.0	2.7	-	-	-
-110	94.6 ± 3.3	32.6 ± 2.5	2.9	-	-	-
-100	157.3 ± 11.2	54.5 ± 4.5	2.9	6.7 ± 0.7	1.7 ± 0.3	3.9
-90	292.1 ± 18.1	112.3 ± 7.1	2.6	9.2 ± 1.1	2.1 ± 0.3	4.3
-80	-	-	-	10.4 ± 1.8	2.3 ± 0.4	4.5
-70	-	-	-	11.9 ± 2.4	2.0 ± 0.4	5.8
-60	-	-	-	8.3 ± 1.4	2.9 ± 0.5	2.8

IV.2.5. Blockage of erg K^+ currents depolarized gonadotropes

After the presence of erg K^+ currents was detected in mouse gonadotropes, it is important to know what the role of these channels is. For this purpose current-clamp experiments were performed on GRIC/R26-YFP male gonadotropes. Membrane potential changes of cultured gonadotropes induced by blocking the erg currents with 1 μ M E-4031 were recorded. The experiments were performed in the perforated-patch whole-cell configuration using 3, 5 and 8 mM $[K^+]_e$ CC Ringer solutions (see Table III.1). In 74% of recorded gonadotrope cells E-4031 induced similar depolarizations of the membrane potential (examples in Fig. IV.15) in all different $[K^+]_e$ solutions ranging from 3 to 18 mV. The average depolarizations were $+5 \pm 1$ mV in 3 mM $[K^+]_e$ ($n = 11$, $P < 0.005$), $+8 \pm 1$ mV in 8 mM $[K^+]_e$ ($n = 11$, $P < 0.0005$), and $+5 \pm 1$ mV in 8 mM $[K^+]_e$ ($n = 17$, $P < 0.005$). The membrane potential depolarizations were not dependent on $[K^+]_e$. In all these experiments E-4031-induced depolarizations occurred after a delay of about 30 s and slowly reached a steady state within 30-60 s. This slow time course was not due to the exchange time of the application system (< 2 s).

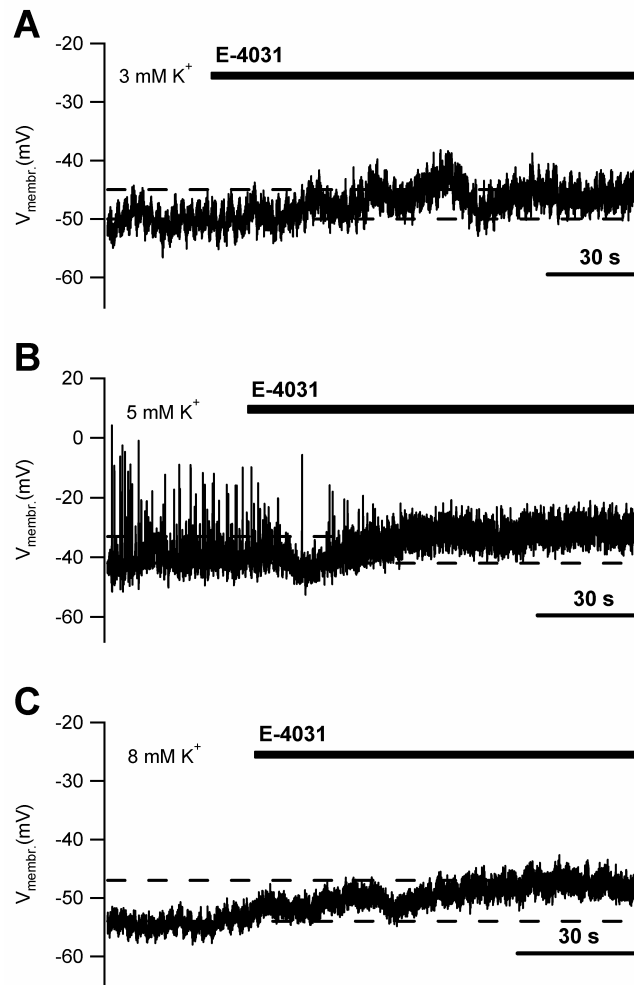


Fig. IV.15 Blockage of the erg currents depolarized the gonadotrope membrane. Examples of membrane potential changes of gonadotropes induced by E-4031 (1 μ M, black bars) in different $[K^+]_e$ concentrations. The resting potential depolarized from -50 mV to -45 mV in 3 mM $[K^+]_e$ (A), from -42 mV to -33 mV in 5 mM $[K^+]_e$ (B) and from -54 mV to -47 mV in 8 mM $[K^+]_e$ (C).

IV.2.6. Blockage of erg channels increases $[Ca^{2+}]_i$ in cultured gonadotropes

Blocking of erg channels in cultured gonadotropes with E-4301 induced a similar increase of $[Ca^{2+}]_i$ (Fig. IV.16) as seen in gonadotropes from acute pituitary slices (see paragraph IV.2.1, Fig. IV.8). The F/F_0 increase was strongly dependent on $[K^+]_e$ concentration (Fig. IV.16, D) in contrast to the current-clamp experiments in which no significant difference in membrane potential depolarization was observed (Fig. IV.2, B). The F/F_0 increase in 8 K^+ CC Ringer was $23 \pm 3\%$, significantly higher than in 5 K^+ CC Ringer ($14 \pm 4\%$) or in 3 K^+ CC Ringer ($7 \pm 2\%$). The $[Ca^{2+}]_i$ responses to E-4031 were characterized by a delay of 20-30 s and a slow time course of F/F_0 increase. The increase in the F/F_0 was abolished by specifically blocking the L-type Ca^{2+} channels with 10 μ M nifedipine (Fig. IV.16, B and D) 2-3 min before application of E-4031.

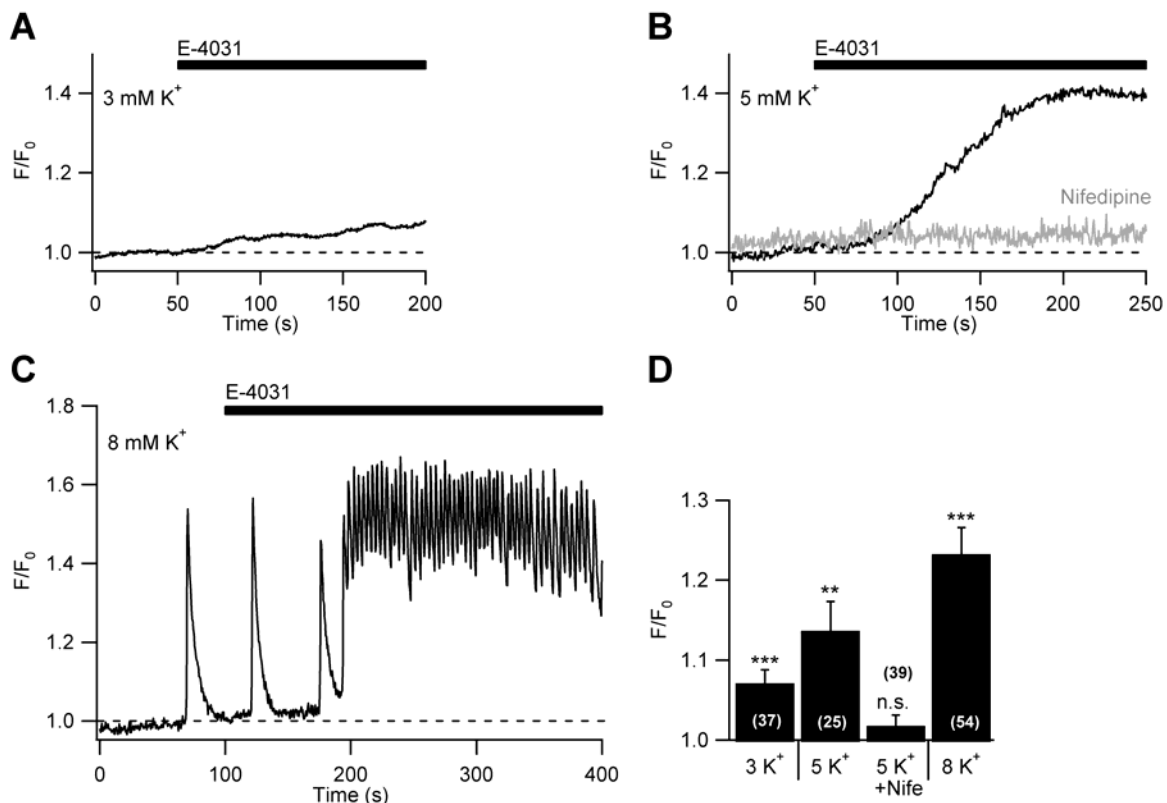


Fig. IV.16: Blockage of erg channels increases $[Ca^{2+}]_i$ in cultured gonadotropes. A, Example of fluorescence increase in 3 K^+ CC Ringer during E-4031 (1 μ M) application. B, Example of fluorescence increase in 5 K^+ CC Ringer during E-4031 (1 μ M) application. The increase in F/F_0 was blocked by nifedipine (10 μ M). C, Example of increase in F/F_0 in 8 K^+ CC Ringer. The transient increase transformed into a plateau F/F_0 increase with superimposed oscillations during E-4031 (1 μ M) application. D, Increase in F/F_0 (mean \pm SEM) induced by E-4031 in different $[K^+]_e$. Number of analyzed gonadotropes is given in parentheses, level of significance, **, $P < 0.01$; ***, $P < 0.001$; n.s., not significant.

IV.2.7. E-4031 and GnRH increased the $[Ca^{2+}]_i$ concentration

The significant $[Ca^{2+}]_i$ increase induced by E-4031 (Fig. IV.8 and IV.16) arose the question if it influences the GnRH-induced $[Ca^{2+}]_i$ increase. To test if the $[Ca^{2+}]_i$ increase by erg channel blockage is part of the $[Ca^{2+}]_i$ increase due to GnRH stimulation, or is additive, further calcium imaging experiments were performed in which the two factors (blockage of erg channels and activation of the GnRH receptor) were combined. In Fig. IV.17, A and D, again a significant increase ($+33 \pm 7\%$) in F/F_0 induced by E-4031 was visible. This increase was smaller than the F/F_0 increase induced by 0.1 nM GnRH ($+86 \pm 9\%$, Fig. IV.17, B and D)). The application of GnRH on top of E-4031 induced a higher increase in F/F_0 fluorescence ($+97 \pm 7\%$) but not statistically significant more than the GnRH-induced increase alone. One interesting observation was that E-4031 significantly shortened the time to reach the peak F/F_0 induced by GnRH from 125 ± 11 s without E-4031 to 65 ± 9 s in the presence of E-4031 ($P < 0.001$). The reverse experiment in which E-4031 was applied in the decaying plateau

phase during GnRH application did not show significant change in F/F_0 ($+61 \pm 8\%$ vs control) compared with GnRH alone ($+58 \pm 6\%$ vs control, Fig. IV.17, C and E).

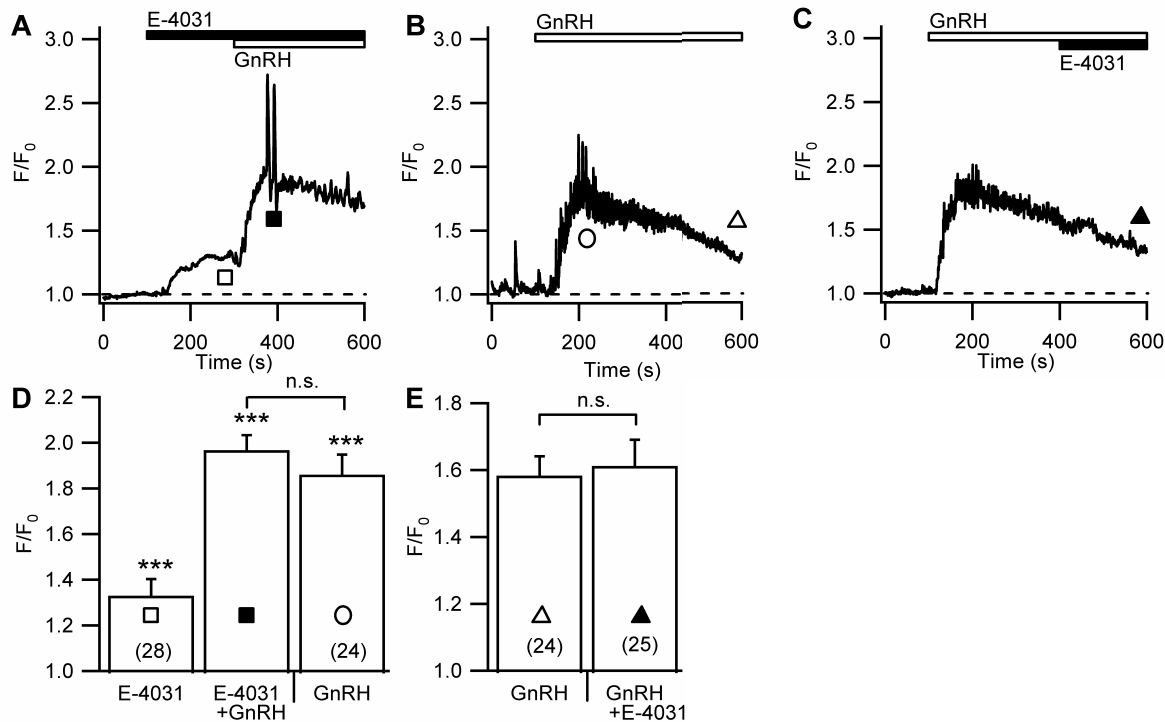


Fig. IV.17: E-4031 and GnRH increase $[Ca^{2+}]_i$. Measurement of the fura-2 fluorescence in 5 mM $[K^+]_e$ Ringer solution. A, F/F_0 measurement before and during E-4031 application as well as during additional application of GnRH (0.1 nM). B, F/F_0 measurement before and during application of GnRH (0.1 nM). C, F/F_0 measurement before and during application of GnRH and subsequent application of E-4031. D, peak increase in F/F_0 (mean \pm SEM) during E-4031 application (empty square) and subsequent application of GnRH in the continued presence of E-4031 (filled square, A) or during GnRH application alone (empty circle, B). E, comparison of F/F_0 in the late plateau phase during GnRH application, either without (empty triangle, B) or with subsequent application of E-4031 (filled triangle, C). Asterisks above the columns denote level of statistical significance versus control, i.e. F/F_0 before drug treatment (paired two-tailed Student's t-test) with **, $P < 0.01$; ***, $P < 0.001$. Significances between the columns indicated by brackets were determined by unpaired Student's t-tests (n.s., not significant).

IV.2.8. E-4031 and GnRH reduce net outward currents

E-4031 depolarized the membrane potential of gonadotropes (Fig. IV.15), presumably by reducing an outward current component due to erg K^+ channels. Next, the amount of outward current at the normal resting potential was determined by blocking the erg currents in voltage-clamped gonadotropes in normal Ringer solution (5 K^+ VC Ringer) with E-4031 (Fig. IV.18). The membrane potential was clamped at -50 mV. Application of E-4031 induced a significant change in the membrane current by -7 ± 2 pA ($n = 5$). Subsequent application of GnRH sometimes triggered transient outward currents mirroring the membrane potential oscillations seen in current-clamp experiments (Fig. IV.3, C and D): always followed by a large delayed, transient reduction of the net outward current of unknown origin (not shown).

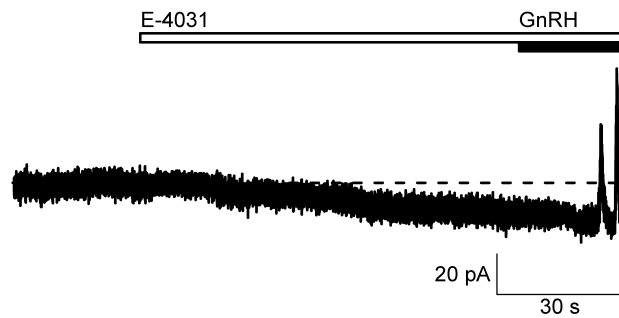


Fig. IV.18 Erg channel blockage reduces an outward current. Gonadotrope cell voltage clamped at -50 mV in an external solution containing 5 mM K^+ . Application of 1 μ M E-4031 reduced the net outward current. Subsequent application of 1 nM GnRH induced transient outward currents.

IV.2.9. Modulation of erg K^+ current by GnRH

The effect of GnRH on erg currents was studied in cultured gonadotropes from GRIC/R26-YFP mice. Changes by GnRH in some biophysical properties of erg currents, i.e. voltage-dependence of activation and availability and time-dependence of activation, were investigated in the perforated-patch configuration in high external K^+ solution (40 K^+ VC Ringer).

Test pulses were applied to measure the time course of modulation of the erg K^+ current by GnRH. The test-pulse protocol consisted of following sequence of pulses: from a holding potential at -20 mV, a 2 s pulse was applied to 20 mV which fully activated the erg K^+ current and a pulse to -120 mV elicited large inward currents which were analyzed in order to monitor the rundown of erg current and the changes induced by GnRH application. GnRH was applied during the test-pulse recordings. Activation and availability protocols were recorded after the erg current amplitude reached a steady state, usually within 2 min after achieving the whole-cell configuration, during 5 min after GnRH application and again after complete block of the erg currents by E-4031.

The change of the voltage dependence of activation of erg currents by GnRH was recorded with the same protocol as shown in Fig. IV.10 and described in paragraph III.4.8. Two populations of gonadotrope cells could be identified. In one group of cells ($n = 4$) the activation curve was situated at more hyperpolarized potentials ($V_{1/2} = -49 \pm 1.6$ mV, $k = 6 \pm 1.3$ mV). For these cells the activation curve was shifted to more depolarized potentials by about 25 mV ($n = 4$) (Fig. IV.19, A). In addition the erg current was reduced by $35 \pm 8\%$ ($P = 0.08$). In the other group of cells ($n = 5$) the activation curve was situated at more depolarized potentials ($V_{1/2} = -37 \pm 2.5$ mV, $k = 10 \pm 0.6$ mV) and there was no shift in the activation curve induced by GnRH. However, GnRH reduced the maximal current by

$33 \pm 12\%$ ($P < 0.05$) in these cells (Fig. IV.19, B). The two groups of gonadotropes did not differ in any other property (e.g. age of animal, days in culture, cell size, or slope k of the Boltzmann function).

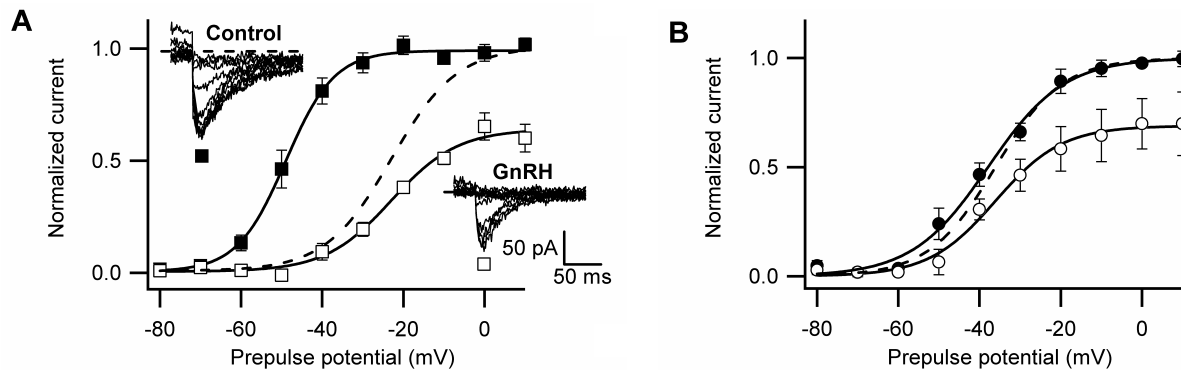


Fig. IV.19 Changes in the voltage dependence of activation induced by GnRH. Two groups of gonadotropes, one in which GnRH caused a shift of the activation curve (A) and the other in which it did not (B). Activation curves recorded before (filled symbols) and during the application of GnRH (open symbols) using the pulse protocol shown in Fig. IV.9, A inset. The insets show the superimposed tail currents recorded at the final potential step to -100 mV before (control) and during GnRH application (GnRH). Peak tail-current amplitudes were normalized and plotted versus the test-pulse potential. Continuous lines represent Boltzmann fits of the means. The dotted line represents the normalized activation curve in the presence of GnRH. A, Control activation curve (filled squares) with $V_{1/2} = -49$ mV and $k = 6$ mV and the shifted activation during GnRH (open squares) with $V_{1/2} = -23$ mV and $k = 8$ mV. GnRH reduced the maximal current by 36%. B, Activation curves of gonadotropes exhibiting no shift in the activation curves. Activation curve before (filled circles) with $V_{1/2} = -38$ mV and $k = 9$ mV and during GnRH application (open circles) with $V_{1/2} = -36$ mV and $k = 8$ mV. GnRH reduced the maximal current by 31%.

The evaluation of the membrane currents determined with the availability protocol (for protocol description see Fig. IV.9, A inset and paragraph III.4.8) showed that the reduction of the maximal tail current amplitude ($35 \pm 7\%$, $P < 0.01$) (Fig. IV.20) was comparable to the reduction seen in the activation curve. Two differently responsive groups of gonadotropes were observed in this case also. In one group, the voltage dependence of erg current availability was located at relatively negative potentials ($V_{1/2} = -68 \pm 1.8$ mV; $n = 8$). In these cells GnRH caused a strong shift (12 ± 2 mV; $P < 0.01$) and reduced the maximal erg current amplitude by $42 \pm 8\%$ ($P < 0.05$). In the other group the availability curves were located at more positive potentials ($V_{1/2} = -51.5 \pm 1.7$ mV; $n = 5$) and GnRH did not shift the voltage dependence of erg current availability (0.3 ± 1.4 mV). The reduction of the maximal erg current in the presence of GnRH in this group was only slightly smaller ($38 \pm 14\%$, $P = 0.08$) than that observed in the group in which the activation shifted.

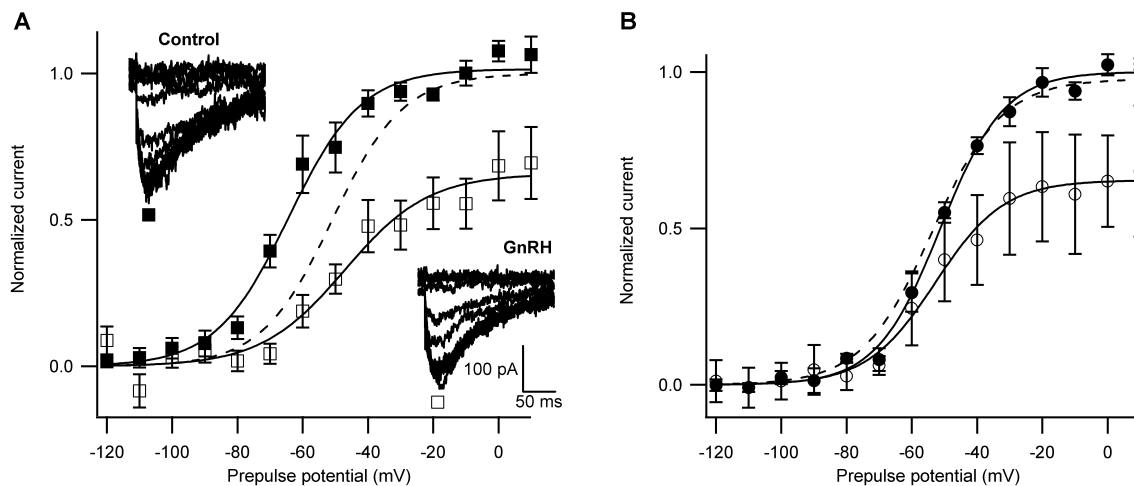


Fig. IV.20 Changes in the voltage dependence of deactivation induced by GnRH. Two groups of gonadotropes, one in which GnRH caused a shift of the availability curve (A) and the other in which it did not (B). Membrane currents were recorded in cultured gonadotropes with the availability pulse protocol before (filled symbols) and during the application of GnRH (open symbols). The insets show the superimposed tail currents recorded at the final potential step to -100 mV before (control) and during GnRH application (GnRH). Tail current amplitudes were normalized to the maximal control current amplitude, means \pm SEM calculated and plotted versus the test pulse potential. Continuous lines represent Boltzmann fits of the means. The dotted line represents the normalized availability curve in the presence of GnRH. A, Availability curves (control: $V_{1/2} = -64$ mV and $k = 11$ mV; GnRH: $V_{1/2} = -51$ mV and $k = 5$ mV, $n = 8$), $V_{1/2}$ was shifted by about 13 mV to more positive membrane potentials while the slope of the availability curve not significantly changed. GnRH reduced the maximal current by 34%. B, Availability curves of gonadotropes exhibiting no shift in the activation curves. Availability curves before (filled circles) with $V_{1/2} = -51$ mV and $k = 10$ mV and during GnRH application (open circles) with $V_{1/2} = -54$ mV and $k = 11$ mV. GnRH reduced the maximal current by 35%.

In summary, the voltage dependence of erg activation and availability was shifted by GnRH in about half of gonadotropes while the maximal current was reduced in all cells.

This inhibition of the maximal erg current by GnRH could be due to a reduction of single-channel conductance, slowing of the time course of activation or recovery from inactivation or because of an acceleration of deactivation. The time constants of recovery from inactivation were measured with the availability protocol (see Fig. IV.9, A inset) and an “envelope-of-tail” protocol (Fig. IV.21, A, inset), were applied.

The time course of erg K^+ current activation was recorded with the “envelope-of-tail” pulse protocol: from a holding potential of -80 mV, a pulse to 20 mV of increasing duration was applied and followed by a potential step to -100 mV which elicited the erg tail inward current (Fig. IV.21, A, inset). The peak amplitudes of the tail currents at -100 mV were normalized to the maximal current and plotted against test pulse duration and the time course was fitted with a single exponential function (Fig. IV.21, B). GnRH did not alter the time course of erg current activation at 20 mV from $\tau_{\text{control}} = 74.8 \pm 5.7$ ms to $\tau_{\text{GnRH}} = 69.7 \pm 8.7$ ms but the maximal current amplitude was decreased by $45 \pm 2\%$ ($n = 6$, $P < 0.005$, Fig. IV.21, A and B).

As previously described, the erg inward currents elicited by the availability protocol were transient during the test pulses negative of -60 mV. The E-4031-sensitive currents were fitted with triple exponential functions and the time constants of recovery from inactivation, fast and slow component of deactivation were plotted against the test-pulse potential (Fig. IV.21, C-E). In the presence of GnRH, the deactivation and recovery from inactivation time constants were not significantly changed at any potential. The time constants of recovery from inactivation varied from $\tau_{\text{rec}} = 3.9 \pm 1.1$ ms at -120 mV to $\tau_{\text{rec}} = 14.7 \pm 2.9$ ms at -70 mV (control), and from $\tau_{\text{rec}} = 2.5 \pm 0.8$ ms at -120 mV to 15.2 ± 4.1 ms at -70 mV (GnRH; n = 6) (Fig. IV.21, C). Time constants of fast deactivation varied from $\tau_{\text{fast}} = 14.1 \pm 3.1$ ms at -120 mV to $\tau_{\text{fast}} = 47.9 \pm 6.7$ ms at -70 mV (control), and from $\tau_{\text{fast}} = 19.9 \pm 4.4$ ms at -120 mV to 59.2 ± 9.2 ms at -70 mV (GnRH; n = 6) (Fig. IV.21, D). Time constants of slow deactivation varied from $\tau_{\text{slow}} = 109 \pm 21$ ms at -120 mV to $\tau_{\text{slow}} = 552 \pm 56$ ms at -70 mV (control), and from $\tau_{\text{slow}} = 204 \pm 60$ ms at -120 mV to $\tau_{\text{slow}} = 579 \pm 141$ ms at -70 mV (GnRH; n = 6) (Fig. IV.21, E).

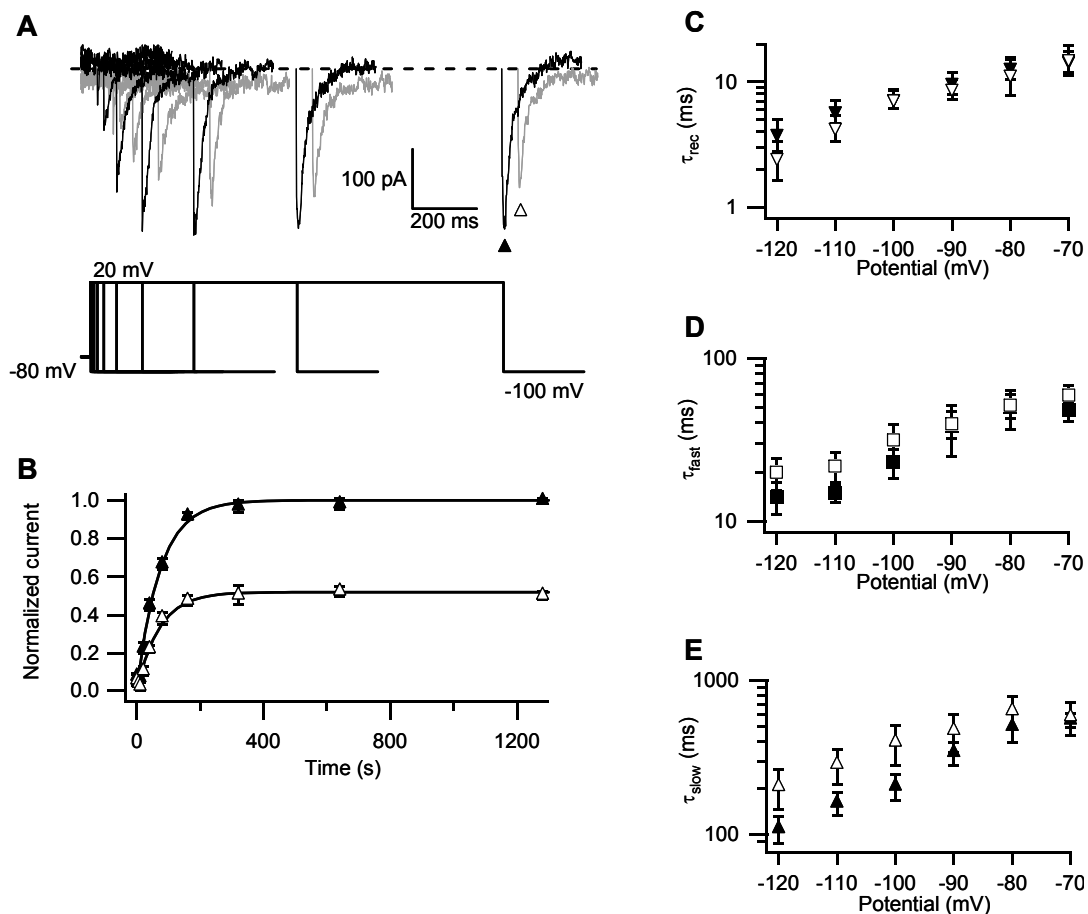


Fig. IV.21. GnRH does not change the time course of activation, deactivation and recovery from inactivation. A, Time course of erg current activation measured with the “envelope-of-tail” protocol: Superimposed E-4031-sensitive currents recorded before (black traces) and during GnRH application (gray traces were shifted by 50 ms to the right to become better visible). Inset showing the pulse protocol. B, Peak amplitudes of erg tail currents were normalized to the maximal control current, the means \pm SEM were plotted versus the test-pulse duration and the time course of activation was fitted with a single exponential function yielding almost the same time constants ($\tau_{control} = 74$ ms, filled triangles; $\tau_{GnRH} = 71$ ms, open triangles; $n = 6$). C-E, Time courses of transient currents elicited by the availability protocol were fitted with the sum of three exponential functions and the time constants were plotted against the test-potential. The time constants of recovery from inactivation (C, τ_{rec}), and the fast (D, τ_{fast}) and slow (E, τ_{slow}) components of deactivation before (filled symbols) and during GnRH application (open symbols; $n = 6$).

IV.3. LH secretion in mouse gonadotropes

The questions arose, whether the observed changes in the membrane potential and $[Ca^{2+}]_i$ because of the pharmacological blockage of erg channels by E-4031 (Fig. IV.13 and IV.14) alone would stimulate LH secretion and if it would affect the amount of LH secretion stimulated by GnRH. The ELISA measurements were done with wild-type pituitary cells

maintained in culture for one day. There was a heterogeneous basal LH secretion varying from 0.6 to 7.7 ng/ml ($n = 12$).

A dose-response curve of GnRH was made in order to determine the maximal response (Fig. IV.22, A). The cells were treated with increasing doses of GnRH (10^{-11} - 10^{-8} M) and a concentration dependence was observed, with almost maximal stimulation at 10^{-8} M, i.e. 10 nM GnRH (Fig. IV.22, A).

A submaximal GnRH concentration (0.1 nM, i.e. 10^{-10} M) was chosen for the final ELISA experiments, because blockage of erg currents might inducing secretion additional to GnRH or might shift the dose-response curve of GnRH. GnRH induced a 2.5-fold increase in LH secretion compared to basal secretion, while 1 μ M E-4031 induced no change (Fig. IV.22, B). When GnRH and E-4031 were applied together, or when GnRH was applied during treatment with E-4031, there was no significantly larger LH increase as compared to that induced by GnRH alone.

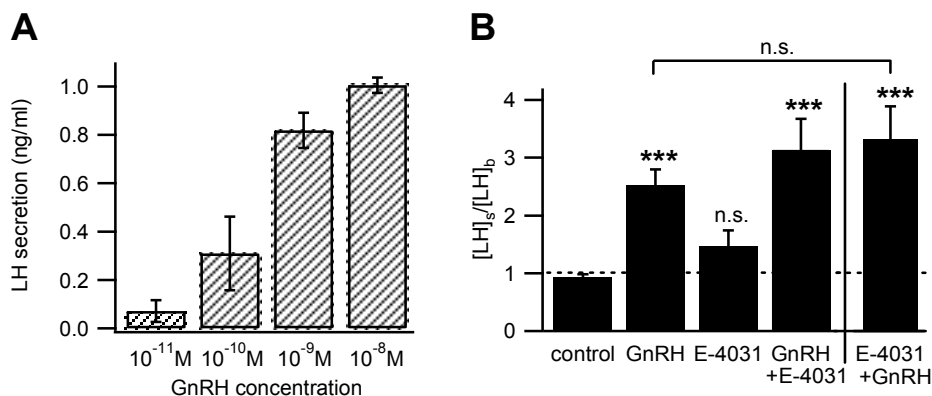


Fig. IV.22: LH secretion of cultured pituitaries measured with ELISA. A, Dose-response curve of LH secretion in response to increasing GnRH concentrations ($n = 6$ mice). B, LH secretion in response to erg channel block and GnRH receptor stimulation. Individual values ($[LH]_s$) were normalized to their control before stimulation ($[LH]_b$). Four left bars, LH secretion before and after addition of no substance (control), 0.1 nM GnRH (GnRH), 1 μ M E-4031 (E-4031), or 0.1 nM GnRH + 1 μ M E-4031 (GnRH + E-4031). Right bar, application of GnRH on top of E-4031 (E-4031 + GnRH). The asterisks denote significances against the individual controls (paired two-tailed Student's t-test, ***, $P < 0.001$, n.s., not significant). The square bracket between the second and fifth column indicates significance of the E-4031-pretreated GnRH-induced versus the GnRH-induced LH secretion (unpaired two-tailed Student's t-test, ns., not significant).

V. Discussion

Genetically modified mice made it possible to study the physiological properties of the entire population of mouse gonadotropes and to study erg K^+ channels and their function specifically in gonadotropes. Patch-clamp technique, calcium-imaging and ELISA measurements were employed in order to characterize functionally the mouse gonadotropes and the role of erg channels in these cells.

V.1. Heterogeneity of mouse gonadotropes

Fluorescent gonadotropes were found with a frequency of $\sim 15\%$ in primary pituitary cell cultures prepared from male GRIC/R26-YFP and GRIC/eR26- τ GFP mice, similar to the percentage reported for GnRH target cells in primary pituitary cell cultures prepared from male rats (Tibolt and Childs 1985). Fluorescent gonadotropes were easily identifiable allowing the study of all gonadotrope cells including those which were not stimulated by GnRH. The results revealed heterogeneity of the physiological properties of gonadotropes and of their response to GnRH (Fig. IV.3). The resting membrane potential of male mouse gonadotropes varied between -13 and -75 mV and 25% of these gonadotropes were spontaneously active. The broad range of resting membrane potentials was similar to ovine gonadotropes where the membrane potential ranged from -20 mV to -75 mV with a mean of -43 mV (Heyward, Chen et al. 1995). Application of GnRH in mouse gonadotropes generated heterogeneous responses ranging from cells which responded with initiation of slow hyperpolarized oscillations of the membrane potential, to cells which started to fire action potentials after GnRH stimulation. In between these two extremes were cells which responded to GnRH by sustained hyperpolarization or with small ongoing depolarization. The dependency of the membrane potential changes in response to different GnRH concentrations was similar to that observed in ovine gonadotropes (Heyward, Chen et al. 1995): while lower concentrations (1-10 nM) of GnRH evoked hyperpolarization followed by membrane potential oscillations and associated burst of action potentials, higher (100 nM) GnRH concentrations induced profound hyperpolarization and then depolarization occurred within 1 min. It has been already shown in rat gonadotropes that the oscillations in the membrane potential induced by GnRH are due to the initial increase in the $[Ca^{2+}]_i$ which activates the

Ca^{2+} -activated SK-type K^+ channels and decrease in $[\text{Ca}^{2+}]_i$ due to the transport of Ca^{2+} into the endoplasmic reticulum (Tse and Hille 1992; Hille, Tse et al. 1994; Hille, Tse et al. 1995; Stojilkovic 2005; Stojilkovic 2006). A similar heterogeneity was observed in the responses of $[\text{Ca}^{2+}]_i$ to GnRH application. GnRH could induce slow oscillations in $[\text{Ca}^{2+}]_i$ with a similar frequency as the membrane potential changes and plateau-like increases in the $[\text{Ca}^{2+}]_i$.

In voltage-clamp experiments in GRIC/R26-YFP gonadotropes the presence of the same major types of ion currents were found as previously described in rat (Stutzin, Stojilkovic et al. 1989; Tse and Hille 1993; Van Goor, Zivadinovic et al. 2001), female mouse (Waring and Turgeon 2006) and ovine (Heyward, Chen et al. 1995) gonadotropes. The biophysical properties of Na^+ currents measured in GRIC/R26-YFP mice gonadotropes were similar to those reported for rats (Tse and Hille 1992; Tse and Hille 1993; Van Goor, Zivadinovic et al. 2001) and ovariectomized female mice (Waring and Turgeon 2006). Outward rectifying K^+ and Ca^{2+} currents were also measured in GRIC/R26-YFP mice (Wen, Schwarz et al. 2008). Only L-type channels were present in mouse gonadotropes and there was no indication of T-type channels, similar to ovine gonadotropes (Heyward, Chen et al. 1995) and contrary to rat gonadotropes (Tse and Hille 1993; Van Goor, Zivadinovic et al. 2001). The total K^+ current density recorded in GRIC/R26-YFP mice was similar to the one found in ovariectomized female mice (Waring and Turgeon 2006). The mean current densities obtained for the transient and delayed-rectifying K^+ -current components were similar to the ones for rat gonadotropes (Van Goor, Zivadinovic et al. 2001) with the exception that the transient currents were smaller than the delayed-rectifying current in GRIC/R26-YFP mice gonadotropes. In addition, the Ca^{2+} -activated SK-type K^+ current was recorded as apamin-sensitive current in all gonadotropes.

V.2. Biophysical properties of erg K^+ currents in gonadotropes

Erg K^+ channels are present not only in the heart, where they mediate the rapidly activating component of the delayed-rectifying K^+ -current (Curran, Splawski et al. 1995; Sanguinetti, Curran et al. 1996), but they are also expressed in lactotropes (Bauer and Schwarz 2001), smooth muscle cells (Ohya, Horowitz et al. 2002; Mewe, Wulfsen et al. 2008) and in different cells in the brain, e.g.: Purkinje neurons in the cerebellum (Sacco, Bruno et al. 2003), serotonergic neurons in the raphe nuclei (Hirdes, Schweizer et al. 2005) and mitral cells in the

olfactory bulb (Hirdes, Napp et al. 2009). This work reports the presence of erg K⁺ currents and their characterization in mouse gonadotropes published in Hirdes et al., 2010.

Comparison of the activation of the erg K⁺ currents in gonadotropes recorded in pituitary slices with that of the erg K⁺ currents in gonadotropes maintained in culture revealed no significant differences between these two preparations. Therefore, most electrophysiological experiments were done in gonadotropes maintained in culture because pharmacology could be better performed on isolated cells. In undissociated gonadotropes, erg K⁺ currents activated at $V_{1/2} = -42$ mV. Activation was close to the observed resting membrane potentials in gonadotropes similar to the erg K⁺ current in raphe neurons ($V_{1/2} = -56$ mV (Hirdes, Schweizer et al. 2005)), in cerebellar Purkinje neurons ($V_{1/2} = -50$ mV (Sacco, Bruno et al. 2003)) and in mitral cells ($V_{1/2} = -52$ mV (Hirdes, Napp et al. 2009)).

Like other voltage-dependent K⁺ channels, erg K⁺ channels are composed of four subunits which can form either homomeric or heteromeric channels (Wimmers, Bauer et al. 2002). In mouse gonadotropes transcripts of two members (erg1a and erg2) were detected by single cell RT-PCR technique, whereas the other members (erg1b and erg3) were not present (Suppl. Fig. 3: (Hirdes, Dinu et al. 2010)). Erg1b and erg3 are characterized by fast deactivation kinetics (Wimmers, Bauer et al. 2002), so the relatively slow currents recorded in mouse gonadotropes could be carried by homomeric erg1a or erg2 or by heteromeric erg1a-erg2 channels. The half activation values of erg K⁺ currents were measured in a solution containing 40 mM K⁺ and free Ca²⁺ in nanomolar concentration and not in a low [K⁺]_e, with normal Ca²⁺ (1 μM) where the activation curve would have been shifted by about 15 mV to more positive membrane potential (Johnson, Mullins et al. 1999). However, in current-clamp experiments performed in a low K⁺ external solution a current component at -50 mV could be blocked by E-4031. This current is most likely mediated by erg K⁺ channels which have a “window current” near -50 mV due to the overlap of voltage-dependent activation and inactivation (Shi, Wymore et al. 1997; Kirchberger, Wulfsen et al. 2006). The pharmacological blockage of erg K⁺ channels by E-4031 depolarized the membrane potential and increased the [Ca²⁺]_i. The increase in the [Ca²⁺]_i could be abolished by nifedipine suggesting that it was mediated by L-type Ca²⁺ channels. Since E-4031 is an open channel blocker (Hancox and James 2008; Perrin, Kuchel et al. 2008), only the small fraction of open erg K⁺ channels at resting potential was blocked by E-4031 thereby inducing the initially small and delayed depolarization which successively opens more erg channels to become blocked, finally inducing a steady-state depolarization. These results demonstrate that erg K⁺ current can contribute to the maintenance of the resting membrane potential of about -50 mV.

A characteristic property of erg channels is that their conductance increases with the increase in the extracellular K^+ concentration. In cardiac myocytes the erg channel conductance increases with the square root of the $[K^+]_e$ concentration ratio (Shibasaki 1987). In mouse gonadotropes the conductance increased only by a factor of 1.6, smaller than the value of 1.94 reported by Shibasaki (1987).

Another factor that increases the erg K^+ current amplitude is higher temperature. In mouse gonadotropes the maximum available erg K^+ current increased by a factor of 1.7 for a 10°C increase (ΔT), relatively less than reported for HERG currents (4.7 for 15°C ΔT , (Vandenberg, Varghese et al. 2006); 2.2 for 12°C ΔT , (Zhou, Gong et al. 1998)) expressed in vitro.

In my experiments 10°C temperature increase substantially accelerated the time courses of deactivation and recovery from inactivation three to four times. This is about twice as much regarding deactivation and slightly higher regarding recovery from inactivation, as reported for HERG in vitro (Zhou, Gong et al. 1998; Vandenberg, Varghese et al. 2006). Contrary to the results by these authors, there was no temperature dependence of the voltage-dependence of erg K^+ current activation in gonadotropes. The observed 10 mV shift in the voltage-dependence of availability may therefore be explained by the fact, that the availability protocol is too short to achieve steady-state deactivation, so a change in the time constant of deactivation influences the amount of remaining current, thus leading to an apparent shift in the voltage dependence. Increased temperatures resulted in depolarizing shifts in $V_{1/2}$ of inactivation for voltage-gated Na^+ channels (Schwarz 1986; Murray, Anno et al. 1990; Ruff 1999) and for the C-type inactivation in Shaker K^+ channels (Meyer and Heinemann 1997) but only small shifts in the $V_{1/2}$ of activation for Shaker K^+ channels (Rodriguez, Sigg et al. 1998) and minimal shift for Na^+ channels (Schwarz 1986; Ruff 1999). When the Q_{10} values for deactivation and recovery from deactivation were compared with the ones in the literature, there is a substantial increase in mouse gonadotropes (2.88 for deactivation at -100 mV and 3.9 for recovery from inactivation at -100 mV) in comparison to CHO cells transfected with HERG (1.7 for deactivation and 2.6 for recovery from inactivation: (Vandenberg, Varghese et al. 2006)), and HEK293 cells transfected with HERG (1.25 and 1.36 for slow and fast deactivation and 3.6 for recovery from inactivation: (Zhou, Gong et al. 1998)). This correlates with the fact that there was no shift in the activation-dependence at higher temperatures. To better understand the whole process of erg K^+ channels temperature-sensitivity is needed an analysis of temperature-dependence of activation and inactivation kinetics.

V.3. Inhibition of erg K⁺ currents by GnRH

GnRH induced a strong inhibition of the erg K⁺ currents in mouse gonadotropes by two biophysical changes: reduction of the maximal erg K⁺ current amplitude by about 40% and a shift in the activation curve in a subpopulation of gonadotropes by about 25 mV to more positive potentials. The inhibition of the erg K⁺ current fraction active near the resting membrane potential by GnRH was comparable to the E-4031 blockage and could explain the small GnRH-induced depolarization observed in most gonadotropes (Fig. IV.3, A, D and E). There are several examples of erg K⁺ current modulation by G_{q/11}-coupled receptors which act by a similar mechanism of action: a reduction of the maximal current and a shift of the activation curve towards more positive potentials, e.g. inhibition by TRH in lactotropes (Bauer, Meyerhof et al. 1990; Bauer and Schwarz 2001; Schledermann, Wulfsen et al. 2001) or by mGlu receptor activation in mitral cells of the olfactory bulb (Hirdes, Napp et al. 2009) and in Purkinje cells of the cerebellum (Niculescu and Schwarz, Abstract). So far, the intracellular signaling cascade mediating the erg K⁺ current reduction by GnRH, TRH or glutamate is still unknown or controversial and is dependent on the different cell types or expression systems.

GnRH induced a shift only in about half of gonadotropes confirming the previously observed heterogeneity of gonadotropes, e.g. only half of LH-containing cells do not release LH in response to GnRH (Smith, Frawley et al. 1984) and half of the YFP-labeled gonadotropes did not trigger LH-induced plaque formation in the reverse hemolytic plaque assay (Wen, Schwarz et al. 2008). The observed heterogeneity could be caused by variable GnRH-receptor expression levels (Lin, Wu et al. 2010), variations in the subunit composition of erg K⁺ channels in mouse gonadotropes (Hirdes, Dinu et al. 2010), variable phosphorylation states (Chen, An et al. 2009), or binding of different types of auxiliary β -subunits (Cui, Kagan et al. 2001), which might alter the susceptibility of the erg K⁺ channels to modulation. This heterogeneity may explain that about 50% of the LH-containing cells do not release LH in response to GnRH (Smith, Frawley et al. 1984) and that about 50% of the YFP-labeled gonadotropes could not produce plaques in the reverse hemolytic plaque assay (Fig. 8: (Wen, Schwarz et al. 2008)).

Specific erg K⁺ current block induced a significant peak increase in [Ca²⁺]_i by more than 30% and GnRH by more than 80%, but the peak increase in [Ca²⁺]_i induced by both substances together was not additive. The reason might be that GnRH already largely reduced the erg K⁺ current close to the threshold potential of L-type Ca²⁺ channel activation, which were

involved in the slow Ca^{2+} increase after erg K^+ channel block. Since the erg current modulation by GnRH cannot be prevented due to the lack of knowledge about the underlying signaling cascade, the contribution of erg K^+ current inhibition to the GnRH-induced $[\text{Ca}^{2+}]_i$ increase cannot be determined at this moment.

Accordingly, the decaying plateau phase of elevated $[\text{Ca}^{2+}]_i$ in the continued presence of GnRH was not altered by specific erg current block. Notably, E-4031 significantly shortened the GnRH-induced $[\text{Ca}^{2+}]_i$ rise time, possibly because the internal $[\text{Ca}^{2+}]_i$ stores are refilled more quickly due to L-type Ca^{2+} channel activation.

The significant increase in the $[\text{Ca}^{2+}]_i$ by blockage of erg K^+ channels by E-4031 was not sufficient to stimulate LH secretion in mouse gonadotropes, possibly because protein kinase C activation is necessary to sensitize the exocytotic response to a submicromolar $[\text{Ca}^{2+}]_i$ concentration range (Jobin, Tomic et al. 1995). As expected, GnRH induced a strong increase in LH secretion in mouse gonadotropes.

V.4. The GnRH-activated signaling cascade involves influx of Ca^{2+}

Binding of GnRH to its receptor in the plasma membrane of gonadotropes activates $\text{G}_{q/11}$ -coupled receptor proteins to produce IP_3 and DAG by hydrolysis of PIP_2 . IP_3 induces an initial increase in $[\text{Ca}^{2+}]_i$ due to release of Ca^{2+} from endoplasmic reticulum (Kraus, Naor et al. 2001; Pawson and McNeilly 2005; Stojilkovic, Zemkova et al. 2005; Jeong and Kaiser 2006; Millar 2006). A model of this signaling cascade is shown in Fig. V.1. GnRH induces an influx of Ca^{2+} through voltage-dependent Ca^{2+} channels to maintain the sustained increase in $[\text{Ca}^{2+}]_i$. The removal of extracellular Ca^{2+} leads to a reduced transient initial peak and plateau $[\text{Ca}^{2+}]_i$ (Shangold, Murphy et al. 1988; Tomic, Cesnajaj et al. 1994; Blum, Reed et al. 2000) and limits the duration of $[\text{Ca}^{2+}]_i$ increase to 200-300 s (Iida, Stojilkovic et al. 1991; Tomic, Cesnajaj et al. 1994). The LH secretion is also dependent on $[\text{Ca}^{2+}]_e$. In a Ca^{2+} -free solution the GnRH-induced LH secretion is reduced to an initial fast and transient LH release presumably reflecting the release from intracellular stores, whereas in the presence of extracellular Ca^{2+} GnRH induces a prolonged increase in LH secretion (McArdle and Poch 1992). LH secretion in a Ca^{2+} -free solution is even abolished if it is stimulated by a depolarization induced by an elevated external K^+ concentration (Chang, Stojilkovic et al.

1988). This demonstrates that Ca^{2+} influx through voltage-dependent Ca^{2+} channels is important for mediating the sustained phase of LH secretion.

Ca^{2+} channels are present in native rat (Tse and Hille 1993; Van Goor, Zivadinovic et al. 2001; Stojilkovic, Zemkova et al. 2005), ovine (Heyward, Chen et al. 1995) and mouse gonadotropes (Wen, Schwarz et al. 2008). In all these cells, about 50% of the Ca^{2+} currents are blocked by nifedipine (10 μM) indicating that this current fraction is mediated by L-type Ca^{2+} channels. An increase of $[\text{Ca}^{2+}]_i$ by influx of Ca^{2+} could physiologically occur by an increase in the action potential frequency, which are carried by Ca^{2+} in gonadotropes (Hille, Tse et al. 1995) unlike by Na^+ in neurons. GnRH triggers regular oscillations of $[\text{Ca}^{2+}]_i$ and the membrane potential and superimposed on the depolarizing phases of these oscillations bursts of action potentials may be generated which can increase Ca^{2+} influx (Hille, Tse et al. 1995). However, there are also quiescent cells which respond to GnRH with short hyperpolarizing potentials or/and small depolarizations. The strong reduction of the erg K^+ current and subsequent depolarization of the membrane potential induced by GnRH could provide a mechanism for initiation of a steady-state Ca^{2+} influx through L-type Ca^{2+} channels at least in gonadotropes which do not fire action potentials. Depolarization-induced steady-state Ca^{2+} influx could be also brought about by GnRH inhibition of A-type K^+ currents which activate at a similar voltage as erg K^+ currents (Van Goor, Zivadinovic et al. 2001; Waring and Turgeon 2006; Wen, Schwarz et al. 2008). Alternatively, GnRH could directly activate a Ca^{2+} current or an unspecific cation current like the one activated by mGlu receptors in mitral/tufted neurons (Heinbockel, Heyward et al. 2004). This work shows that a small depolarization is able to activate voltage-dependent Ca^{2+} channels because a depolarization to -50 mV increases $[\text{Ca}^{2+}]_i$ in voltage-clamped mouse gonadotropes. Voltage-dependent Ca^{2+} channels in gonadotropes start to activate at membrane potentials positive to -50 mV (Wen, Schwarz et al. 2008), similarly to those observed in somato-mammotrope GH3 cells (Scherubl and Hescheler 1991). Thus, one role of the erg K^+ channels in gonadotropes might be to limit steady-state Ca^{2+} influx at rest and to enable Ca^{2+} replenishment during GnRH stimulation. The functional importance of the GnRH-induced reduction of erg currents within the complex GnRH-activated events leading to increase in $[\text{Ca}^{2+}]_i$ and LH secretion remains to be determined.

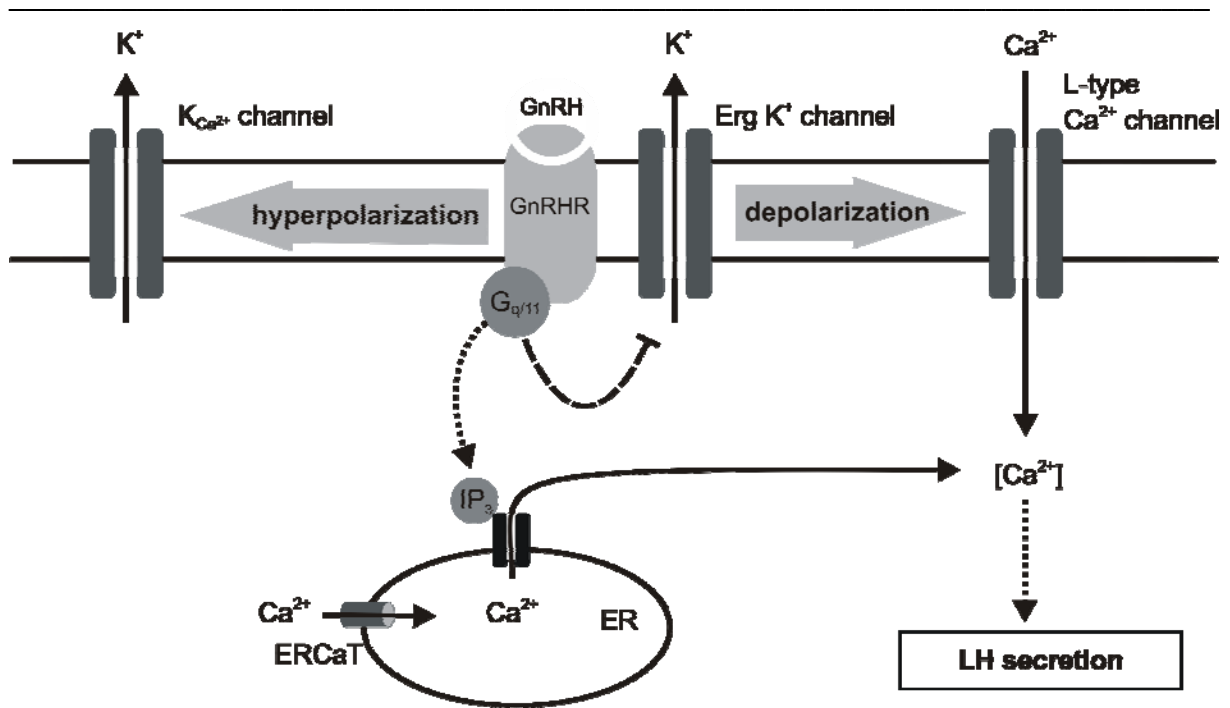


Fig. V.1: Hypothetical model of intracellular signaling cascade activated by binding of GnRH to its receptor in the plasma membrane of gonadotropes. Binding of GnRH to its receptor (GnRHR) in the plasma membrane activates $G_{q/11}$ -proteins thereby generating IP_3 (inositol-1,4,5-trisphosphate). IP_3 binds to the IP_3 receptor (IP_3 -R) leading to release of Ca^{2+} from the endoplasmic reticulum (ER). Ca^{2+} is pumped into the ER by the endoplasmic reticulum Ca^{2+} transporter (ERCaT). The changes in the intracellular Ca^{2+} level induce opening and closing of Ca^{2+} -dependent potassium channels ($K_{Ca^{2+}}$). Activation of $G_{q/11}$ G proteins also inhibits erg K^+ channels via an as yet unknown intracellular signal cascade, inducing a membrane potential depolarization allowing influx of external Ca^{2+} through activated voltage-dependent Ca^{2+} channels.

VI. References

1. Abbott, G. W., F. Sesti, et al. (1999). "MiRP1 forms IKr potassium channels with HERG and is associated with cardiac arrhythmia." Cell **97**(2): 175-87.
2. Alonso-Ron, C., F. Barros, et al. (2009). "Participation of HERG channel cytoplasmic structures on regulation by the G protein-coupled TRH receptor." Pflugers Arch **457**(6): 1237-52.
3. Baker, B. L. and D. S. Gross (1978). "Cytology and distribution of secretory cell types in the mouse hypophysis as demonstrated with immunocytochemistry." Am J Anat **153**(2): 193-215.
4. Ball, S. G. (2007). "Vasopressin and disorders of water balance: the physiology and pathophysiology of vasopressin." Ann Clin Biochem **44**(Pt 5): 417-31.
5. Barros, F., D. Gomez-Varela, et al. (1998). "Modulation of human erg K⁺ channel gating by activation of a G protein-coupled receptor and protein kinase C." J Physiol **511** (Pt 2): 333-46.
6. Barros, F., G. Mieskes, et al. (1993). "Protein phosphatase 2A reverses inhibition of inward rectifying K⁺ currents by thyrotropin-releasing hormone in GH3 pituitary cells." FEBS Lett **336**(3): 433-9.
7. Bauer, C. K., B. Engeland, et al. (1998). "RERG is a molecular correlate of the inward-rectifying K current in clonal rat pituitary cells." Receptors Channels **6**(1): 19-29.
8. Bauer, C. K., W. Meyerhof, et al. (1990). "An inward-rectifying K⁺ current in clonal rat pituitary cells and its modulation by thyrotrophin-releasing hormone." J Physiol **429**: 169-89.
9. Bauer, C. K., R. Schafer, et al. (1999). "A functional role of the erg-like inward-rectifying K⁺ current in prolactin secretion from rat lactotrophs." Mol Cell Endocrinol **148**(1-2): 37-45.
10. Bauer, C. K. and J. R. Schwarz (2001). "Physiology of EAG K⁺ channels." J Membr Biol **182**(1): 1-15.
11. Bian, J., J. Cui, et al. (2001). "HERG K(+) channel activity is regulated by changes in phosphatidyl inositol 4,5-bisphosphate." Circ Res **89**(12): 1168-76.
12. Bianchi, L., B. Wible, et al. (1998). "herg encodes a K⁺ current highly conserved in tumors of different histogenesis: a selective advantage for cancer cells?" Cancer Res **58**(4): 815-22.

13. Blum, J. J., M. C. Reed, et al. (2000). "A mathematical model quantifying GnRH-induced LH secretion from gonadotropes." Am J Physiol Endocrinol Metab **278**(2): E263-72.
14. Brelidze, T. I., A. E. Carlson, et al. (2009). "Absence of direct cyclic nucleotide modulation of mEAG1 and hERG1 channels revealed with fluorescence and electrophysiological methods." J Biol Chem **284**(41): 27989-97.
15. Chandy, K. G. and G. A. Gutman (1995). Voltage-gated potassium channel genes. In: Handbook of Receptors and Channels. R. A. North. Boca Raton, Ann Arbor, London, Tokyo, CRC Press: 1-171.
16. Chang, J. P., S. S. Stojilkovic, et al. (1988). "Gonadotropin-releasing hormone stimulates luteinizing hormone secretion by extracellular calcium-dependent and -independent mechanisms." Endocrinology **123**(1): 87-97.
17. Chen, J., B. S. An, et al. (2009). "Gonadotropin-releasing hormone-mediated phosphorylation of estrogen receptor-alpha contributes to fosB expression in mouse gonadotrophs." Endocrinology **150**(10): 4583-93.
18. Chen, J., A. Zou, et al. (1999). "Long QT syndrome-associated mutations in the Per-Arnt-Sim (PAS) domain of HERG potassium channels accelerate channel deactivation." J Biol Chem **274**(15): 10113-8.
19. Childs, G. V. (2006). Gonadotropes and lactotropes. Knobil and Neill's physiology of reproduction. N. J. Knobil E. Amsterdam, Elsevier: 1483-1579.
20. Clayton, R. N. and K. J. Catt (1981). "Gonadotropin-releasing hormone receptors: characterization, physiological regulation, and relationship to reproductive function." Endocr Rev **2**(2): 186-209.
21. Cockerill, S. L., A. B. Tobin, et al. (2007). "Modulation of hERG potassium currents in HEK-293 cells by protein kinase C. Evidence for direct phosphorylation of pore forming subunits." J Physiol **581**(Pt 2): 479-93.
22. Coetzee, W. A., Y. Amarillo, et al. (1999). "Molecular diversity of K⁺ channels." Ann N Y Acad Sci **868**: 233-85.
23. Cole, K. S. and J. W. Moore (1960). "Ionic current measurements in the squid giant axon membrane." J Gen Physiol **44**: 123-67.
24. Corrette, B. J., C. K. Bauer, et al. (1995). Electrophysiology of anterior pituitary cells. The ELECTROPHYSIOLOGY of NEUROENDOCRINE CELLS. H. Scherubl and J. Hescheler, CRC Press Inc.: 101-143.

25. Cui, J., A. Kagan, et al. (2001). "Analysis of the cyclic nucleotide binding domain of the HERG potassium channel and interactions with KCNE2." *J Biol Chem* **276**(20): 17244-51.
26. Cui, J., Y. Melman, et al. (2000). "Cyclic AMP regulates the HERG K(+) channel by dual pathways." *Curr Biol* **10**(11): 671-4.
27. Curran, M. E., I. Splawski, et al. (1995). "A molecular basis for cardiac arrhythmia: HERG mutations cause long QT syndrome." *Cell* **80**(5): 795-803.
28. Daughaday, W. H., M. Kapadia, et al. (1985). "Insulin-like growth factors I and II of nonmammalian sera." *Gen Comp Endocrinol* **59**(2): 316-25.
29. Eggan, K., K. Baldwin, et al. (2004). "Mice cloned from olfactory sensory neurons." *Nature* **428**(6978): 44-9.
30. Engeland, B., A. Neu, et al. (1998). "Cloning and functional expression of rat ether-a-go-go-like K⁺ channel genes." *J Physiol* **513** (Pt 3): 647-54.
31. Evans, V. R., A. B. Manning, et al. (1994). "Alpha-melanocyte-stimulating hormone and N-acetyl-beta-endorphin immunoreactivities are localized in the human pituitary but are not restricted to the zona intermedia." *Endocrinology* **134**(1): 97-106.
32. Fan, J. S., M. Jiang, et al. (1999). "Effects of outer mouth mutations on hERG channel function: a comparison with similar mutations in the Shaker channel." *Biophys J* **76**(6): 3128-40.
33. Gainer, H. and S. Wray (1994). Cellular and molecular biology of oxytocin and vasopressin. *The Physiology of Reproduction*. N. J. Knobil E. New York, Raven Press: 1099-1129.
34. Ganetzky, B., G. A. Robertson, et al. (1999). "The eag family of K⁺ channels in *Drosophila* and mammals." *Ann N Y Acad Sci* **868**: 356-69.
35. Goldstein, S. A., K. W. Wang, et al. (1998). "Sequence and function of the two P domain potassium channels: implications of an emerging superfamily." *J Mol Med* **76**(1): 13-20.
36. Grynkiewicz, G., M. Poenie, et al. (1985). "A new generation of Ca²⁺ indicators with greatly improved fluorescence properties." *J Biol Chem* **260**(6): 3440-50.
37. Gurrola, G. B., B. Rosati, et al. (1999). "A toxin to nervous, cardiac, and endocrine ERG K⁺ channels isolated from *Centruroides noxius* scorpion venom." *FASEB J* **13**(8): 953-62.
38. Gutman, G. A., K. G. Chandy, et al. (2005). "International Union of Pharmacology. LIII. Nomenclature and molecular relationships of voltage-gated potassium channels." *Pharmacol Rev* **57**(4): 473-508.

39. Hadley, E. M. and E. J. Levine (2007). *Endocrinology*. B. Cummings.
40. Hamill, O. P., A. Marty, et al. (1981). "Improved patch-clamp techniques for high-resolution current recording from cells and cell-free membrane patches." *Pflugers Arch* **391**(2): 85-100.
41. Hancox, J. C. and A. F. James (2008). "Refining insights into high-affinity drug binding to the human ether-a-go-go-related gene potassium channel." *Mol Pharmacol* **73**(6): 1592-5.
42. Hancox, J. C., H. J. Witchel, et al. (1998). "Alteration of HERG current profile during the cardiac ventricular action potential, following a pore mutation." *Biochem Biophys Res Commun* **253**(3): 719-24.
43. Heinbockel, T., P. Heyward, et al. (2004). "Regulation of main olfactory bulb mitral cell excitability by metabotropic glutamate receptor mGluR1." *J Neurophysiol* **92**(5): 3085-96.
44. Herzberg, I. M., M. C. Trudeau, et al. (1998). "Transfer of rapid inactivation and sensitivity to the class III antiarrhythmic drug E-4031 from HERG to M-eag channels." *J Physiol* **511 (Pt 1)**: 3-14.
45. Heyward, P. M., C. Chen, et al. (1995). "Inward membrane currents and electrophysiological responses to GnRH in ovine gonadotropes." *Neuroendocrinology* **61**(6): 609-21.
46. Hille, B. (2001). *Ion Channels of Excitable Membranes*. Sunderland, Sinauer Associates, Inc.
47. Hille, B., A. Tse, et al. (1994). "Calcium oscillations and exocytosis in pituitary gonadotropes." *Ann N Y Acad Sci* **710**: 261-70.
48. Hille, B., A. Tse, et al. (1995). "Signaling mechanisms during the response of pituitary gonadotropes to GnRH." *Recent Prog Horm Res* **50**: 75-95.
49. Hiller-Sturmhofel, S. and A. Bartke (1998). "The endocrine system: an overview." *Alcohol Health Res World* **22**(3): 153-64.
50. Hirdes, W., C. Dinu, et al. (2010). "Gonadotropin-releasing hormone inhibits ether-a-go-go-related gene K⁺ currents in mouse gonadotropes." *Endocrinology* **151**(3): 1079-88.
51. Hirdes, W., L. F. Horowitz, et al. (2004). "Muscarinic modulation of erg potassium current." *J Physiol* **559**(Pt 1): 67-84.
52. Hirdes, W., N. Napp, et al. (2009). "Erg K⁺ currents modulate excitability in mouse mitral/tufted neurons." *Pflugers Arch* **459**(1): 55-70.

53. Hirdes, W., M. Schweizer, et al. (2005). "Fast erg K⁺ currents in rat embryonic serotonergic neurones." J Physiol **564**(Pt 1): 33-49.
54. Ho, W. K., Y. E. Earm, et al. (1996). "Voltage- and time-dependent block of delayed rectifier K⁺ current in rabbit sino-atrial node cells by external Ca²⁺ and Mg²⁺." J Physiol **494** (Pt 3): 727-42.
55. Hodgkin, A. L. and A. F. Huxley (1952). "The components of membrane conductance in the giant axon of Loligo." J Physiol **116**(4): 473-96.
56. Hodgkin, A. L. and A. F. Huxley (1952). "A quantitative description of membrane current and its application to conduction and excitation in nerve." J Physiol **117**(4): 500-44.
57. Horn, R. and A. Marty (1988). "Muscarinic activation of ionic currents measured by a new whole-cell recording method." J Gen Physiol **92**(2): 145-59.
58. Iida, T., S. S. Stojilkovic, et al. (1991). "Spontaneous and agonist-induced calcium oscillations in pituitary gonadotrophs." Mol Endocrinol **5**(7): 949-58.
59. Jeong, K. H. and U. B. Kaiser (2006). Gonadotropin-releasing hormone regulation of gonadotropin biosynthesis and secretion. In: Knobil and Neill's physiology of reproduction. N. J. Knobil E. Amsterdam, Elsevier Academic Press. **1**: 1635-1701.
60. Jiang, Y., A. Lee, et al. (2003). "X-ray structure of a voltage-dependent K⁺ channel." Nature **423**(6935): 33-41.
61. Jobin, R. M., M. Tomic, et al. (1995). "Gonadotropin-releasing hormone-induced sensitization of calcium-dependent exocytosis in pituitary gonadotrophs." Endocrinology **136**(8): 3398-405.
62. Johnson, J. P., Jr., F. M. Mullins, et al. (1999). "Human ether-a-go-go-related gene K⁺ channel gating probed with extracellular ca²⁺. Evidence for two distinct voltage sensors." J Gen Physiol **113**(4): 565-80.
63. Jones, E. M., E. C. Roti Roti, et al. (2004). "Cardiac IKr channels minimally comprise hERG 1a and 1b subunits." J Biol Chem **279**(43): 44690-4.
64. Kao, J. P. (1994). "Practical aspects of measuring [Ca²⁺] with fluorescent indicators." Methods Cell Biol **40**: 155-81.
65. Karle, C. A., E. Zitron, et al. (2002). "Rapid component I(Kr) of the guinea-pig cardiac delayed rectifier K(+) current is inhibited by beta(1)-adrenoreceptor activation, via cAMP/protein kinase A-dependent pathways." Cardiovasc Res **53**(2): 355-62.
66. Kelberman, D., K. Rizzoti, et al. (2009). "Genetic regulation of pituitary gland development in human and mouse." Endocr Rev **30**(7): 790-829.

67. Kiehn, J., A. E. Lacerda, et al. (1996). "Molecular physiology and pharmacology of HERG. Single-channel currents and block by dofetilide." Circulation **94**(10): 2572-9.
68. Kirchberger, N. M., I. Wulfsen, et al. (2006). "Effects of TRH on heteromeric rat *erg1a/1b* K⁺ channels are dominated by the *regr1b* subunit." J Physiol **571**(Pt 1): 27-42.
69. Kraus, S., Z. Naor, et al. (2001). "Intracellular signaling pathways mediated by the gonadotropin-releasing hormone (GnRH) receptor." Arch Med Res **32**(6): 499-509.
70. Kubo, Y., J. P. Adelman, et al. (2005). "International Union of Pharmacology. LIV. Nomenclature and molecular relationships of inwardly rectifying potassium channels." Pharmacol Rev **57**(4): 509-26.
71. Kukuljan, M., S. S. Stojilkovic, et al. (1992). "Apamin-sensitive potassium channels mediate agonist-induced oscillations of membrane potential in pituitary gonadotrophs." FEBS Lett **301**(1): 19-22.
72. Kupershmidt, S., D. J. Snyders, et al. (1998). "A K⁺ channel splice variant common in human heart lacks a C-terminal domain required for expression of rapidly activating delayed rectifier current." J Biol Chem **273**(42): 27231-5.
73. Lees-Miller, J. P., C. Kondo, et al. (1997). "Electrophysiological characterization of an alternatively processed ERG K⁺ channel in mouse and human hearts." Circ Res **81**(5): 719-26.
74. Leng, S. X., J. E. McElhaney, et al. (2008). "ELISA and multiplex technologies for cytokine measurement in inflammation and aging research." J Gerontol A Biol Sci Med Sci **63**(8): 879-84.
75. Lesage, F., E. Guillemare, et al. (1996). "TWIK-1, a ubiquitous human weakly inward rectifying K⁺ channel with a novel structure." EMBO J **15**(5): 1004-11.
76. Lin, C. J., G. C. Wu, et al. (2010). "Regulation of two forms of gonadotropin-releasing hormone receptor gene expression in the protandrous black porgy fish, *Acanthopagrus schlegeli*." Mol Cell Endocrinol **323**(2): 137-46.
77. Lippiat, J. D. (2008). "Whole-cell recording using the perforated patch clamp technique." Methods Mol Biol **491**: 141-9.
78. Lobe, C. G., K. E. Koop, et al. (1999). "Z/AP, a double reporter for cre-mediated recombination." Dev Biol **208**(2): 281-92.
79. London, B., M. C. Trudeau, et al. (1997). "Two isoforms of the mouse ether-a-go-go-related gene coassemble to form channels with properties similar to the rapidly activating component of the cardiac delayed rectifier K⁺ current." Circ Res **81**(5): 870-8.
80. Ludwig, J., H. Terlau, et al. (1994). "Functional expression of a rat homologue of the voltage gated ether-a-go-go potassium channel reveals differences in selectivity and

- activation kinetics between the *Drosophila* channel and its mammalian counterpart." EMBO J **13**(19): 4451-8.
81. Malgaroli, A., L. Vallar, et al. (1987). "Dopamine inhibits cytosolic Ca²⁺ increases in rat lactotroph cells. Evidence of a dual mechanism of action." J Biol Chem **262**(29): 13920-7.
82. Marmont, G. (1949). "Studies on the axon membrane; a new method." J Cell Physiol **34**(3): 351-82.
83. McArdle, C. A. and A. Poch (1992). "Dependence of gonadotropin-releasing hormone-stimulated luteinizing hormone release upon intracellular Ca²⁺ pools is revealed by desensitization and thapsigargin blockade." Endocrinology **130**(6): 3567-74.
84. McDonald, T. V., Z. Yu, et al. (1997). "A minK-HERG complex regulates the cardiac potassium current I(Kr)." Nature **388**(6639): 289-92.
85. Mewe, M., M. Mauerhofer, et al. (2010). "Modulation of cardiac ERG1 K(+) channels by cGMP signaling." J Mol Cell Cardiol **49**(1): 48-57.
86. Mewe, M., I. Wulfsen, et al. (2008). "Erg K+ channels modulate contractile activity in the bovine epididymal duct." Am J Physiol Regul Integr Comp Physiol **294**(3): R895-904.
87. Meyer, R. and S. H. Heinemann (1997). "Temperature and pressure dependence of Shaker K+ channel N- and C-type inactivation." Eur Biophys J **26**(6): 433-45.
88. Millar, R. P. (2006). Gonadotrophin releasing hormone. In: Handbook of biologically active peptides, Elsevier Academic Press: 635-644.
89. Morais Cabral, J. H., A. Lee, et al. (1998). "Crystal structure and functional analysis of the HERG potassium channel N terminus: a eukaryotic PAS domain." Cell **95**(5): 649-55.
90. Murray, K. T., T. Anno, et al. (1990). "Voltage clamp of the cardiac sodium current at 37 degrees C in physiologic solutions." Biophys J **57**(3): 607-13.
91. Neher, E. and B. Sakmann (1992). "The patch clamp technique." Sci Am **266**(3): 44-51.
92. Ohya, S., B. Horowitz, et al. (2002). "Functional and molecular identification of ERG channels in murine portal vein myocytes." Am J Physiol Cell Physiol **283**(3): C866-77.
93. Pawson, A. J. and A. S. McNeilly (2005). "The pituitary effects of GnRH." Anim Reprod Sci **88**(1-2): 75-94.
94. Perrin, M. J., P. W. Kuchel, et al. (2008). "Drug binding to the inactivated state is necessary but not sufficient for high-affinity binding to human ether-a-go-go-related gene channels." Mol Pharmacol **74**(5): 1443-52.
95. Pongs, O. (1992). "Molecular biology of voltage-dependent potassium channels." Physiol Rev **72**(4 Suppl): S69-88.

96. Rauer, S. and A. Conrad (2001). "Competitive inhibition ELISA for the detection of *Borrelia burgdorferi* antigens--failure to detect antigen in the cerebrospinal fluid from patients with neuroborreliosis." J Med Microbiol **50**(6): 577-8.
97. Reid, G., C. K. Bauer, et al. (1996). "Most lactotrophs from lactating rats are able to respond to both thyrotropin-releasing hormone and dopamine." Mol Cell Endocrinol **124**(1-2): 121-9.
98. Reinhart, J., L. M. Mertz, et al. (1992). "Molecular cloning and expression of cDNA encoding the murine gonadotropin-releasing hormone receptor." J Biol Chem **267**(30): 21281-4.
99. Restano-Cassulini, R., T. Olamendi-Portugal, et al. (2008). "Two novel ergtoxins, blockers of K⁺-channels, purified from the Mexican scorpion *Centruroides elegans elegans*." Neurochem Res **33**(8): 1525-33.
100. Robertson, G. A., J. M. Warmke, et al. (1996). "Potassium currents expressed from *Drosophila* and mouse eag cDNAs in *Xenopus* oocytes." Neuropharmacology **35**(7): 841-50.
101. Rodriguez, B. M., D. Sigg, et al. (1998). "Voltage gating of Shaker K⁺ channels. The effect of temperature on ionic and gating currents." J Gen Physiol **112**(2): 223-42.
102. Rodriguez, C. I., F. Buchholz, et al. (2000). "High-efficiency deleter mice show that FLPe is an alternative to Cre-loxP." Nat Genet **25**(2): 139-40.
103. Rodriguez, I., P. Feinstein, et al. (1999). "Variable patterns of axonal projections of sensory neurons in the mouse vomeronasal system." Cell **97**(2): 199-208.
104. Ruff, R. L. (1999). "Effects of temperature on slow and fast inactivation of rat skeletal muscle Na⁽⁺⁾ channels." Am J Physiol **277**(5 Pt 1): C937-47.
105. Sacco, T., A. Bruno, et al. (2003). "Functional roles of an ERG current isolated in cerebellar Purkinje neurons." J Neurophysiol **90**(3): 1817-28.
106. Saganich, M. J., E. Vega-Saenz de Miera, et al. (1999). "Cloning of components of a novel subthreshold-activating K⁽⁺⁾ channel with a unique pattern of expression in the cerebral cortex." J Neurosci **19**(24): 10789-802.
107. Sanguinetti, M. C., M. E. Curran, et al. (1996). "Spectrum of HERG K⁺-channel dysfunction in an inherited cardiac arrhythmia." Proc Natl Acad Sci U S A **93**(5): 2208-12.
108. Sanguinetti, M. C., C. Jiang, et al. (1995). "A mechanistic link between an inherited and an acquired cardiac arrhythmia: HERG encodes the IKr potassium channel." Cell **81**(2): 299-307.
109. Schafer, R., I. Wulfsen, et al. (1999). "The erg-like potassium current in rat lactotrophs." J Physiol **518** (Pt 2): 401-16.

-
110. Scherubel, H. and J. Hescheler (1991). "Steady-state currents through voltage-dependent, dihydropyridine-sensitive Ca²⁺ channels in GH3 pituitary cells." Proc Biol Sci **245**(1313): 127-31.
111. Schledermann, W., I. Wulfsen, et al. (2001). "Modulation of rat *erg1*, *erg2*, *erg3* and HERG K⁺ currents by thyrotropin-releasing hormone in anterior pituitary cells via the native signal cascade." J Physiol **532**(Pt 1): 143-63.
112. Schonherr, R. and S. H. Heinemann (1996). "Molecular determinants for activation and inactivation of HERG, a human inward rectifier potassium channel." J Physiol **493** (Pt 3): 635-42.
113. Schonherr, R., B. Rosati, et al. (1999). "Functional role of the slow activation property of ERG K⁺ channels." Eur J Neurosci **11**(3): 753-60.
114. Schroeder, B. C., S. Waldegger, et al. (2000). "A constitutively open potassium channel formed by KCNQ1 and KCNE3." Nature **403**(6766): 196-9.
115. Schwarz, J. R. (1986). "The effect of temperature on Na currents in rat myelinated nerve fibres." Pflugers Arch **406**(4): 397-404.
116. Schwarz, J. R. and C. K. Bauer (1999). "The ether-a-go-go-Related Gene K(+) Current: Functions of a Strange Inward Rectifier." News Physiol Sci **14**: 135-142.
117. Sealfon, S. C., H. Weinstein, et al. (1997). "Molecular mechanisms of ligand interaction with the gonadotropin-releasing hormone receptor." Endocr Rev **18**(2): 180-205.
118. Shangold, G. A., S. N. Murphy, et al. (1988). "Gonadotropin-releasing hormone-induced Ca²⁺ transients in single identified gonadotropes require both intracellular Ca²⁺ mobilization and Ca²⁺ influx." Proc Natl Acad Sci U S A **85**(17): 6566-70.
119. Shi, W., H. S. Wang, et al. (1998). "Cloning of a mammalian elk potassium channel gene and EAG mRNA distribution in rat sympathetic ganglia." J Physiol **511** (Pt 3): 675-82.
120. Shi, W., R. S. Wymore, et al. (1997). "Identification of two nervous system-specific members of the *erg* potassium channel gene family." J Neurosci **17**(24): 9423-32.
121. Shibasaki, T. (1987). "Conductance and kinetics of delayed rectifier potassium channels in nodal cells of the rabbit heart." J Physiol **387**: 227-50.
122. Slominski, A., D. J. Tobin, et al. (2004). "Melanin pigmentation in mammalian skin and its hormonal regulation." Physiol Rev **84**(4): 1155-228.
123. Smith, P. F., L. S. Frawley, et al. (1984). "Detection of LH release from individual pituitary cells by the reverse hemolytic plaque assay: estrogen increases the fraction of gonadotropes responding to GnRH." Endocrinology **115**(6): 2484-6.

124. Smith, P. L., T. Baukrowitz, et al. (1996). "The inward rectification mechanism of the HERG cardiac potassium channel." Nature **379**(6568): 833-6.
125. Snyders, D. J. and A. Chaudhary (1996). "High affinity open channel block by dofetilide of HERG expressed in a human cell line." Mol Pharmacol **49**(6): 949-55.
126. Spector, P. S., M. E. Curran, et al. (1996). "Class III antiarrhythmic drugs block HERG, a human cardiac delayed rectifier K⁺ channel. Open-channel block by methanesulfonanilides." Circ Res **78**(3): 499-503.
127. Spinelli, W., I. F. Moubarak, et al. (1993). "Cellular electrophysiology of WAY-123,398, a new class III antiarrhythmic agent: specificity of IK block and lack of reverse use dependence in cat ventricular myocytes." Cardiovasc Res **27**(9): 1580-91.
128. Srinivas, S., T. Watanabe, et al. (2001). "Cre reporter strains produced by targeted insertion of EYFP and ECFP into the ROSA26 locus." BMC Dev Biol **1**: 4.
129. Stocker, M. (2004). "Ca²⁺-activated K⁺ channels: molecular determinants and function of the SK family." Nat Rev Neurosci **5**(10): 758-70.
130. Stojilkovic, S. S. (2005). "Ca²⁺-regulated exocytosis and SNARE function." Trends Endocrinol Metab **16**(3): 81-3.
131. Stojilkovic, S. S. (2006). "Pituitary cell type-specific electrical activity, calcium signaling and secretion." Biol Res **39**(3): 403-23.
132. Stojilkovic, S. S., M. Kukuljan, et al. (1992). "Integration of cytoplasmic calcium and membrane potential oscillations maintains calcium signaling in pituitary gonadotrophs." Proc Natl Acad Sci U S A **89**(9): 4081-5.
133. Stojilkovic, S. S., J. Reinhart, et al. (1994). "Gonadotropin-releasing hormone receptors: structure and signal transduction pathways." Endocr Rev **15**(4): 462-99.
134. Stojilkovic, S. S., H. Zemkova, et al. (2005). "Biophysical basis of pituitary cell type-specific Ca²⁺ signaling-secretion coupling." Trends Endocrinol Metab **16**(4): 152-9.
135. Strauss, U., M. Herbrik, et al. (2001). "Whole-cell patch-clamp: true perforated or spontaneous conventional recordings?" Pflugers Arch **442**(4): 634-8.
136. Sturm, P., S. Wimmers, et al. (2005). "Extracellular potassium effects are conserved within the rat erg K⁺ channel family." J Physiol **564**(Pt 2): 329-45.
137. Stutzin, A., S. S. Stojilkovic, et al. (1989). "Characteristics of two types of calcium channels in rat pituitary gonadotrophs." Am J Physiol **257**(5 Pt 1): C865-74.
138. Thomas, D., J. Kiehn, et al. (2004). "Adrenergic regulation of the rapid component of the cardiac delayed rectifier potassium current, I(Kr), and the underlying hERG ion channel." Basic Res Cardiol **99**(4): 279-87.

139. Tibolt, R. E. and G. V. Childs (1985). "Cytochemical and cytophysiological studies of gonadotropin-releasing hormone (GnRH) target cells in the male rat pituitary: differential effects of androgens and corticosterone on GnRH binding and gonadotropin release." Endocrinology **117**(1): 396-404.
140. Tomic, M., M. Cesnajak, et al. (1994). "Developmental and physiological aspects of Ca²⁺ signaling in agonist-stimulated pituitary gonadotrophs." Endocrinology **135**(5): 1762-71.
141. Trudeau, M. C., J. W. Warmke, et al. (1995). "HERG, a human inward rectifier in the voltage-gated potassium channel family." Science **269**(5220): 92-5.
142. Tse, A. and B. Hille (1992). "GnRH-induced Ca²⁺ oscillations and rhythmic hyperpolarizations of pituitary gonadotropes." Science **255**(5043): 462-4.
143. Tse, A. and B. Hille (1993). "Role of voltage-gated Na⁺ and Ca²⁺ channels in gonadotropin-releasing hormone-induced membrane potential changes in identified rat gonadotropes." Endocrinology **132**(4): 1475-81.
144. Turgeon, J. L. and D. W. Waring (1990). "Rapid augmentation by progesterone of agonist-stimulated luteinizing hormone secretion by cultured pituitary cells." Endocrinology **127**(2): 773-80.
145. Tutor, A. S., E. Delpon, et al. (2006). "Association of 14-3-3 proteins to beta1-adrenergic receptors modulates Kv11.1 K⁺ channel activity in recombinant systems." Mol Biol Cell **17**(11): 4666-74.
146. Van Goor, F., D. Zivadinovic, et al. (2001). "Differential expression of ionic channels in rat anterior pituitary cells." Mol Endocrinol **15**(7): 1222-36.
147. Vandenberg, J. I., A. Varghese, et al. (2006). "Temperature dependence of human ether-a-go-go-related gene K⁺ currents." Am J Physiol Cell Physiol **291**(1): C165-75.
148. Verheijck, E. E., A. C. van Ginneken, et al. (1995). "Effects of delayed rectifier current blockade by E-4031 on impulse generation in single sinoatrial nodal myocytes of the rabbit." Circ Res **76**(4): 607-15.
149. Vilorio, C. G., F. Barros, et al. (2000). "Differential effects of amino-terminal distal and proximal domains in the regulation of human erg K(+) channel gating." Biophys J **79**(1): 231-46.
150. Wang, J., C. D. Myers, et al. (2000). "Dynamic control of deactivation gating by a soluble amino-terminal domain in HERG K(+) channels." J Gen Physiol **115**(6): 749-58.
151. Wang, J., M. C. Trudeau, et al. (1998). "Regulation of deactivation by an amino terminal domain in human ether-a-go-go-related gene potassium channels." J Gen Physiol **112**(5): 637-47.

152. Wang, S., S. Liu, et al. (1997). "A quantitative analysis of the activation and inactivation kinetics of HERG expressed in *Xenopus* oocytes." *J Physiol* **502** (Pt 1): 45-60.
153. Waring, D. W. and J. L. Turgeon (2006). "Estradiol inhibition of voltage-activated and gonadotropin-releasing hormone-induced currents in mouse gonadotrophs." *Endocrinology* **147**(12): 5798-805.
154. Warmke, J., R. Drysdale, et al. (1991). "A distinct potassium channel polypeptide encoded by the *Drosophila* eag locus." *Science* **252**(5012): 1560-2.
155. Warmke, J. W. and B. Ganetzky (1994). "A family of potassium channel genes related to eag in *Drosophila* and mammals." *Proc Natl Acad Sci U S A* **91**(8): 3438-42.
156. Weinsberg, F., C. K. Bauer, et al. (1997). "The class III antiarrhythmic agent E-4031 selectively blocks the inactivating inward-rectifying potassium current in rat anterior pituitary tumor cells (GH3/B6 cells)." *Pflugers Arch* **434**(1): 1-10.
157. Wen, S., J. R. Schwarz, et al. (2008). "Functional characterization of genetically labeled gonadotropes." *Endocrinology* **149**(6): 2701-11.
158. Wimmers, S., C. K. Bauer, et al. (2002). "Biophysical properties of heteromultimeric erg K⁺ channels." *Pflugers Arch* **445**(3): 423-30.
159. Yang, T., S. Kupersmidt, et al. (1995). "Anti-minK antisense decreases the amplitude of the rapidly activating cardiac delayed rectifier K⁺ current." *Circ Res* **77**(6): 1246-53.
160. Zankov, D. P., H. Yoshida, et al. (2009). "Adrenergic regulation of the rapid component of delayed rectifier K⁺ current: implications for arrhythmogenesis in LQT2 patients." *Heart Rhythm* **6**(7): 1038-46.
161. Zaza, A., M. Micheletti, et al. (1997). "Ionic currents during sustained pacemaker activity in rabbit sino-atrial myocytes." *J Physiol* **505** (Pt 3): 677-88.
162. Zhou, Z., Q. Gong, et al. (1998). "Properties of HERG channels stably expressed in HEK 293 cells studied at physiological temperature." *Biophys J* **74**(1): 230-41.
163. Zhu, X., A. S. Gleiberman, et al. (2007). "Molecular physiology of pituitary development: signaling and transcriptional networks." *Physiol Rev* **87**(3): 933-63.

VII. Appendix

VII.1. Contributions

- I would like to state that the Na⁺-current and erg K⁺-current temperature-dependence experiments, as well as the LH-secretion measurements were performed completely by me. For all the other electrophysiological and the calcium-imaging experiments I would like to thank Dr. Wiebke Hirdes for contributing to the gathering and analysis of the data.
- Also, I would like to note that the immunofluorescence experiments on pituitary slices were done by Shuping Wen.

VII.2. List of tables

Table III.1: Ionic composition of different extracellular (Ringer) solutions and intracellular solution used for recording of the erg currents	29
Table III.2: Ionic composition of extra- and intracellular solutions used for recording sodium currents	29
Table IV.1: Temperature dependence of erg current activation, availability and current density in gonadotropes	49
Table IV.2: Temperature dependence of time courses of recovery from inactivation and deactivation with the corresponding Q ₁₀ values	50

VII.3. List of figures

Fig. II.1: Schematic representation of principal K ⁺ subunits families and subfamilies	4
Fig. II.2: The ether-á-go-go gene K ⁺ channel family (EAG)	5

Fig. II.3: Structure of EAG K ⁺ channels	6
Fig. II.4: Schematic representation of the erg-mediated current	9
Fig. II.5: Physiological function of erg currents in cardiac myocytes	11
Fig. II.6: Diagram illustrating the effects of reduction of the erg current in prolactin secretion	13
Fig. II.7: Gonadotropes membrane potential at rest, GnRH-induces electrical activity and Ca ²⁺ signaling	15
Fig. III.1: Cre recombinase mediated YFP and GFP expression in gonadotropes	18
Fig. III.2: Chemical structure of fura-2	20
Fig. III.3: Excitation spectra of 1 μM fura-2	21
Fig. III.4: Membrane behavior compared with an electrical circuit	23
Fig. III.5: Voltage clamp negative feedback circuit	24
Fig. III.6: Simplified diagram of the patch-clamp amplifier and substitute circuit of the whole-cell configuration	25
Fig. III.7: Schematic diagram of various patch-clamp recording configurations	26
Fig. III.8: Sandwich ELISA technique steps	33
Fig. IV.1: YFP expression in gonadotropes	36
Fig. IV.2: Recording of resting membrane potential of gonadotropes	37
Fig. IV.3: GnRH induced different types of membrane potential responses	39
Fig. IV.4: Calcium imaging revealed heterogeneity of GnRH responses	40
Fig. IV.5: Effects of depolarizing the membrane potential of mouse gonadotropes	41
Fig. IV.6: Na ⁺ currents activation	42
Fig. IV.7: Voltage dependence of steady-state inactivation of Na ⁺ currents	42
Fig. IV.8: Blockage of erg channels increases [Ca ²⁺] _i in gonadotropes in acute pituitary slices	44
Fig. IV.9: Availability of erg currents in cultured gonadotropes	45
Fig. IV.10: Activation of erg currents in cultured gonadotropes	46
Fig. IV.11: Increase in [K ⁺] _e elevates erg channel conductance	47
Fig. IV.12: Temperature dependence of erg K ⁺ currents availability	48
Fig. IV.13: Temperature dependence of erg K ⁺ current activation	48
Fig. IV.14: Effects of temperature on the erg current rates of recovery from inactivation and deactivation	50
Fig. IV.15: Blockage of the erg currents depolarized the gonadotrope membrane	52
Fig. IV.16: Blockage of erg channels increases [Ca ²⁺] _i in cultured gonadotropes	53

Fig. IV.17: E-4031 and GnRH increase $[Ca^{2+}]_i$	54
Fig. IV.18 Erg channel blockage reduces an outward current	55
Fig. IV.19 Changes in the voltage dependence of activation induced by GnRH	56
Fig. IV.20 Changes in the voltage dependence of deactivation induced by GnRH	57
Fig. IV.21. GnRH does not change the time course of activation, deactivation and recovery from inactivation	59
Fig. IV.22: LH secretion of cultured pituitaries measured with ELISA	60
Fig. V.1: Hypothetical model of intracellular signaling cascade activated by binding of GnRH to its receptor in the plasma membrane of gonadotropes	68

VII.4. Abbreviations

4-AP	4-Aminopyridine
HEPES	4-(2-hydroxyethyl)-1-piperazineethanesulfonic acid
TMB	3,3',5,5'-tetramethylbenzidine
AM	Acetoxymethyl
ACTH	Adrenocorticotrophic hormone
MgATP	Adenosine 5'-triphosphate magnesium salt
ADH	Antidiuretic hormone / vasopressin
ACSF	Artificial cerebrospinal fluid
BSA	Bovine serum albumin
CaCl ₂	Calcium chloride
Ca ²⁺	Calcium ion
C	Capacitance
CO ₂	Carbon dioxide
CsCl	Cesium chloride
CsOH	Cesium hydroxide
q	Charge
CHO	Chinese hamster ovary
CAGS	CMV enhancer
cDNA	Complementary deoxyribonucleic acid
G	Conductance

Cre	Cre recombinase
I	Current
CC	Current clamp
I/V	Current versus voltage
cAMP	Cyclic adenosine monophosphate
cGMP	Cyclic guanosine monophosphate
cNBD	Cyclic nucleotide binding domain
CMV	Cytomegalovirus
DIV	Days <i>in vitro</i>
DNA	Deoxyribonucleic acid
DAG	Diacylglycerol
DMSO	Dimethylsulfoxide
GRIC/R26-YFP	Double heterozygous “knock-in” mice resulting from GRIC mice bred to ROSA26-YFP mice
GRIC/eR26- τ GFP	Double heterozygous “knock-in” mice resulting from GRIC mice bred to eROSA26- τ GFP mice
DMEM	Dulbecco’s modified Eagle medium
erg	eag-related gene
elk	eag-like
EBSS	Earle’s balanced salt solution
EIA	Enzyme immunoassay
ELISA	Enzyme-linked immunosorbent assay
eag	Ether-á-go-go
EGTA	Ethylene glycol tetraacetic acid
$[Ca^{2+}]_e$	External calcium concentration
$[K^+]_e$	External potassium concentration
F	Farad
F	Fluorescence intensity ratio
FSH	Follicle-stimulating hormone
GRIC	GnRHR-IRES-Cre “knock-in” mice
GRIC ^{neo+}	<u>G</u> nRHR- <u>I</u> RES- <u>C</u> re with neomycin resistance “knock-in” mice
GnRH	Gonodotropin-releasing hormone
GnRHR	Gonadotropin-releasing hormone receptor
GPCR	G-protein-coupled receptor

g	Gravity
GFP	Green fluorescent protein
GH	Growth hormone
GH ₃	Growth hormone and prolactin secreting tumor cell line
HCl	Hydrogen chloride
H ₂ O ₂	Hydrogen peroxide
HPG	Hypothalamic-pituitary-gonadal axis
HEK	Human embryonic kidney
HERG	Human erg potassium channel gene
C57BL/6J	Inbred strain of laboratory mice
IP ₃	Inositol trisphosphate
IRES	Internal ribosome entry site
[Ca ²⁺] _i	Internal calcium concentration
K _{ir}	Inward rectifier potassium channels
LQT2	long QT-syndrome type 2
LH	Luteinizing hormone
MgCl ₂	Magnesium chloride
I _{max}	Maximum current
MΩ	Megaohms
MSH	Melanocyte-stimulating hormone
E _m	Membrane potential
V _{1/2}	Membrane potential at which current is 50% of the maximum
mRNA	Messenger ribonucleic acid
MEM	Minimal essential medium
F ₀	Minimal fluorescence in control condition
MiRP	MinK-related peptide
OT	Oxytocin
PVN	Paraventricular nuclei
PIP ₂	Phosphatidylinositol 4,5-bisphosphate
KCl	Potassium chloride
KOH	Potassium hydroxide
K ⁺	Potassium ion
PRL	Prolactin
PKA	Protein kinase A

PKC	Protein kinase C
I_{Kr}	Rapidly activating component of cardiac delayed rectifier K^+ current / HERG
R	Resistance
E_{rev}	Reversal potential
RNA	Ribonucleic acid
RT	Room temperature
n	Sample number
R_s	Series resistance
S	Siemens
AgCl	Silver chloride
SA	Sinoatrial node
k	Slope factor
$NaHCO_3$	Sodium bicarbonate
NaCl	Sodium chloride
G_{Na}	Sodium conductance
NaH_2PO_4	Sodium dihydrogen phosphate
NaOH	Sodium hydroxide
Na^+	Sodium ion
E_{Na}	Sodium reversal potential
I_{Na}	Sodium peak current
SEM	Standard error of the mean
GH_3/B_6	Subclone of GH_3 cells
SON	Supraoptic nuclei
T	Temperature
Q_{10}	Temperature coefficient
$Q_{10deact}$	Temperature coefficient for deactivation
Q_{10rec}	Temperature coefficient for recovery
ΔT	Temperature difference
TEA-Cl	Tetraethylammonium chloride
TTX	Tetrodotoxin
TSH	Thyroid-stimulating hormone
TRH	Thyrotropin-releasing hormone
t	Time

$\tau_{20^{\circ}\text{C}}$	Time constants at 20°C
$\tau_{30^{\circ}\text{C}}$	Time constants at 30°C
τ_{fast}	Time constants of fast component of deactivation
τ_{rec}	Time constants of recovery from inactivation
τ_{slow}	Time constants of slow component of deactivation
TMD	Transmembrane domain
U/ml	Units per milliliter
V	Voltage and/or volt
VC	Voltage clamp
K_v	Voltage-dependent potassium channels
YFP	Yellow fluorescent protei

VIII. Acknowledgements

Foremost, I would like to express my sincere gratitude to my advisors Prof. Dr. Jürgen R. Schwarz and Dr. Wiebke Hirdes for the continuous support of my Ph.D study and research. Prof. Schwarz's perpetual energy and enthusiasm in research had motivated all the students from the Institute of Neural Signal Transduction, including me. In addition, he is always accessible and willing to help his students with their research. Dr. Wiebke Hirdes, with her enthusiasm, her inspiration, and her great efforts to explain things clearly and simply, helped to make research fun for me. Throughout my thesis-writing period, they provided encouragement, advice, good teaching, good company, and lots of good ideas. I could have not imagined having better advisors and mentors for my Ph.D study and, as a result, research life became smooth and rewarding for me.

I am especially grateful to Prof. Dr. Olaf Pongs, who was essential in this research and provided facilities and fruitful discussions. I thank him sincerely for offering a great scientific environment with lots of mental resources and great financial support.

My sincere thanks also go to our collaborators, Dr. Ulrich Boehm and his crew who shared with us the GRIC/R26-YFP and GRIC/eR26- τ GFP mice. A particular thank to Shuping Wen for her help with analyzing the GRIC/R26-YFP and to Oliver Mai for creating the GRIC/eR26- τ GFP mice and also to: Christian, Soumya, Devesh, Zahara, Nergiz and their technicians Dagmar and Annette for offering good advice and help whenever I needed them.

I was delighted to interact with Prof. Dr. Christiane K. Bauer from the Department of Vegetative Physiology and Pathophysiology by having her as my co-advisor. I would like to thank her and also Dr. Günter Glassmeier for their encouragement and technical guidance.

I am grateful: to the scientific workshop service of the ZMNH, namely Fritz Kutschera and Torsten Renz, for never failing to come up with a solution for a problem, to the IT service and development (EDV) people for sheer endless computer-problem solving, and the ever-friendly administrative staff.

I would like to show my gratitude to Dr. Michaela Schweizer and Raithore Chudamani for their technical help in the primary culture, and Dr. Gabriele Loers for her advice and fruitful help with ELISA measurements.

I am grateful to Dr. Irm Hermans-Borgmeyer for accepting me as a student in the Graduate Study Program in Molecular Biology (Aufbaustudium Molekularbiologie) and for organizing the German course for all non-native speakers in the ZMNH. The accumulated experience

broadened my perspective on the practical aspects of research and improved my social life in Germany.

I would like to thank my thesis committee: PD Dr. Sabine Lüthje, Prof. Dr. Dirk Isbrandt and Prof. Dr. Dirk Warnecke for their encouragement, insightful comments, and for their invaluable support and time.

I cannot thank enough all those colleagues who supported me in different ways, some of whom are now my closest friends. I am especially grateful to the innumerable people who I have annoyed in the past years with my questions, complaints and problems. I sincerely thank all my colleagues for offering a very nice environment in the lab, for their discussions, advice, technical help and time: Dragoş, Phanindra, Sönke, Lijuan, Martin, Vitya, Joanna, Gregor, Malte, Niklas, Yu, Frederick, Alexander and some former labmates: Jacqueline, Simone, Quyen, Christoph. Special thanks to Iris Ohmert for her constant help and good advice for laboratory practice.

A particular thank to Mr. Lee Jennings for his time dedicated to read this thesis as a native English speaker.

I thank my friends, particularly Cristina, Simona, Ioana, Radu, Dana, Aparna, Monica, Eka, Sathish, Gionata, Luca, Praveen, Stephanie for their continuous support and interest in what I do and for all the fun we have had in the last three years.

I am grateful to Sebastian to be the very special person he is and for the incredible amount of patience he had with me.

Lastly, and most importantly, I wish to thank my entire extended family and especially my parents who always provide me with encouragement and a loving environment. Without their endless support, this thesis would not have been achieved. I dedicate this thesis to them.